A STUDY OF 2-PION PRODUCTION IN 10 GeV/c K^+ MESON INTERACTIONS IN HYDROGEN

Barry Alper

Linacre College

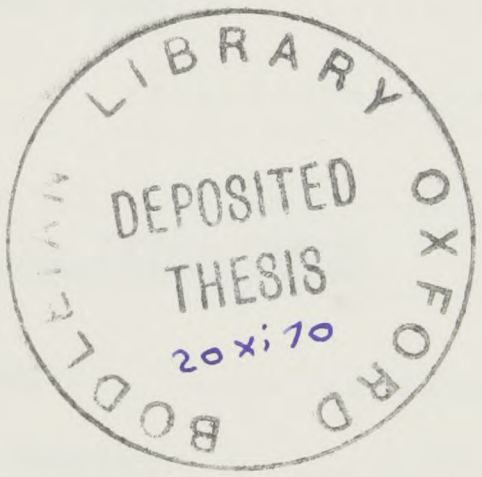

Thesis submitted for the degree of Doctor of Philosophy
in the University of Oxford

September, 1970

C O N T E N T S

A B S T R A C T

This thesis contains an analysis of the two reactions,

$$K^+p \rightarrow K^+\pi^+\pi^-p$$

and

$$K^+p \rightarrow K^o\pi^+\pi^op$$

at an incident K^+ momentum of 10 GeV/c, which were observed in the C.E.R.N. 2m Hydrogen Bubble Chamber.

The resonances $\Delta^{++}(1236)$, $K^{*o}(890)$ and $K^{*o}(1420)$ are strongly produced in these data. To investigate the possible existence of a scalar $K_N(1100)$ resonance, calculations were performed on the $K^{*o} - \Delta^{++}(1236)$, quasi two-body state, using modified one-pion-exchange formulae. The presence of a large $I = \frac{1}{2}$, s-wave phase shift in the region of 1.1 GeV/c^2 is indicated but is not required to be resonant.

The enhancement between 1.2 and 1.45 GeV/c^2 in $K\pi\pi$ mass, present in these data, is determined to have a dominant spin-parity of 1^+ throughout. Evidence for two 1^+ resonances in this mass region is obtained from an analysis of the variations, with mass, of the decay properties of this system.

A low mass $p\pi\pi$ enhancement is present in the data from $K^+\pi^+\pi^-p$ final state, only. A study of the production and decay characteristics of this system would seem to suggest that it is composed of the $I = \frac{1}{2}$ resonances in the spin-parity series $\frac{1}{2}^+$, $3/2^-$, $5/2^+$, known from elastic π-p phase shift analyses.

P R E F A C E

The two final states $K^+\pi^+\pi^-p$ and $K^o\pi^o\pi^+p$ are rich in interesting features and provide useful material for studying many aspects of hadron physics. Meson resonances, both strange and non-strange and non-strange baryon resonances are all present in these data, produced in some cases by diffraction dissociation. The experimental work for obtaining the data on these two channels has, for the most part, been carried out at Birmingham and Glasgow Universities; however, the analyses contained in this thesis on these two channels have been performed in Oxford only.

The thesis is arranged as follows: Chapter 1 is an introductory chapter. The first part contains an outline of the measuring and fitting, in Oxford, of the events satisfying the $K^+\pi^+\pi^-p$ topology. The general characteristics of the two channels are discussed in the second part using the method suggested by Van Hove for displaying 4-body final states. Chapter 2 contains an analysis of $K^{*-}\Delta$ systems using one-pion-exchange models. The production and decay into $K\pi\pi$ of the Q enhancement is the subject of Chapter 3. The systematics and most of the mathematics related to this chapter are placed in the appendices. Finally Chapter 4 contains a study of the $p\pi^+\pi^-$ system.

ACKNOWLEDGEMENTS

I would like to thank Professors D.H. Wilkinson, F.R.S., and D.H. Perkins, F.R.S., for a place in the Bubble Chamber Group of the Nuclear Physics Laboratory, and the Science Research Council for the award of a Research Studentship.

It is a great pleasure to thank my supervisor, Dr. M.G. Bowler, for his assistance, encouragement and enthusiasm throughout the last three years.

I am very grateful to Drs. R.J. Cashmore and D.H. Saxon for many valuable discussions and suggestions, and to my colleagues at Birmingham and Glasgow Universities for making their data available to me. Finally, I would like to thank Mrs. E. Browne, for her fine typing of this manuscript.

C H A P T E R 1

INTRODUCTION

1 History of the Experiment

The 10 GeV/c K^+p Bubble Chamber Experiment is a collaboration between the Universities of Birmingham, Glasgow and Oxford. Film exposures have been taken with the C.E.R.N. 2-metre Bubble Chamber at various times since December 1965. The separation of kaons in the beam was obtained by means of radio-frequency deflecting cavities. Due to the pressure from other experiments on the Oxford measuring facilities, we have assisted in the experimental runs and subsequent measurement of those events obtained before 1967 only. Consequently the major part of the data presented here has been measured at Birmingham and Glasgow Universities.

In this thesis, the two final states of primary interest are :

$$K^+p \rightarrow K^+\pi^+\pi^-p \qquad (1)$$

and

$$K^+p \rightarrow K^o\pi^+\pi^op \qquad (2)$$

All details of the beam, measurement of the chamber field and the reconstruction, in Oxford of the events satisfying the 'two-prong one-vee' topology of reaction (2) have been summarised by Hemingway [1] and Sumner [2]. They analysed the events from the three runs of December 1965, June 1966 and July 1966 and found that the proton and muon contamination

in the December 1965 and July 1966 beams was considerably higher than in the June 1966 run. The average number of protons per frame was ~ 0.1 in the June run but more than five times higher than this in the other two.

2 Measurement of the 4-prongs at Oxford

The events of reaction (1) above satisfy a '4-prong no-vee' topology in the chamber. The high contamination of the beam in the December and July runs mentioned above, meant that it was unsafe to measure the 4-prong topology, where no strange particle decay is observed, from those runs. Consequently, of these three runs only the 4-prongs from the June run were measured. A single separate scan for 4-prongs was carried out on the 20,000 frames at Oxford for this run.

The subsequent measurements were processed with the Oxford Bubble Chamber Group system of programs [3], which are based on the Rutherford Laboratory sequence of GEOMETRY, KINEMATICS and JUDGE. The optical constants for the geometrical reconstruction of events were determined by Hemingway [1] using the program MONGOOSE [4].

The following five hypotheses were used in the kinematic fitting to the 4-prongs.

$K^+p \rightarrow K^+\pi^+\pi^-p$	(a)	(4-constraint fit)
$K^+p \rightarrow K^+K^+K^-p$	(b)	(4-constraint fit)
$K^+p \rightarrow K^+\pi^+\pi^-p\pi^0$	(c)	(1-constraint fit)
$K^+p \rightarrow K^+\pi^+\pi^+\pi^-n$	(d)	(1-constraint fit)
$K^+p \rightarrow \pi^+\pi^+\pi^-p\ K^0$	(e)	(1-constraint fit)

Four-constraint or three-constraint fits were accepted over any one-constraint fit that existed for the same event. This approach was checked by ionization scanning all four-constraint events and only those consistent with the ionization determined for the fit by the kinematics program, were accepted. An acceptable four-constraint fit was defined as one with a χ^2 probability of $\geqslant$ 0.1 per cent.

As our primary interest was in the four-constraint (4-C) fits only, the events at this stage were divided into five classes as follows :

i) Unique 4 or 3-C fits consistent with ionization

ii) Ambiguous 4 or 3-C fits all interpretations consistent with ionization

iii) Rejected events with obvious non beam tracks or very early or late tracks

iv) Events which failed to reconstruct geometry or fit kinematics

v) Events which fit kinematics but not to hypotheses (a) or (b).

The ambiguous events, class (ii), were found to lie predominantly in a region of low $K\pi\pi$ mass with a short recoil proton. It was suspected that many of these ambiguities would be removed if, in certain cases, the proton had been correctly identified as a stopping track, as greater accuracy in the determination of the momentum can be obtained from measurement of range rather than curvature. With this identification corrected where appropriate, these events together

with those from class (iv), were remeasured. Very little change in the ambiguous events from class (ii) resulted from this remeasurement. Of 89 that had a two-fold ambiguity after the first measurement, 78 still had the same ambiguity after the second. These class (ii) events will be discussed later.

In Table 1.1 is given the number of unique and ambiguous fits from Oxford to hypotheses (a) and (b), obtained after the second measurement. The χ^2 probability distribution for the unique events from reaction (1) is given in Fig. 1.1.

3 Mass resolution of the $K^+\pi^+\pi^-$ System

The experimental errors on the invariant mass combinations for the events of reaction (1) are particularly important in the low mass $K^+\pi^+\pi^-$ region where detailed structure is suspected (see Chapter 3). As no errors were made available to the author for the data from Birmingham and Glasgow Universities, the analysis outlined below was carried out on the Oxford data only. However, as similar measuring systems were employed at the three universities, the errors determined at Oxford are hopefully typical of the whole.

The invariant mass of the $K\pi\pi$ system is given by

$$M^2 = \left(\sum_i E_i\right)^2 - \left(\sum_i p_i\right)^2 \qquad (3)$$

where the summation is over the 3 particles. Since the E_i are derived from the p_i, the errors are determined from the

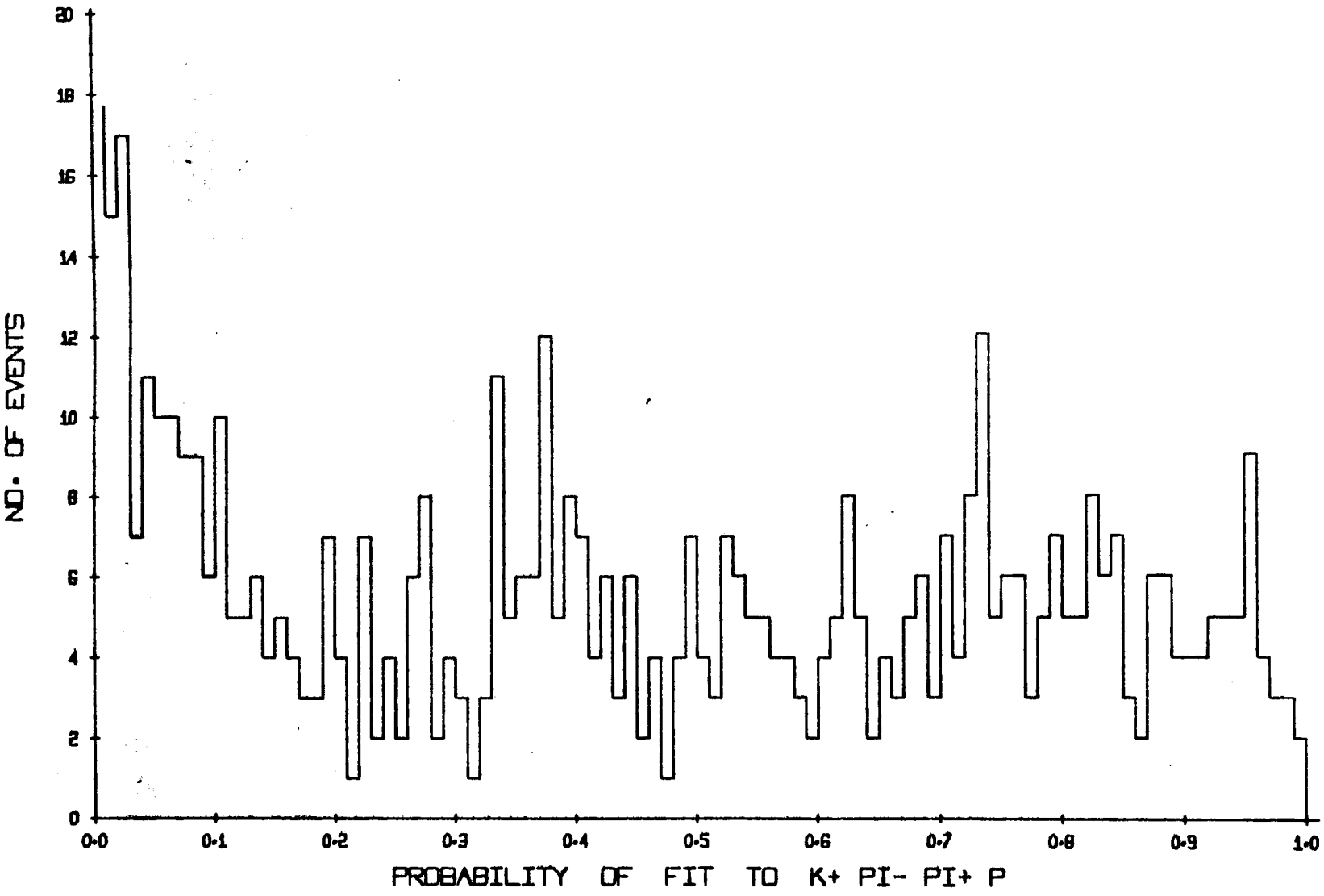
NO. OF EVENTS
20
18
16
14
12
10
8
6
4
2
0
0·0
0·1
0·2
0·3
0·4
0·5
0·6
0·7
0·8
0·9
1·0
PROBABILITY OF FIT TO K+ PI- PI+ P

Fig. 1.1

Table 1.1

Summary of the 4-constraint fits to the

Oxford 4-prongs

Final State	No. of unique events	No. of fits with 2-fold ambiguity
1) $K^+\pi^+\pi^-p$	882	281
2) $K^+K^+K^-p$	29	9

latter variables only. Therefore we write

$$(\Delta M^2)^2 = \sum_i \left[\sum_{x,y} \frac{\partial M^2}{\partial p_{x_i}} \frac{\partial M^2}{\partial p_{y_i}} \Delta(p_{x_i}, p_{y_i}) \right] \qquad (4)$$

where x,y are summations over the Cartesian components, and $\Delta(p_{x_i}, p_{y_i})$ is the Cartesian error matrix element derived from kinematics. To evaluate the partial derivatives we use

$$E_i^2 = \sum_y (p_{y_i})^2 + m_i^2 \qquad (5)$$

and write

$$2E_i \frac{\partial E_i}{\partial p_{x_i}} = 2 \sum_y p_{y_i} \frac{\partial p_{y_i}}{\partial p_{x_i}}$$

$$= 2 p_{x_i} \qquad (6)$$

Using Eq. (6) after differentiating Eq. (3) we get

$$\frac{\partial M^2}{\partial p_{x_i}} = 2 E_{tot.} \frac{p_{x_i}}{E_i} - 2 p_{tot.} \qquad (7)$$

where $E_{tot.}$ and $p_{tot.}$ are respectively the energy and momentum of the K$\pi\pi$ system. Substituting Eq. (7) into Eq. (4) the error on M^2 may be evaluated for each event. The error on the mass is then given by

$$\Delta M = \frac{\Delta M^2}{2M} \qquad (8)$$

The distribution of ΔM against M is shown in Fig. 1.2 using this procedure. The resolution is largely independent of mass and is approximately $\pm$ 10 MeV/c^2. A similar analysis [5] on the events of reaction (2) yielded a value of $\pm$ 20 MeV/c^2.

4 The one-constraint events

For the 'two-prongs, one-vee' topology of reaction (2), the K^o is uniquely identified and the proton can usually be distinguished by ionization. The amount of freedom that is available for fixing the identification of the remaining particles is therefore drastically reduced. This is not the case with the 4-prongs, where many possible permutations of track identification are possible. At 10 GeV/c, in many cases π^+ and K^+ assignments can be interchanged freely for any particular track, with the attributed ionizations remaining unaltered. This introduces considerable freedom in the one-constraint fits and in most cases many possible interpretations were found to occur for each event. Ionization scanning of these events was attempted by the author. A unique interpretation consistent with ionization was found in only a relatively small fraction of the events. Table 1.2 summarised the results of scanning a quarter of the Oxford sample of film. The numbers have been cut off above 3-fold ambiguities. As can be seen the number of 2-fold ambiguities is comparable to the uniques, making any use of these events extremely limited.

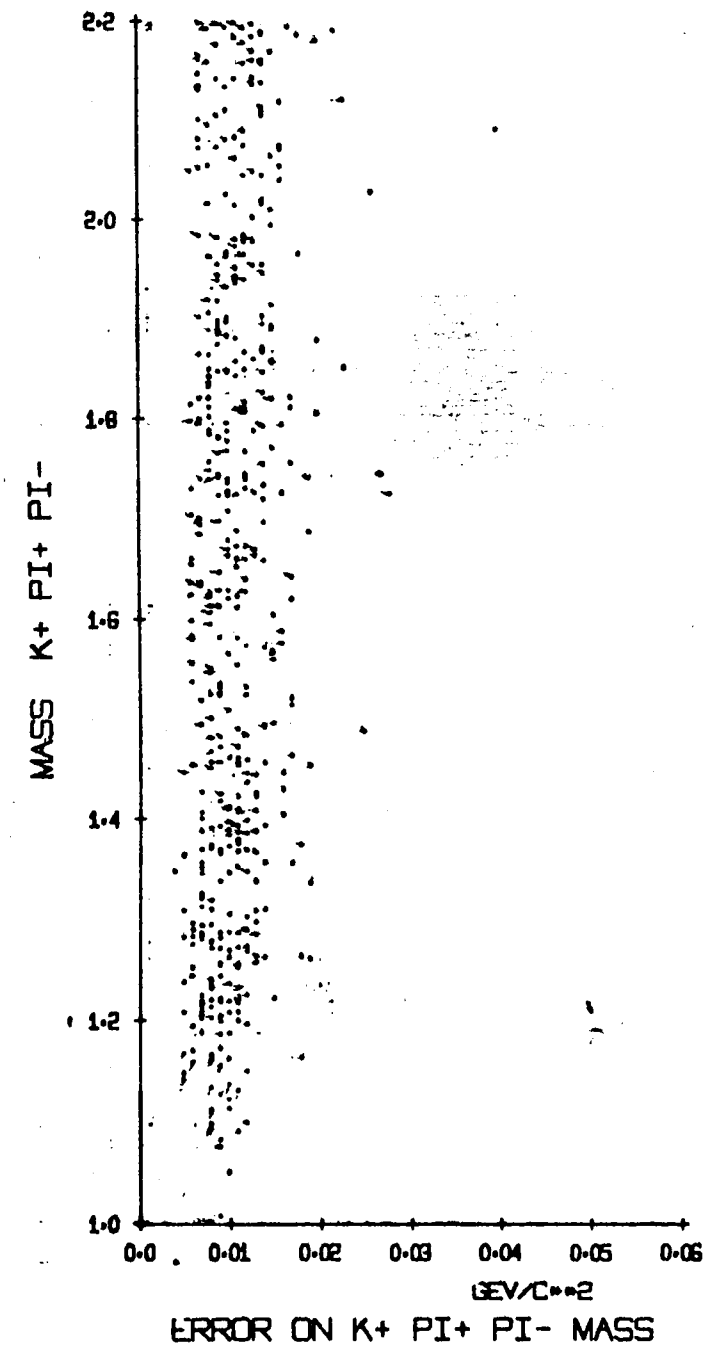
2·2
2·0
1·8
1·6
1·4
1·2
1·0
MASS K+ PI+ PI-
0·0
0·01
0·02
0·03
0·04
0·05
0·06
GEV/C**2
ERROR ON K+ PI+ PI- MASS

Fig. 1.2

Table 1.2

Summary of the 1-constraint fits to the sample of Oxford 4-prongs which was ionization scanned

Final State	No. of unique events	No. of fits with 2-fold ambiguity	No. of fits with 3-fold ambiguity
1) $K^+\pi^+\pi^-p\pi^0$	204	290	31
2) $\pi^+\pi^+\pi^-pK^0$	107	120	23
3) $K^+\pi^+\pi^+\pi^-n$	48	72	33

In Fig. 1.3, the beam 'stretch functions' are shown for the variables azimuth, dip and reciprocal of momentum for the unique fits to hypothesis (c) before and after ionization scanning a sample of film. The stretch function, which is given by

$$\frac{X_{fitted} - X_{measured}}{[\langle \delta X_{meas.} \delta X_{meas.} \rangle - \langle \delta X_{fit.} \delta X_{fit.} \rangle]^{\frac{1}{2}}} \qquad (9)$$

for a quantity X, where $\langle \quad \rangle$ signifies the error matrix, should approximate to a Gaussian distribution with mean 0 and width 1 for the three variables plotted. The events, before ionization scanning are clearly not normally distributed, being almost flat. This is not due to poor chamber constants since the 4-constraint fits produced significantly better distributions. It must be due to incorrect assignments. The distributions after ionization scanning are better, though they are still too wide, suggesting misidentified events remain.

A check on the correctness of the assignments to hypothesis (e) can be made from a comparison with the 4-constraint fits to this hypothesis where the K^o decay is seen. From a measure of the cross-section of this channel with the K^o seen, the number of unseen K^o's in the sample of film scanned is expected to be $\sim$ 95 events. This is consistent with the number found in the one-constraint fits, only if all the ambiguous fits are ignored (see Table 1.2). The $p\pi^+$ and

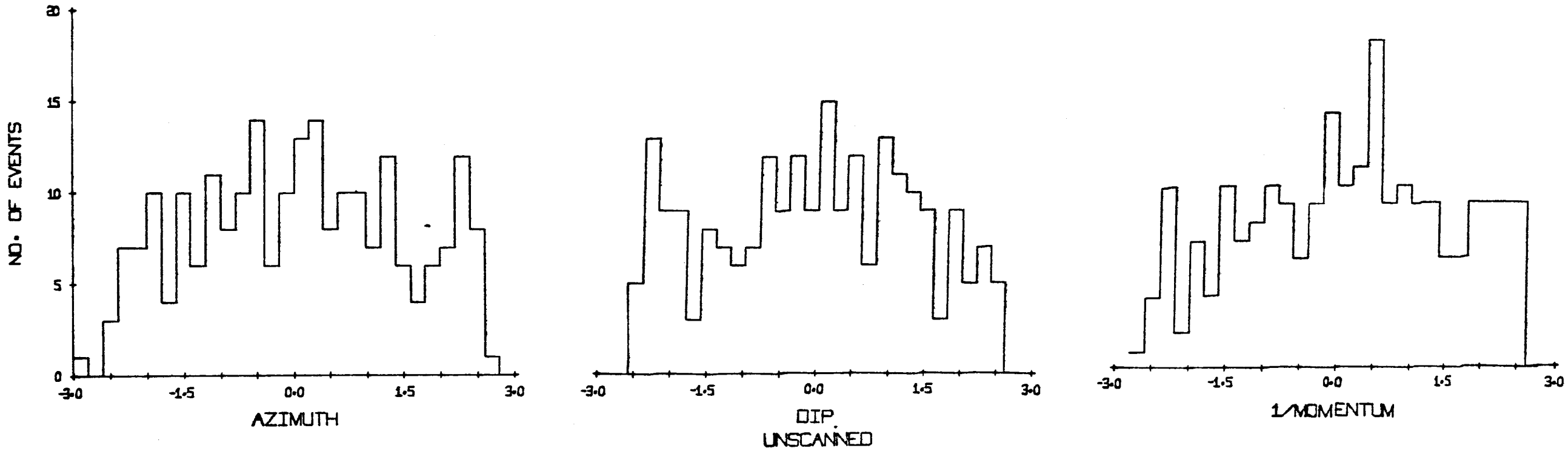

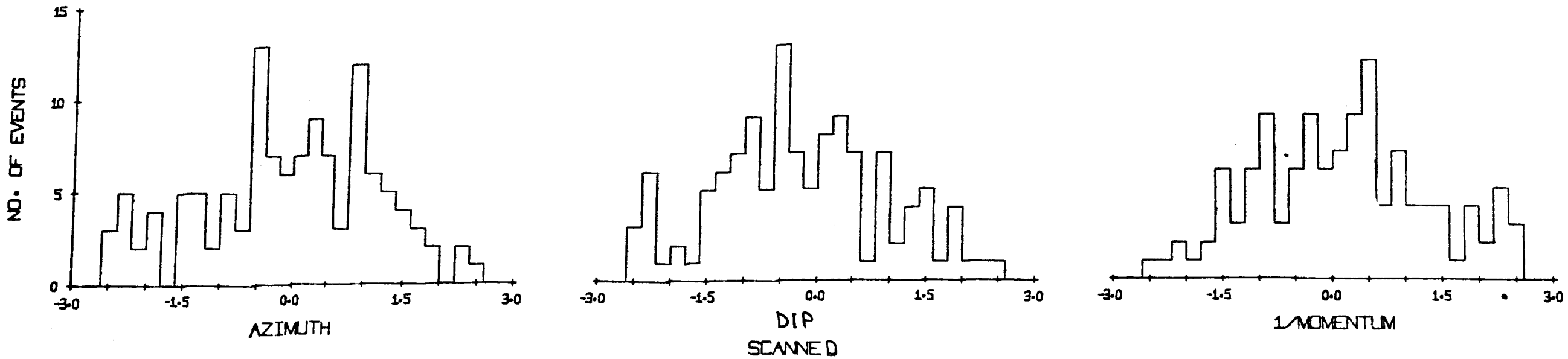

STRETCH FUNCTIONS

Fig. 1.3

$K^{o}\pi^{+}$ mass projections from these unique one-constraint and four-constraint fits are compared in Fig. 1.4. The clear $\Delta^{++}(1236)$ and $K^{*+}(890)$ signals seen in the latter events are barely visible in the former.

The use of one-constraint fits from the 4-prongs at 10 GeV/c seems very limited. They will not be studied further here.

5 The available data

Table 1.3 shows the number of events, both unique and with a two-fold ambiguity from various channels referred to in this thesis, that were made available by the three universities at the time of writing. The cross-sections have been determined by Birmingham University using Taus and a normalization to $K^{+}p$ total cross-sections. The errors quoted include a contribution from statistical errors and the difference in path length obtained from these two methods [6].

6 The Van Hove Plot

At high energies, the study of more than 3-body final states in strong interaction processes, has been hindered by the difficulty of finding meaningful variables and fruitful ways of plotting the data. This problem is manifestly present in the data from reactions (1) and (2) (see Section 1) as the $\pi\pi$, $K\pi$, $K\pi\pi$, $p\pi$ and $p\pi\pi$ systems can all resonate. A display of the numerous invariant mass and momentum transfer

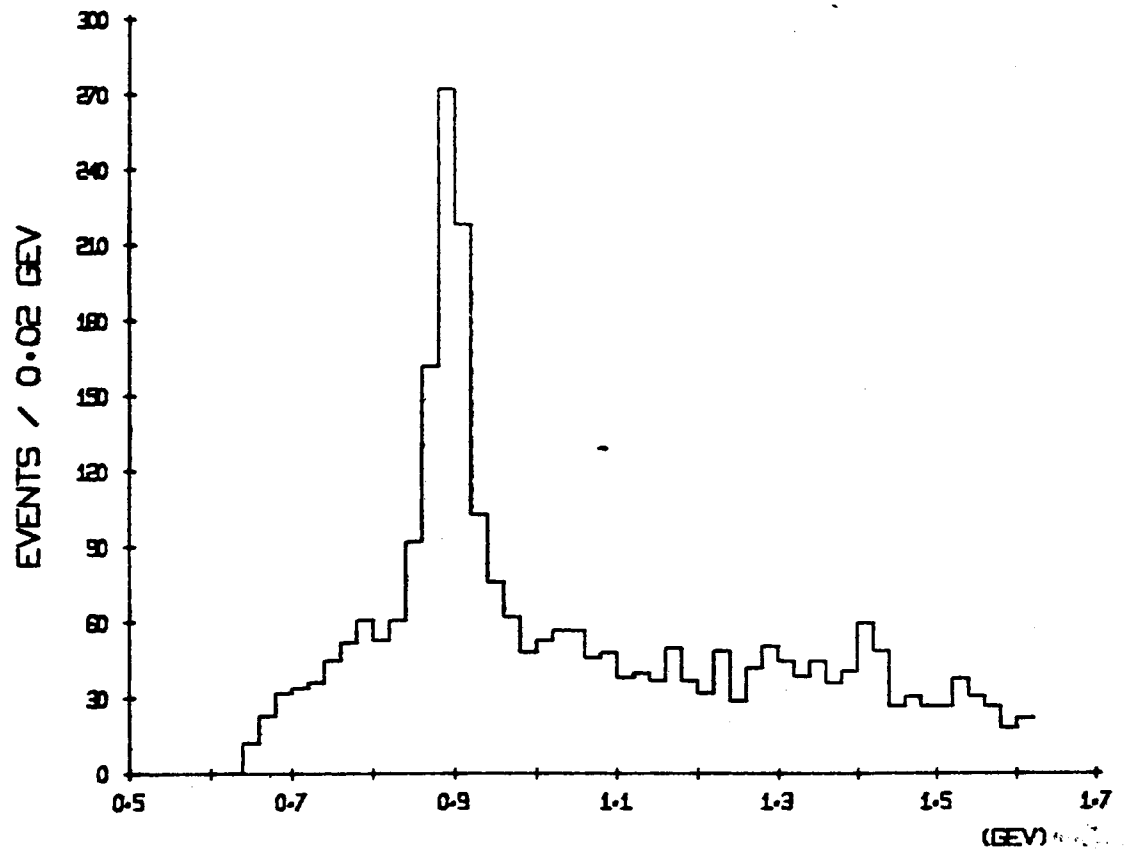

MASS K0 PI+ (4-C)

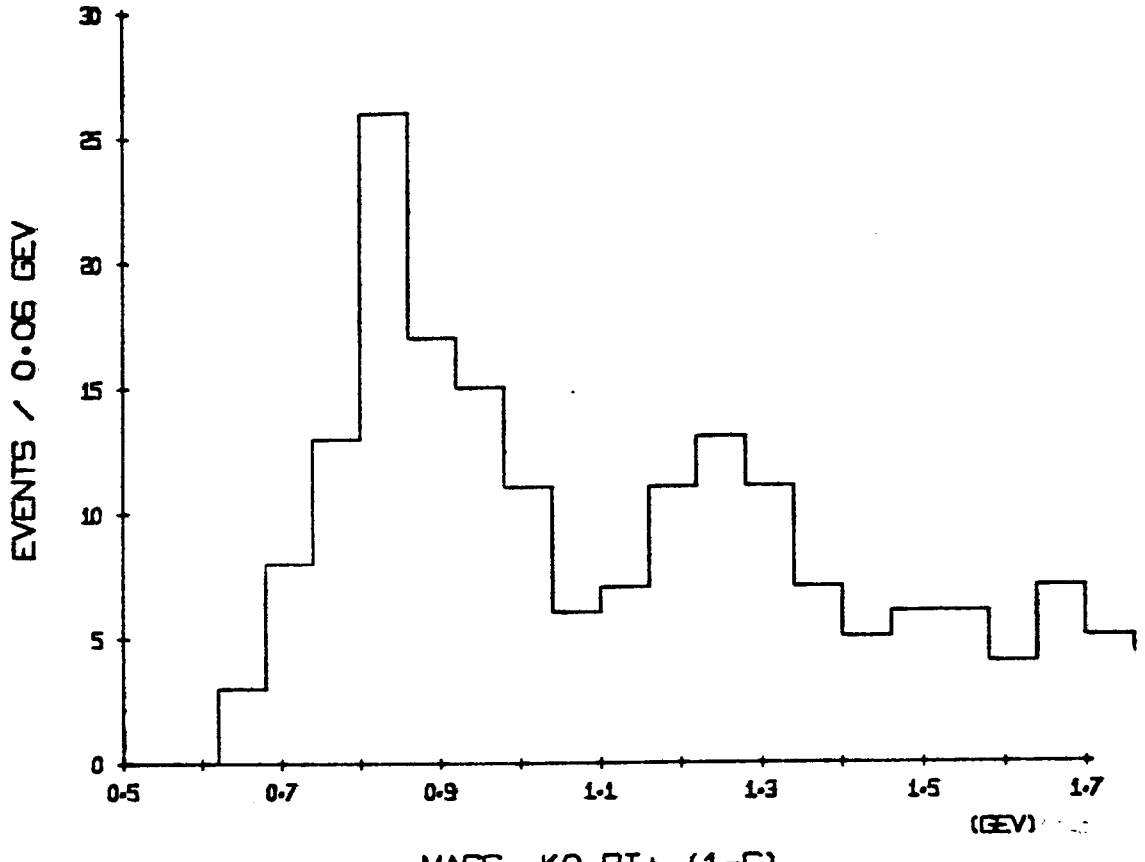

MASS K0 PI+ (1-C)

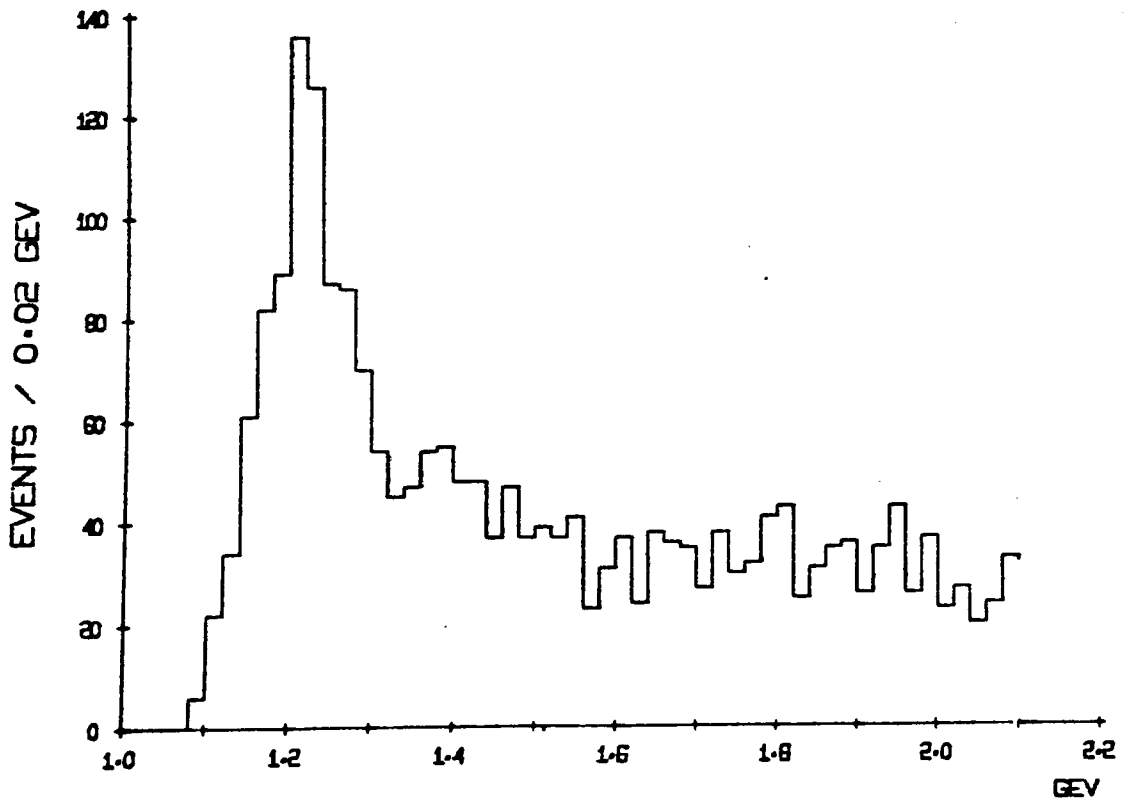

MASS P PI+ (4-C)

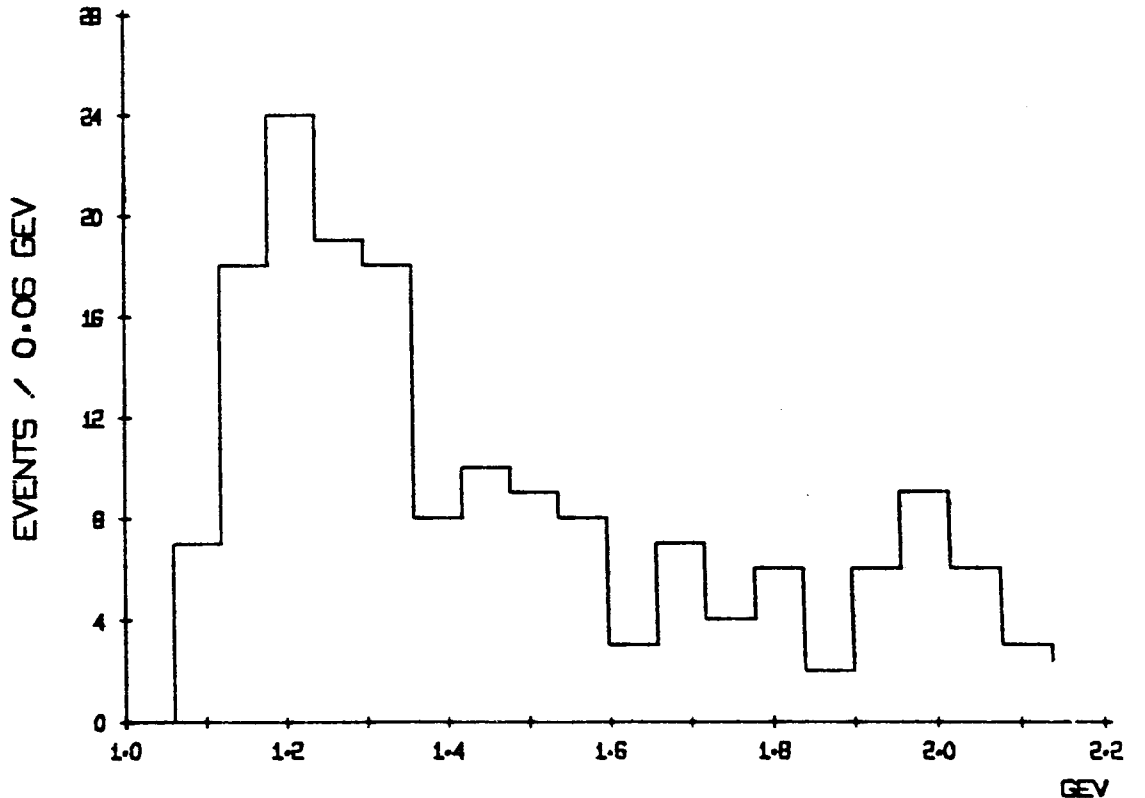

MASS P PI+ (1-C)

Fig. 1.4

Table 1.3

Total data sample available and cross-section estimates

Final State	No. of unique events	No. of fits with 2-fold ambiguity	Total cross-section μb
$K^+\pi^+\pi^-p$ (4-c)	6077	2059	1190±130
$K^o\pi^+\pi^o p$ (1-c)	4244	308	1090±115
$K^o\pi^+ p$ (4-c)	1142	28	226±32
$K^o\pi^+\pi^+\pi^- p$ (4-c)	1528	90	374±45

distributions would give information on the production of these systems but would not lead to any appreciation of the overall characteristics of that particular final state.

In strong interactions it has been known for a long time that single particle transverse momentum distributions are generally independent of the reaction involved and of the momentum of the incident particle. They peak at around 300 - 400 MeV/c in all cases. At high energies this momentum is generally small compared with the longitudinal component. Consequently, most of the information on an event is contained in the longitudinal components. Recently Van Hove [7] has suggested a technique for studying the correlations between the longitudinal momenta of the particles in a 4-body final state which uses this property. The principles are outlined below.

In the centre of mass of a 4-body final state, conservation of longitudinal momentum is given by

$$\sum_{i=1}^{4} p^*_{L,i} = 0 \qquad (10)$$

and conservation of energy by

$$\sum_{i=1}^{4} E_i = \sum_{i=1}^{4} [p^*_{L,i}{}^2 + r_i{}^2]^{\frac{1}{2}} = W \qquad (11)$$

Here $r_i{}^2 = p^*_{T,i}{}^2 + m_i{}^2$, i.e. it equals the sum of the squares of the mass and transverse momentum of each particle.

At high energies generally the relation $r_i^2 \ll p^{*2}_{L,i}$ holds and (1) may be approximated by

$$\sum_{i=1}^{4} |p^*_{L,i}| \lesssim W \qquad (12)$$

The constraints (10) and (12) require every event in longitudinal phase space to fall within a polyhedron with 14 faces, a cuboctahedron, with each face being either a square or an equilaterial triangle [8]. As the energies get higher, the nearer (12) gets to equality and the nearer to the surface of the polyhedron the events lie. A coordinate system for plotting the polyhedron may be defined by

$$X = \sqrt{\frac{3}{8}}\ (p^*_{L_1} + p^*_{L_2} + p^*_{L_3})$$

$$Y = \sqrt{\frac{1}{8}}\ (p^*_{L_1} + 3\ p^*_{L_2})$$

$$Z = p^*_{L_1}$$

The plot may be reduced to 2-dimensions by radially projecting each event outwards onto the surface of the polyhedron.

Figure 1.5 shows the surface of the cuboctahedron unfolded onto a plane for reactions (1) and (2) for that half corresponding to $p^*_L < 0$ for the proton. The longitudinal momenta of the three mesons for any particular point on the plot are proportional to the perpendicular distances from that point to the three axes shown. The proton momentum is

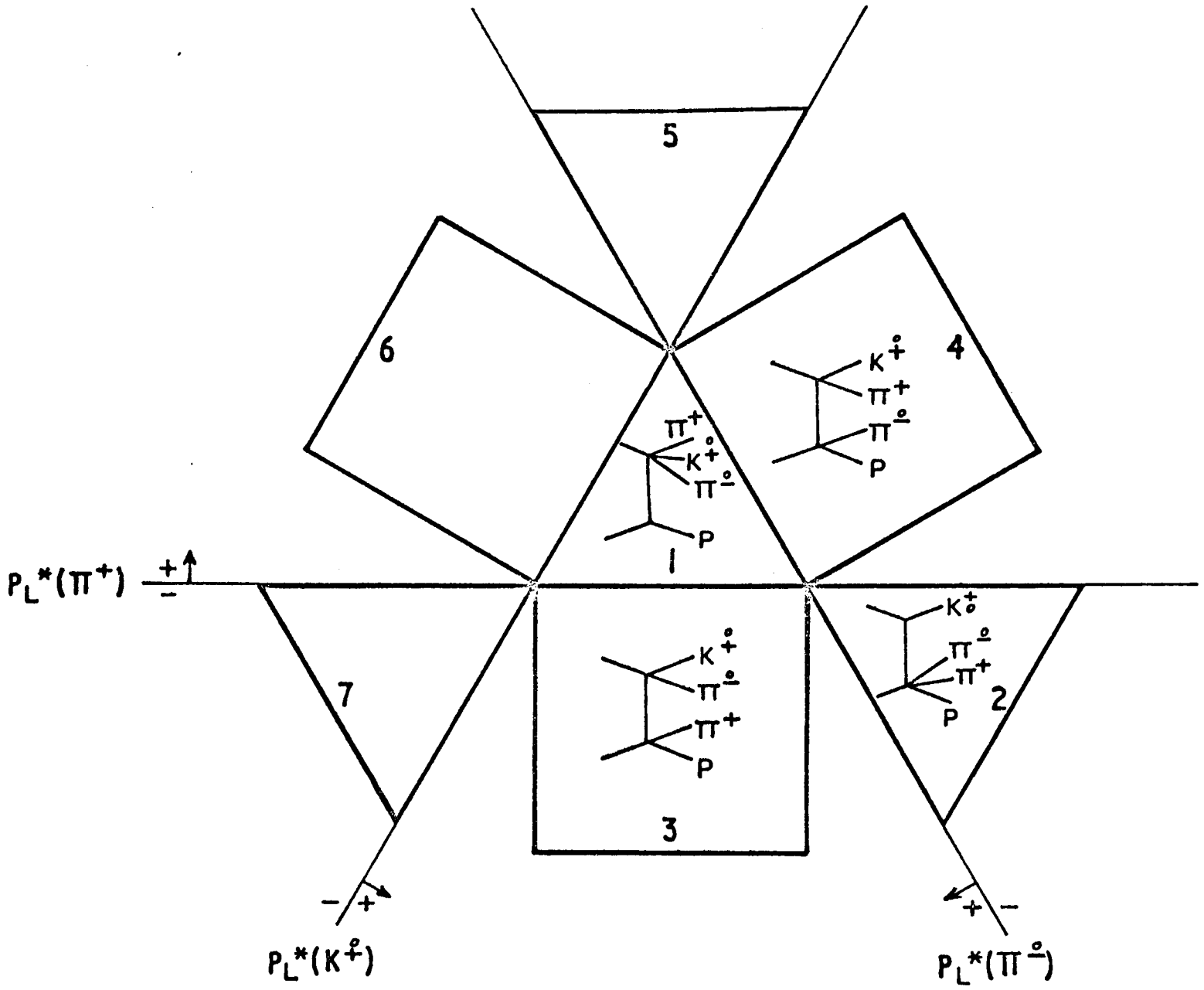

(Faces 5, 6 and 7 correspond to backward K's)

FIG. 1.5 CUBOCTAHEDRON PLOT

measured negatively in from the hexagonal boundary to a constant minimum value over Face (1). On each face has been drawn a peripheral diagram characterising the kinematic configuration for that face. The triangles correspond to three particles at one vertex and one at the other, whilst the squares correspond to two at each. Phase space dependence is complex, but it tends to crowd events near the boundaries.

Using the program FBODY [9], the unique events from the two reactions have been plotted in Figs. 1.6 and 1.7 on the surface of a cuboctahedron. The events not shown which correspond to forward protons, contribute only $\sim 3\%$ to the total sample. The plots illustrate the dominance of diffractive processes at high energies. Faces 1 and 2 for reaction (1) and Face 1 for reaction (2) are all highly populated by the data. These correspond to diagrams where at one vertex the initial and final state particles are the same and are therefore natural candidates for diffractive processes. It may be noted that unlike reaction (1) the process attributed to Face 2 for reaction (2) cannot go by diffractive means and there are correspondingly few events on that face. Face 1 corresponds to production of low mass $K\pi\pi$ systems. These events are studied in Chapter 3. Face 2 corresponds to low mass $p\pi^+\pi^-$ systems and is studied in Chapter 4. The bulk of the remaining events from both final states lie on Face 3. They correspond to $K^{*o} - \Delta^{++}$ production and are studied in Chapter 2.* The few events

* The association of a face with a particular process was checked by plotting separately the data that satisfied the selection criteria applied in subsequent chapters to isolate the process of interest. In each case, the events lay almost entirely on the face of the plot to which they were attributed.

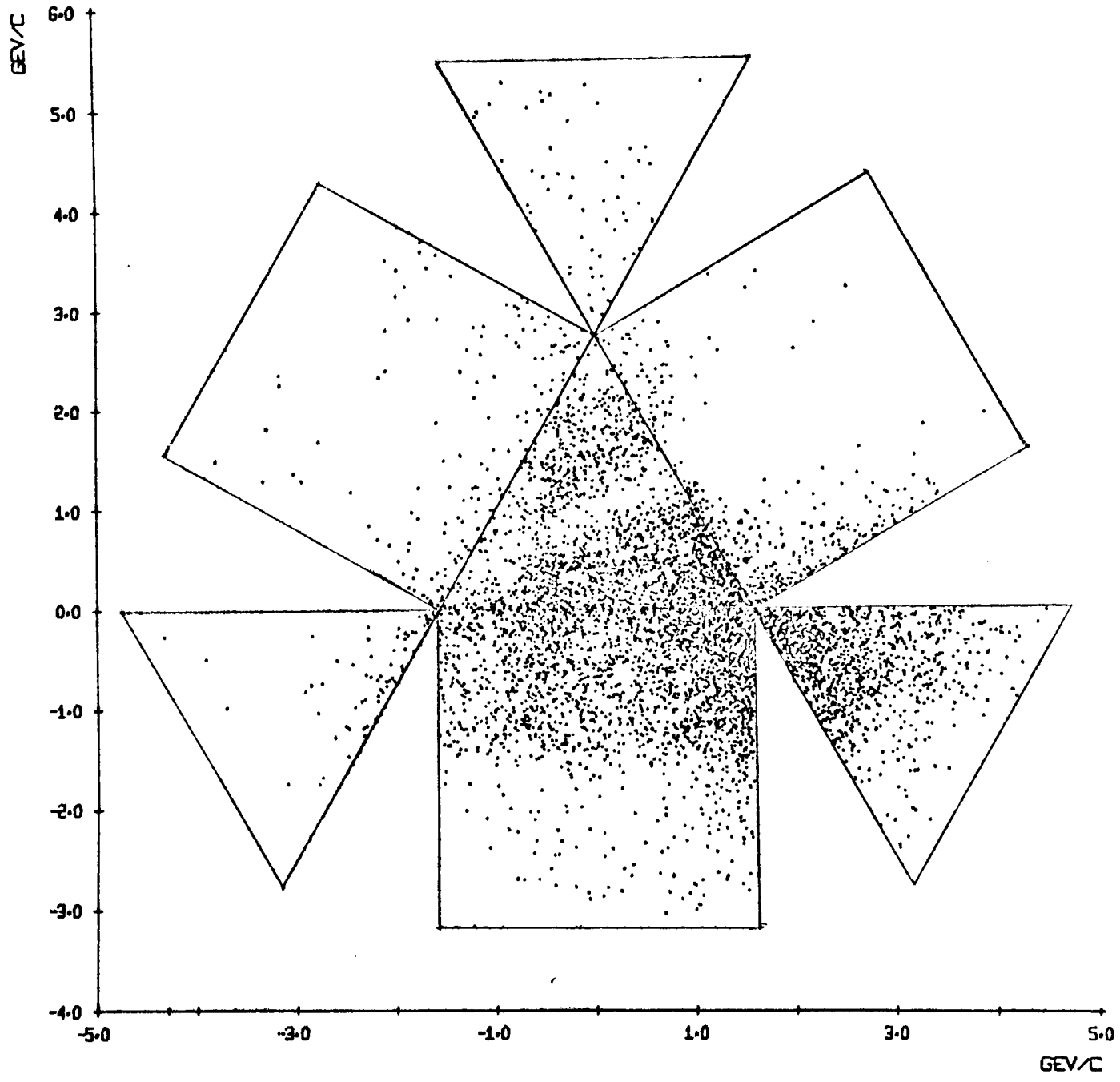

K+ PI+ PI- P FINAL STATE
VAN HOVE 4-BODY PLOT

Fig. 1.6

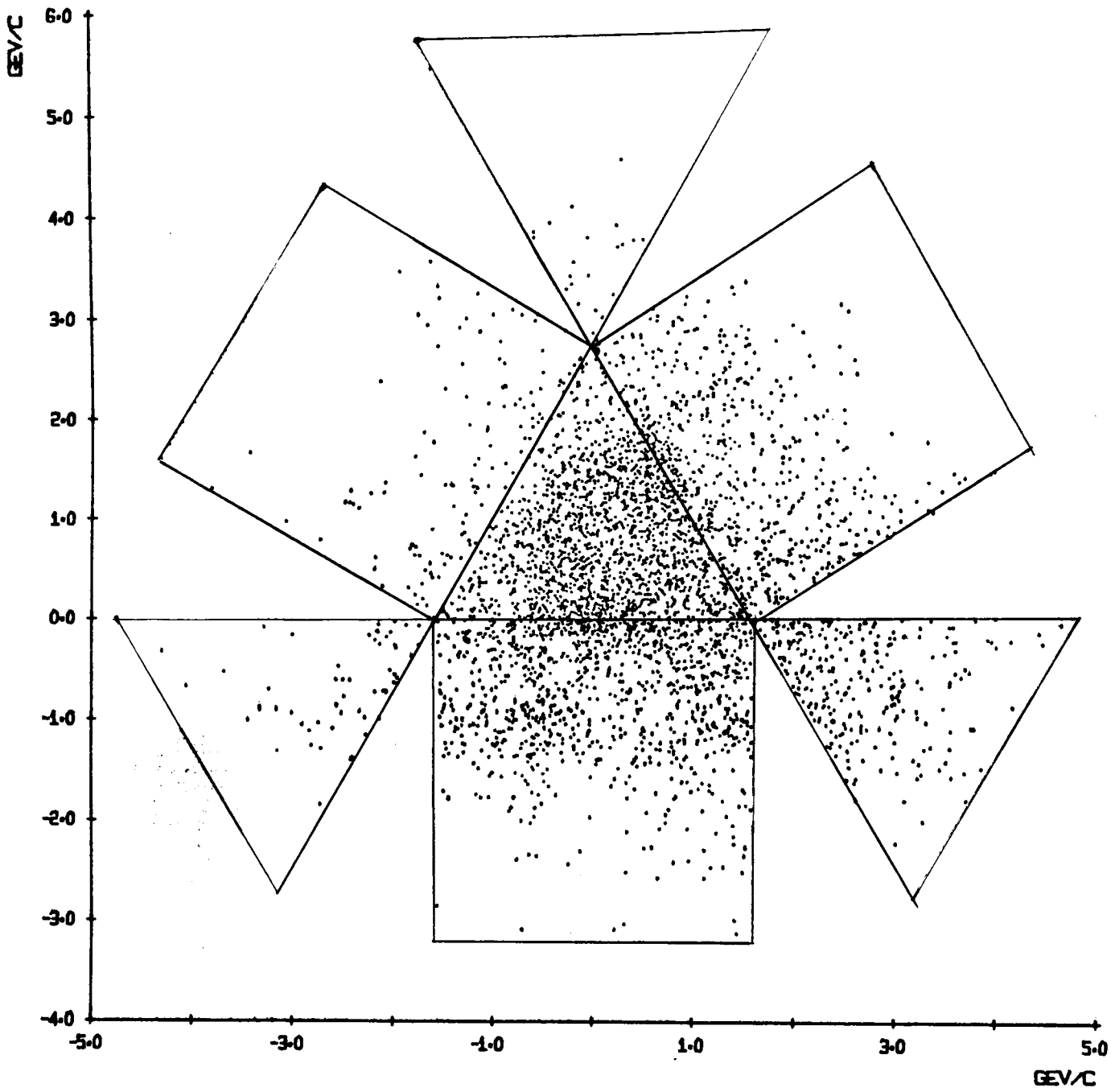

KO PIO PI+ P FINAL STATE
VAN HOVE 4-BODY PLOT

Fig. 1.7

from reaction (2) falling on Face 4 correspond to $K^{*+} - \Delta^{+}$ production. Isospin factors for this process assuming a one-pion-exchange model, severely cut down production of these events compared with those on Face 3. There is negligible contribution to this face from reaction (1) where the $K^{+}\pi^{+}$ system at the meson vertex corresponds to an exotic state.

On Face 1 of Fig. 1.6 there is a depletion of events which runs along the bisector of the K^{+} and π^{+} axes. The events plotted correspond to the unique fits to the $K^{+}\pi^{+}\pi^{-}p$ final state. The higher probability kinematic fit for those events from this final state with a two-fold ambiguity are plotted in Fig. 1.8. These events lie almost entirely in this depleted region. The Van Hove plot clearly demonstrates the origin of these ambiguities. This region corresponds to events with the K^{+}, π^{+} and π^{-} travelling forwards and the proton strongly backwards in the centre of mass with the K^{+} and π^{+} having similar forward momenta. There is a further tendency for the events to crowd near the end corresponding to small π^{-} momentum. In the laboratory these events have the K^{+} and π^{+} travelling with a similar large forward momentum. There is insufficient resolution for the kinematics program to distinguish a kaon from a pion in these cases, and the two ambiguities correspond to an exchange in the identification of the two particles. This is an inherent problem at 10 GeV/c and the plot clearly demonstrates why the remeasurement of a sample of these ambiguous events had little beneficial effect. In the studies of later chapters only the unique events have been used except in Chapter 3 where the low mass

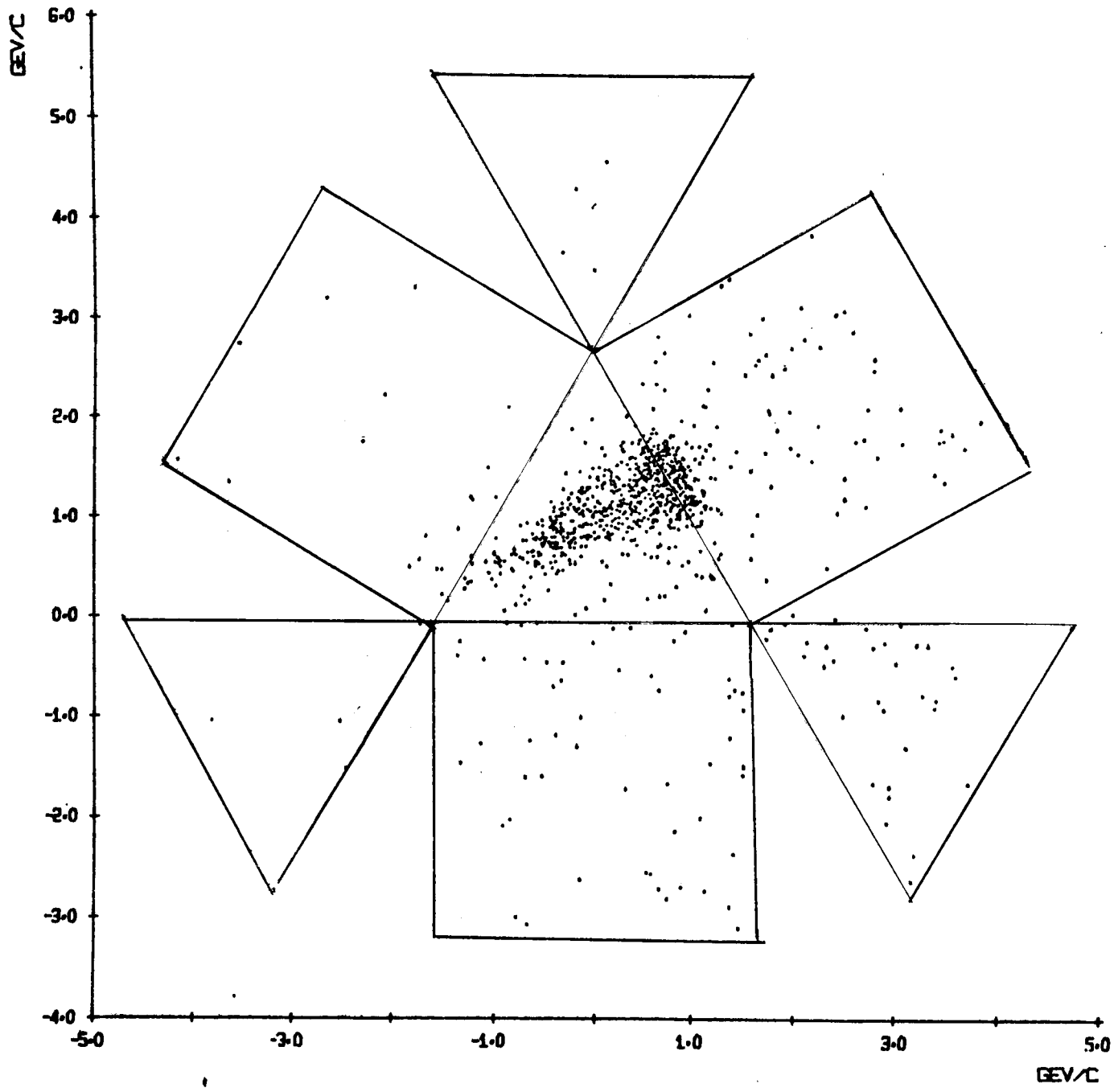

AMBIGUOUS EVENTS
(HIGHER PROB. FIT)

K+ PI+ PI- P FINAL STATE

Fig. 1.8

$K\pi\pi$ system is analysed. The treatment of the ambiguous events will be discussed further there.

The cuboctahedron plots have been useful for obtaining an overall impression of the characteristics of these two 4-body channels. Their use on a more quantitative basis is however, severely limited by the complex phase space dependence across the surface.

REFERENCES

[1] R.J. Hemingway — D.Phil. Thesis, Oxford 1967 (unpublished).

[2] D.J. Sumner — D.Phil. Thesis, Oxford 1967 (unpublished).

[3] GEOMETRY — A.R. Norton - Oxford Geometry Manual 1968.

KINEMATICS — A.G. Wilson 'A kinematic fitting program for bubble chamber events' NIRL/M/38 - 1962.

SOLOMON — W.W.M. Allison: A program to execute decision logic on post kinematics library tapes OUNPL Programming note 1968.

SHEBA — W.W.M. Allison: A program to deal with ionization information. OUNPL Programming note 1968.

WASP — A.R. Norton - Oxford track analysis statistics program OUNPL Programming note 1968.

[4] R.J. Hemingway and D.H. Stork — Optical constants for bubble chambers OUNPL Internal report 1966.

[5] R.J. Cashmore — Private communication

[6] P. Watkins — Private communication

[7] L. Van Hove — Nucl. Phys. B9, 331 (1969)

[8] See J. Bartsch et al. — CERN/D.Ph. II/Phys 70-6 for further details.

[9] R. Horgan — Three- and Four-Body Van Hove Plots OUNPL Programming note 1970.

C H A P T E R 2

THE $K\pi$ INTERACTION

1 Introduction

This chapter will be devoted primarily to a study of the $K\pi$ interaction. At the present time K-π colliding beams are not technically feasable so indirect methods have to be found to study these processes. The most common approach is to select a class of events which is believed to be dominated by One-Pion-Exchange (OPE) and to assume that the properties of this virtual pion are close to, or extrapolate smoothly to those of a pion on its mass shell. For K^+p collisions, those events represented by the Feynman graph of Fig. 2.1, where e is believed to be a pion, are the most appropriate. They lie on Face 3 of the Van Hove cuboctahedron discussed in Chapter 1.

A study of $K\pi$ systems leads to an understanding of the strangeness S = 1 meson states in the natural spin-parity series ($J^P = 0^+, 1^-, 2^+ \ldots$) with isospin $I = 1/2$ and $I = 3/2$ both possible. The $I = 1/2$, $K^*(890)$ with $J^P = 1^-$ and $K^*(1420)$ with $J^P = 2^+$ are well established. The possible existence of a scalar ($J^P = 0^+$) resonance is in question. The Veneziano Model would expect it to have a mass of 0.89 GeV/c^2 as a daughter [1] of the $K^*(890)$, whereas the Quark Model would prefer a mass* nearer 1.1 GeV/c^2. Both models

---

* This point is discussed further in Chapter 3, Section 1.

FEYNMAN GRAPH

for one-pion-exchange

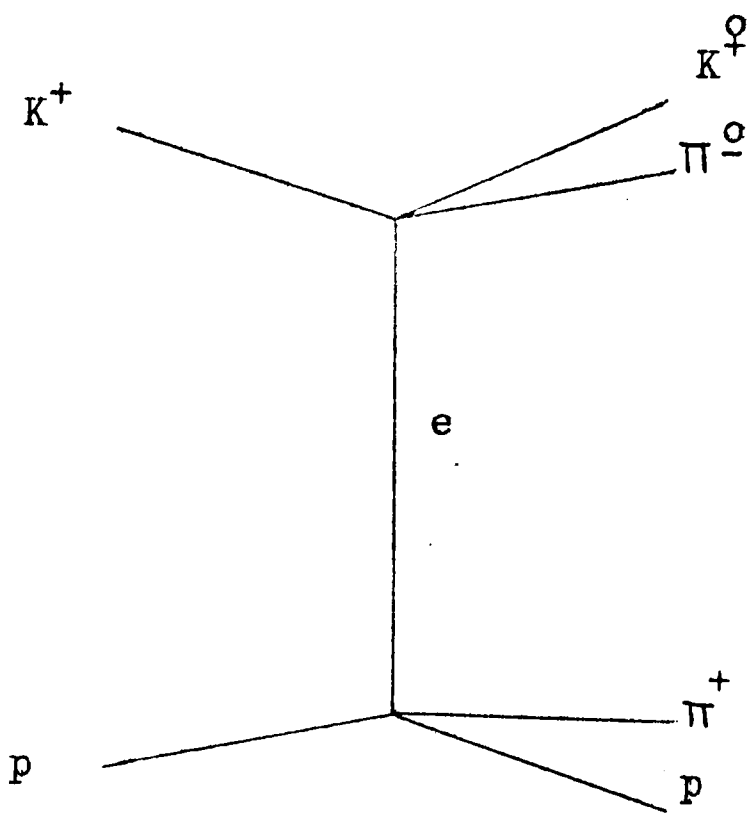

Fig.2.1

predict no resonant I = 3/2 Kπ interaction. Lovelace [2], using a unitarised form of the Veneziano Model has made quantitative predictions of the I = 3/2 interaction. A comparison of his predictions with experiment would be very useful.

Trippe et al. [3] have suggested the possible existence of a wide 0^+ Kπ resonance centred near 1.1 GeV/c^2. They studied a similar class of events to those represented in Fig. 2.1 at an incident K^+ momentum of 7.3 GeV/c. Their suggestion was motivated by the observation of a high background of events in $K^+\pi^-$ mass occurring between the $K^*(890)$ and $K^*(1420)$ peaks which was not present above this region. The same effect is seen in the reaction $K^+p \rightarrow K^+\pi^+\pi^-p$ in this experiment (Fig. 2.2). The events shown correspond to the selection of the Δ^{++}(1.12 to 1.4 GeV/c^2) produced with a momentum transfer of $\Delta^2 < 0.5$ (GeV/c)^2. The Trippe analysis had a relatively small number of $K^o\pi^o\pi^+p$ events making any determination of the relative I = 3/2 contribution almost impossible.

Attempts have been made to determine the I = 3/2 Kπ interaction [4] by studying events where a $K^-\pi^-$ or $K^+\pi^+$ pair occur at the meson vertex of Fig. 2.1 but the analyses have been hampered by large backgrounds from more dominant channels.

The study of Kπ cross-sections and scattering angular distributions as a function of Δ^2 needs very high statistics. Analyses along these lines are being carried out by various groups [5] using the data on a K^+p World Data Summary Tape where these high statistics are available. This requires

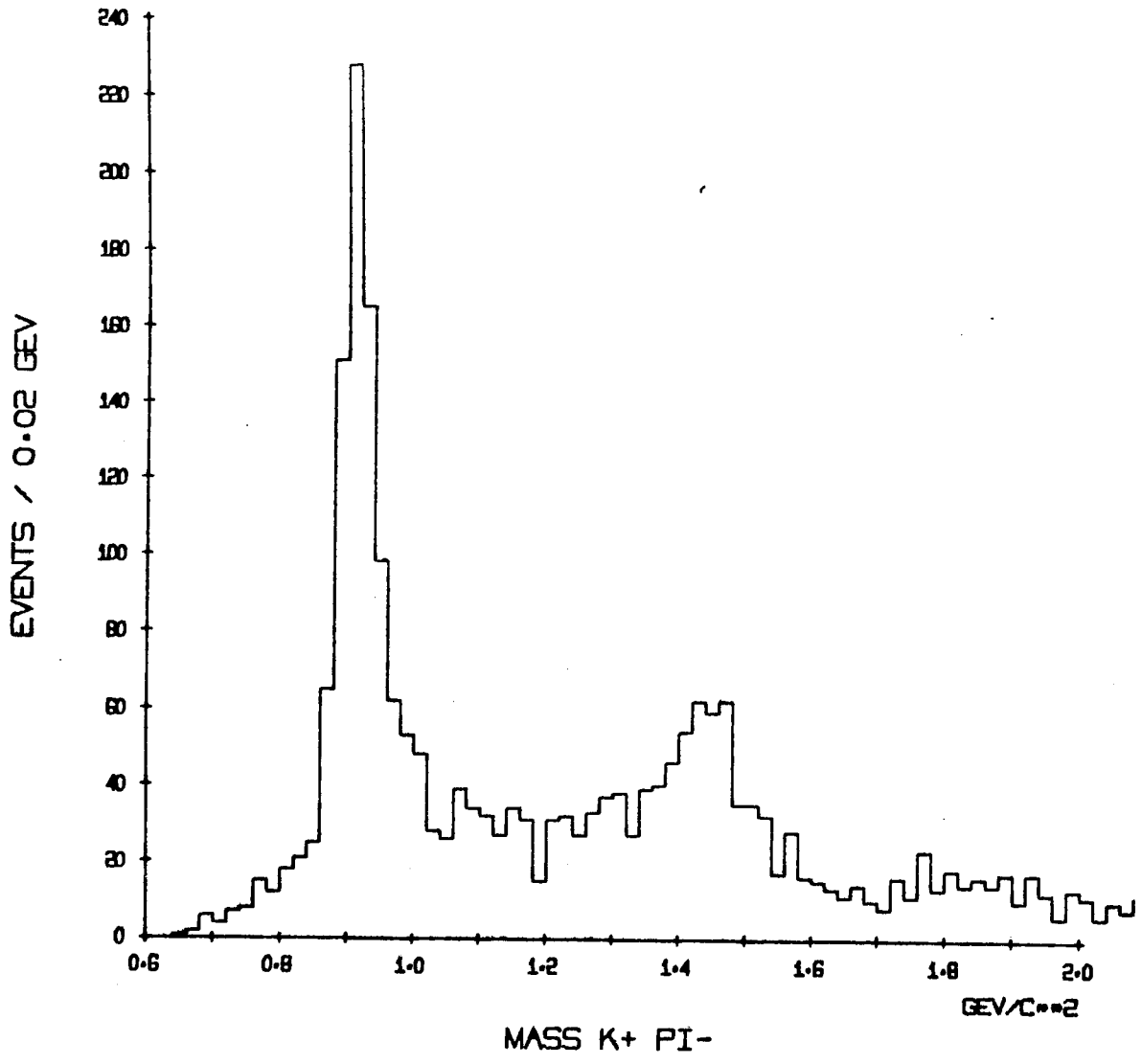
EVENTS / 0.02 GEV
240
220
200
180
160
140
120
100
80
60
40
20
0
0.6
0.8
1.0
1.2
1.4
1.6
1.8
2.0
GEV/C**2
MASS K+ PI-

Fig. 2.2

combining events with a range of K^+ beam momenta from 3.0 to 12.7 GeV/c. Backgrounds from other processes, which will vary from momentum to momentum, will be poorly determined and their effects uncertain. The analysis carried out here is on data from 10 GeV/c only.

2 The Baryon Vertex

A measure of the validity of some of the assumptions required to apply the OPE model to the Kπ vertex can be made by testing the model on the π^+p vertex where the on-mass-shell properties are known. The scattering angular distribution $W(\Theta, \Phi)$ of the proton in the π^+p centre of mass is expanded in the form

$$W(\Theta, \Phi) = \sum_{L\,M} W_L^M \; Y_L^{M\,*}(\Theta, \Phi)$$

where the angles are with respect to a Z-axis taken as the direction of the incoming proton and a Y-axis as the normal to the production plane. The variation of the moments W_1^0, W_2^0, W_3^0 and W_4^0 with $p\pi^+$ mass are shown in Fig. 2.3, for the final states $K^+\pi^+\pi^-p$ and $K^0\pi^0\pi^+p$, for those events with $\Delta^2 < 0.5$. All moments are normalised to $W_0^0 = 1$. The dashed lines correspond to the on-mass-shell dependence of the π^+p moments. The two final states are in extremely good agreement with each other, demonstrating that the π^+p interaction is not dependent on the process occurring at the other vertex. They both follow the on-mass-shell dependence quite closely throughout most of the region. The

+ from $K^+\pi^+\pi^-p$

× from $K^o\pi^+\pi^op$

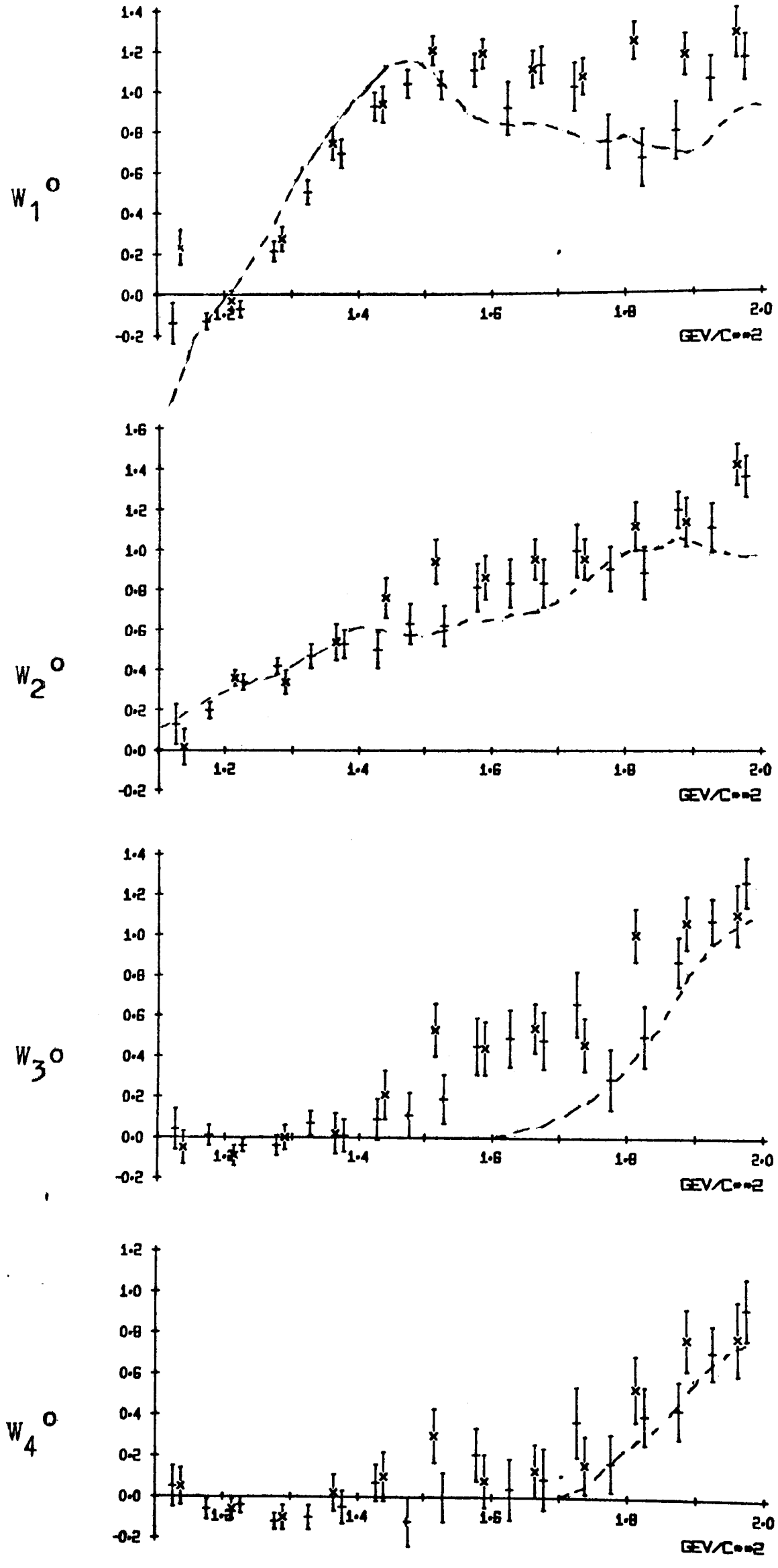

MOMENTS FOR PPI+ SCATTERING

Fig. 2.3

notable exceptions are that the data appear too high in W_1^0 and W_3^0 for $p\pi^+$ masses $\gtrsim$ 1.6 GeV/c^2 and they do not follow the curve for W_1^0 to large negative values below 1.2 GeV/c^2. This latter effect has been noticed in other experiments [6]. Schlein has suggested [7] that this may be due to the use of $\cos\Theta$ rather than t_p (the momentum transfer from proton to proton). For off-shell quasi-elastic scattering they are related by

$$\cos\Theta = \frac{t_p - 2m_p^2 + 2E_{in}\,E_{out}}{2\,|p_{in}|\,.\,|p_{out}|} \qquad (1)$$

whereas for on-mass-shell scattering the relation is $\cos\Theta = 1 + t_p/2p^2$ where p is the three momentum in the 2 particle centre of mass. The physical limits of $\cos\Theta = \pm 1$ cover different ranges of the variable t_p for the two processes, the differences becoming the most significant at values of large Δ^2 and small $p\pi^+$ mass. This may explain the discrepancy in W_1^0 at low mass, although the other moments do not appear to be affected. It should be emphasized that there is apparently no unique way to relate the on- and off-shell scattering angles. The invariance, for example, of the Mandelstam variable u_p would lead to a different result. An adequate theory is lacking.

The shapes of the π^+p on- and off-shell cross-sections are compared in Fig. 2.4. The data (histogrammed) follows the trends of the on-shell scattering in that it dips around 1.55 GeV/c^2 and rises to a second peak near 1.9 GeV/c^2.

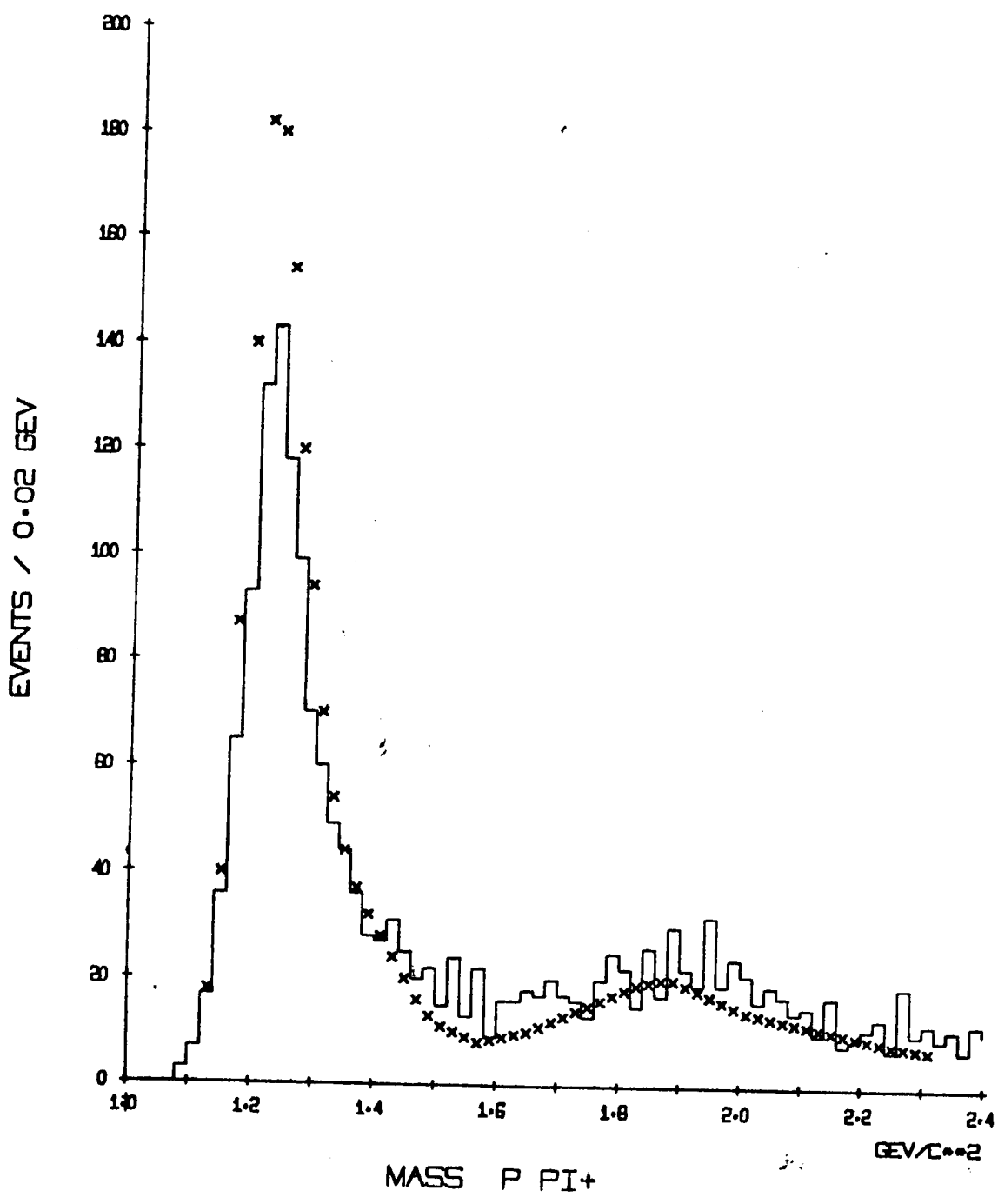

On-and off-shell cross-sections

Fig. 2.4

The height of the on-shell $\Delta^{++}(1236)$ peak relative to the second peak is considerably higher than that observed in the data, but at low $p\pi^+$ masses off-shell corrections are expected to be large (see Section 3).

For π^+p scattering the Treiman-Yang angle (Φ) should be isotropically distributed. Figure 2.5 shows the variations of W_1^1, W_2^1, W_3^1 and W_4^1 with mass, for the $K^+\pi^+\pi^-p$ final state. A strong Φ dependence appears above 1.4 GeV/c^2. This effect, together with the large W_1^0 and W_3^0 mentioned earlier, is related to the presence of the Q enhancement at low $K\pi\pi$ masses (see Chapter 3) and illustrates the fact that to reproduce the $K\pi\pi$ mass spectrum the π^+ needs to be more forward peaked than a simple Deck model for Q production would predict. A model in which the pion is 'Reggeised', can reproduce these trends [8].

3 The Dürr-Pilkuhn modified OPE Model

The simplicity of the OPE graph and the successful comparison below 1.4 GeV/c^2 of the on- and off-shell π^+p moments of Section 2 suggests the possibility of carrying out a fit to the three variables: $m(K^+\pi^-)$, $t(=-\Delta^2)$, and $M(p\pi^+)$ with such a model, for a range of $K^+\pi^-$ mass. The events to be fitted satisfy the following criteria: (a) $M(p\pi^+)$ in the range 1.12 to 1.4 GeV/c^2; (b) Δ^2, the momentum transfer to the π^+p system < 0.5 (GeV/c)^2 and (c) $m(K^+\pi^-) < 1.7$ GeV/c^2. These, we will assume, may be represented to a good approximation by the Feynman graph of Fig. 2.1 with the π^+p

The height of the on-shell $\Delta^{++}(1236)$ peak relative to the second peak is considerably higher than that observed in the data, but at low $p\pi^+$ masses off-shell corrections are expected to be large (see Section 3).

For π^+p scattering the Treiman-Yang angle (Φ) should be isotropically distributed. Figure 2.5 shows the variations of W_1^1, W_2^1, W_3^1 and W_4^1 with mass, for the $K^+\pi^+\pi^-p$ final state. A strong Φ dependence appears above 1.4 GeV/c^2. This effect, together with the large W_1^0 and W_3^0 mentioned earlier, is related to the presence of the Q enhancement at low $K\pi\pi$ masses (see Chapter 3) and illustrates the fact that to reproduce the $K\pi\pi$ mass spectrum the π^+ needs to be more forward peaked than a simple Deck model for Q production would predict. A model in which the pion is 'Reggeised', can reproduce these trends [8].

3 The Dürr-Pilkuhn modified OPE Model

The simplicity of the OPE graph and the successful comparison below 1.4 GeV/c^2 of the on- and off-shell π^+p moments of Section 2 suggests the possibility of carrying out a fit to the three variables: $m(K^+\pi^-)$, $t(=-\Delta^2)$, and $M(p\pi^+)$ with such a model, for a range of $K^+\pi^-$ mass. The events to be fitted satisfy the following criteria: (a) $M(p\pi^+)$ in the range 1.12 to 1.4 GeV/c^2; (b) Δ^2, the momentum transfer to the π^+p system < 0.5 (GeV/c)^2 and (c) $m(K^+\pi^-) < 1.7$ GeV/c^2. These, we will assume, may be represented to a good approximation by the Feynman graph of Fig. 2.1 with the π^+p

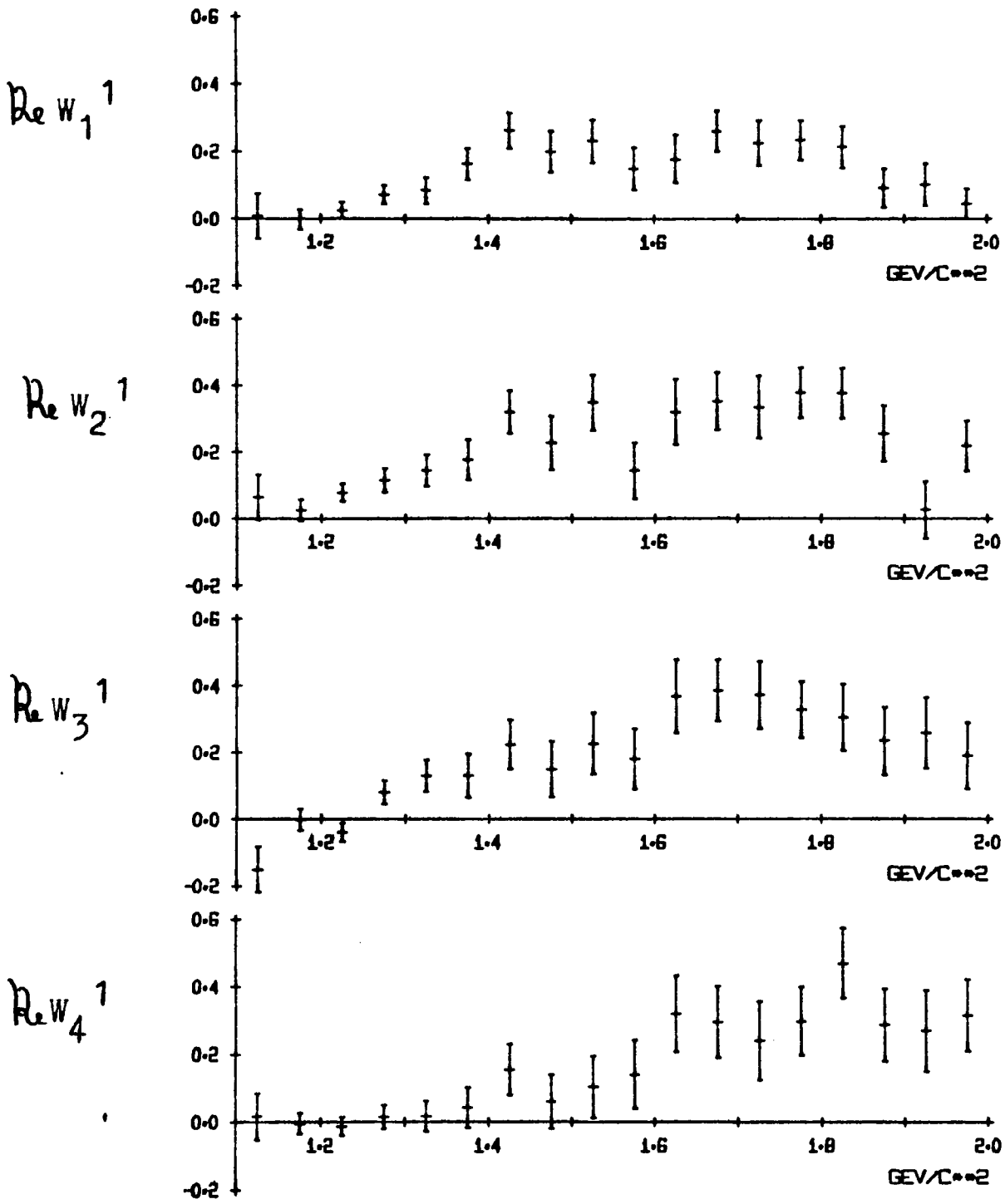

MOMENTS FOR P PI+ SCATTERING
FROM K+ PI+ PI- P FINAL STATE

Fig. 2.5

interaction dominated by the $P_{33}(1236)$ resonance.

The cross-section for such a reaction may be written as

$$\sigma = \frac{1}{4} \quad \frac{1}{(2\pi)8} \quad \frac{1}{(\bar{Q}W)} \int |M|^2 \; dR_4 \qquad (2)$$

where

$\bar{Q}$ = centre of mass incident K^+ momentum

W = centre of mass total energy

R_4 = 4-body Lorentz invariant phase space.

M is the transition amplitude, which for this process we approximate by

$$|M|^2 = |A\,(M(\pi^+ p), t)|^2 \; \frac{1}{(t-\mu^2)^2} \; |A(m(K^+\pi^-), t)|^2 \qquad (3)$$

The A's are transition amplitudes for the quasi elastic scattering processes at the baryon and meson vertices and μ is the pion rest mass. This form neglects any possible interference or final state interactions that may occur between particles from different vertices. We outline below the theory of writing expression (2) in a more suitable form for carrying out an analysis of these data.

Using the recursion relation of Hagedorn [9], R_4 may be expanded into products of 2-body phase space to give

$$dR_4(W, m_{K^+}, m_{\pi^-}, M_{\pi^+}, M_p) = dm^2 \; R_2(m, m_{K^+}, m_{\pi^-}) \; dM^2 \; R_2(M, M_p, M_{\pi^+})$$

$$\times \; R_2(W, m, M) \qquad (4)$$

Here m stands for $m(K^+\pi^-)$ and M for $M(p\pi^+)$.

The cross-section for the 2-body scattering process at the meson vertex is given by

$$\sigma(m) = \frac{1}{16\pi^2} \frac{1}{mq(t)} \int |A(m,t)|^2 dR_2 (m, m_{K^+}, m_{\pi^-}) \qquad (5)$$

where q(t) is the π^- off-shell incident momentum in the $K\pi$ centre of mass. An essentially identical relation to (5) holds for $\sigma(M)$, the total cross section at the baryon vertex. Substituting $\sigma(m)$ and $\sigma(M)$ into (2) only the factor $R_2(W,m,M)$ remains to be evaluated. This may be written as

$$R_2 = \frac{2\pi \bar{Q}_{out}}{4W} \int d(\cos\theta) \qquad (6)$$

where $\bar{Q}_{out}$ is the momentum of the π^+p system in the overall centre of mass and the scattering angle $\cos\theta$ is given by

$$t = m^2 + M^2 - 2 E_{K^*} E_{\Delta^{++}} - 2 \bar{Q} \cdot \bar{Q}_{out} \cos\theta.$$

Using the above relation (6) may be rewritten as

$$R_2(W,m,M) = \frac{2\pi}{8W\bar{Q}} \int dt \qquad (7)$$

Substituting (7) into (2) we get finally

$$\frac{d\sigma}{dm\, dM\, dt} = \frac{1}{4\pi^3} \frac{1}{(\bar{Q}W)^2} m^2 q(t) \sigma(m) \frac{1}{(t-\mu^2)^2} M^2 Q(t) \sigma(M) \qquad (8)$$

The pole approximation consists of replacing the off-shell $q\sigma(m)$ and $Q\sigma(M)$ terms by the on-shell forms. This approximation produces very poor results for one pion exchange particularly when compared with the experimental t distributions. The inclusion of form factors for extended particles is the natural modification. Considerable success has been obtained with the Dürr Pilkuhn method [10] particularly in πp processes [11]. The approach is to modify each on-shell angular momentum amplitude A_ℓ by simple penetration factors derived from potential theory. These factors are dependent on the incident pion momentum and hence on t. The ones of relevance here are listed in Table 2.1. The unknown quantities R_ℓ are essentially a measure of the effective range of the potential. Following Trippe the term $q(t)\sigma(m)$ in (8) is replaced by

$$q(\mu^2)\left\{4\pi\lambda^2\left[\frac{4}{9}\,3|A_1|^2\,DP_{(1)}{}^2+\frac{4}{9}\,5|A_2|^2\,DP_{(2)}{}^2\right]+\sigma_s\right\} \tag{9}$$

$$\text{where}\quad A_\ell=\frac{\Gamma/2}{(m_r-m)-i\Gamma/2}\quad\text{with}\quad \Gamma=\Gamma_r\left(\frac{q}{q_r}\right)^{2\ell+1}\frac{m_r}{m} \tag{10}$$

and the $DP_{(\ell)}$ are the Dürr-Pilkuhn factors defined in Table 2.1.

We take, for $\ell=1$, $E_r=0.89$ and $\Gamma_r=0.05$

and for $\ell=2$, $E_r=1.42$ and $\Gamma_r=0.09$.

For $\ell=2$ an additional inelasticity factor of $(0.5)^2$ is used.

Table 2.1

Dürr Pilkuhn off-shell factors

Term	Expression
DP(1)	$\dfrac{q(t)}{q(\mu^2)} \left[\dfrac{(1+R_1{}^2 q^2(\mu^2))}{(1+R_1{}^2 q^2(t))}\right]^{\frac{1}{2}}$
DP(2)	$\left(\dfrac{q(t)}{q(\mu^2)}\right)^2 \left[\dfrac{(9+3R_2{}^2 q^2(\mu^2)+R_2{}^4 q^4(\mu^2))}{(9+3R_2{}^2 q^2(t)+R_2{}^4 q^4(t))}\right]^{\frac{1}{2}}$
DP(Δ)	$\dfrac{Q(t)}{Q(\mu^2)} \left[\dfrac{((M+M_p)^2-t)}{((M+M_p{}^2)-\mu^2)} \cdot \dfrac{(1+R_\Delta{}^2 Q^2(\mu^2))}{(1+R_\Delta{}^2 Q^2(t))}\right]^{\frac{1}{2}}$

where $q(t) = \left\{((m-m_K)^2-t)((m+m_K)^2-t)\right\}^{\frac{1}{2}}/2m$

and $Q(t) = \left\{((M-M_p)^2-t)((M+M_p)^2-t)\right\}^{\frac{1}{2}}/2M$

The factor $\frac{4}{9}$ is the Clebsch Gordan term for $K^+\pi^- \rightarrow K^+\pi^-$ in an $I = 1/2$ state. The σ_s, the remaining $K^+\pi^-$ cross-section is assumed to be s-wave and has no extrapolation term in the Dürr-Pilkuhn model. The term $[Q(t)\sigma(M)]_{off\ shell}$ is replaced by $Q(\mu^2)\ DP^2(\Delta)\sigma(M)_{on\text{-}shell}$ where $\sigma(M)_{on\text{-}shell}$ is taken from the summary by Focacci and Giacomelli [12]. Following Wolf [13] an additional form factor $f(t) = \left[\frac{(c-\mu^2)}{(c-t)}\right]^2$ is included in the overall intensity. The overall formula reduces to the pole equation as $t \rightarrow \mu^2$.

Using this model a maximum likelihood fit was carried out on the variables (m,M,t) with c, R_1, R_2, R_Δ and six values of σ_s at 200 MeV/c^2 intervals from 0.7 to 1.7 GeV/c^2 as free parameters. For values of σ_s between these regions, linear interpolation was used. 2078 events were used in the fits. The values of the parameters c, R_1, R_2 and R_Δ resulting from the fits are given in Table 2.2 and of σ_s in Fig. 2.6. Also shown in this figure are the values of σ_s obtained from similar fits by Trippe et al. [14]. Both show a significant contribution of σ_s below 1.3 GeV/c^2 with a rapid fall off above this region. The values from the 7.3 GeV/$_c$ data are higher than those from 10 GeV/c though apart from the 1.1 GeV/c^2 point they are not inconsistent. The curve $\frac{4}{9}\ 4\pi\lambda^2$ is the unitarity limit for an $I = 1/2$ s-wave $K\pi$ resonance. The fits at 10 GeV/c do not indicate the presence of a resonant s-wave interaction in any region below 1.4 GeV/c^2, though possible interference with an s-wave $I = 3/2$ $K\pi$ state has been neglected. Recently Lovelace [2] has cast doubt on the validity of the Dürr-Pilkuhn prescription

Table 2.2

Values of parameters obtained from the maximum likelihood fits

Parameter	Value
R_1	3.41 ± 1.3
R_2	3.61 ± 1.8
R_Δ	2.18 ± 0.25
C	2.3 ± 1.2

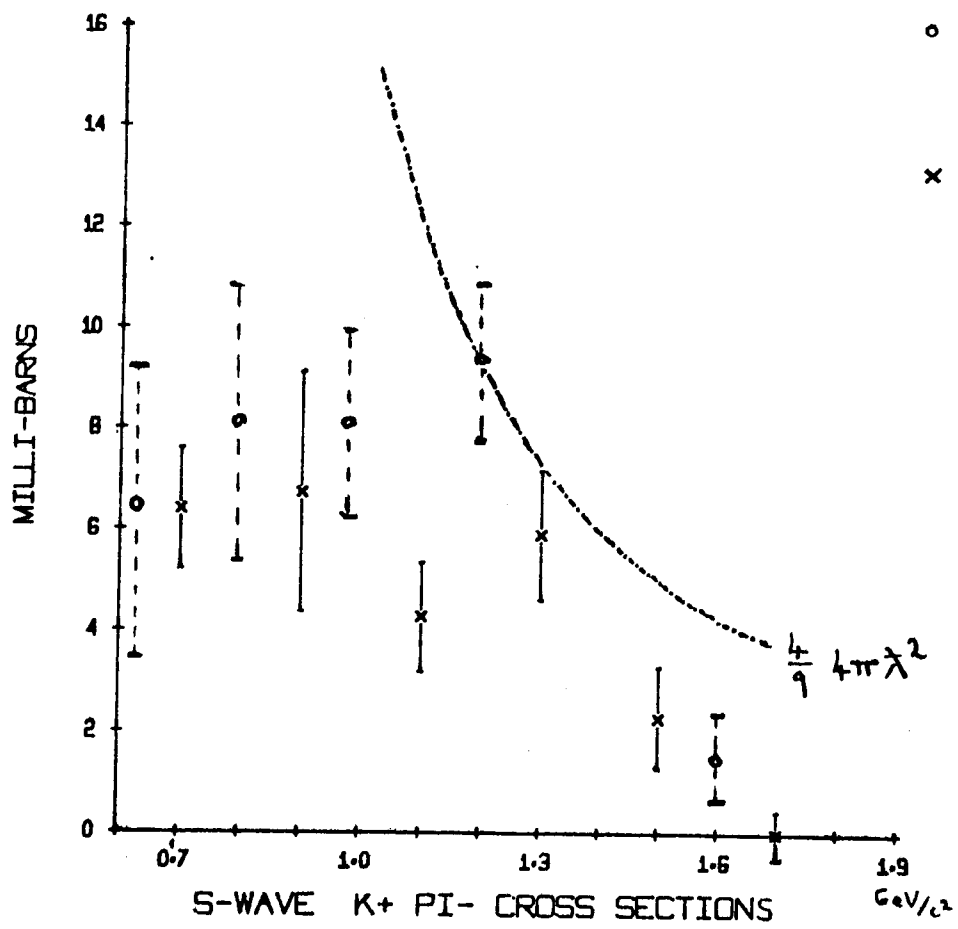
16
14
12
10
8
6
4
2
0
MILLI-BARNS
0·7
1·0
1·3
1·6
1·9
GeV/c²
S-WAVE K+ PI- CROSS SECTIONS
$\frac{4}{9}\,4\pi\lambda^2$
° Trippe
× This experiment

Fig. 2.6

of no off-shell extrapolation term for the s-wave case. The model he proposes is in qualitative agreement with the Dürr-Pilkuhn for p-and d-waves but not for s-waves. Essentially, the dominant $I = 1/2$ s-wave dependence in this region he would attribute to the residue of the daughter of the $K^*(890)$. This has a dependence on t_K, the momentum transfer from K^+_{in} to K^+_{out}, which in turn is dependent on $m^2(K^+\pi^-)$ and t. The situation is further complicated by the presence of any s-wave $I = 3/2$ scattering which would have a different off-shell dependence. It is therefore unclear what off-shell prescription should be used in the s-wave case. The results of Fig. 2.6 can be taken as an indication that there is an appreciable excess of events between the $K^*(890)$ and $K^*(1420)$ over the tails of these resonances, but it must be regarded as a qualitative result only.

With reference to the quality of the maximum likelihood fits, Figs. 2.7 and 2.8 show respectively the $K^+\pi^-$ and $p\pi^+$ mass distributions, and the t distributions for three regions of $K^+\pi^-$ mass. The crosses are the predictions of the fits. These have been multiplied by an additional common normalisation factor of 1.55. It should be noted that the fitting technique uses a likelihood function normalised to unity and is consequently independent of the overall normalisation of the data. That the best fits to the model predict a cross-section that is nearly 40% too low must be regarded as a weakness of the model. A similar factor (of value 1.6) was needed in the earlier work of Trippe at 7.3 GeV/c [14], suggesting it is not an error in the measurement of the

(a)

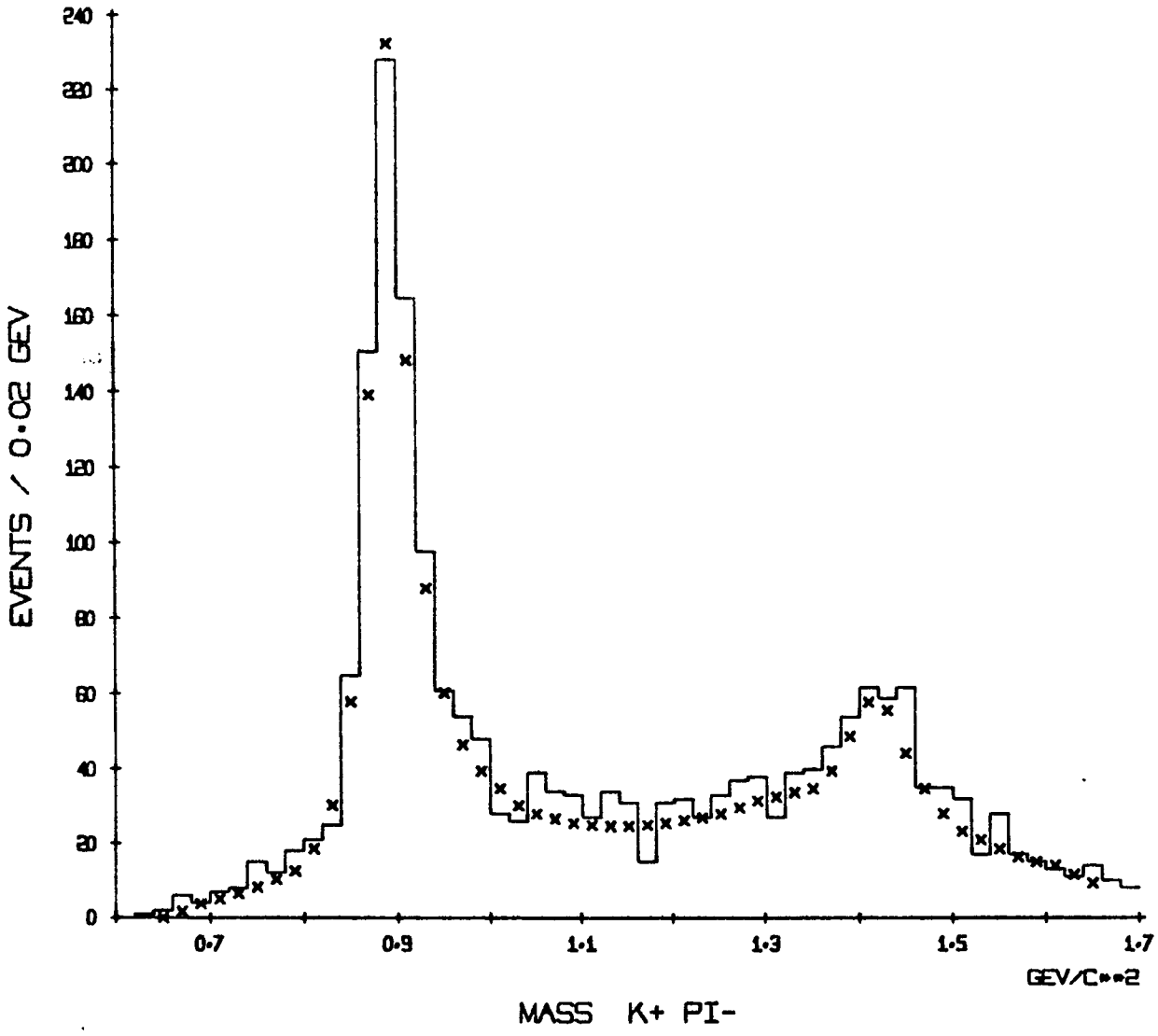
EVENTS / 0.02 GEV
0
20
40
60
80
100
120
140
160
180
200
220
240
0.7
0.9
1.1
1.3
1.5
1.7
GEV/C**2
MASS K+ PI-

(b)

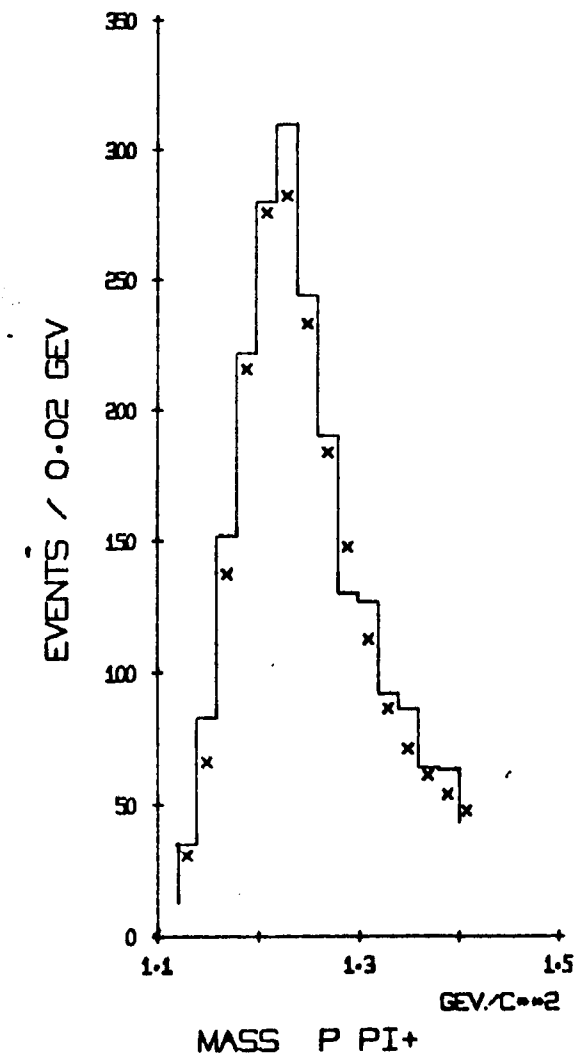
EVENTS / 0.02 GEV
0
50
100
150
200
250
300
350
1.1
1.3
1.5
GEV/C**2
MASS P PI+

Fig. 2.7

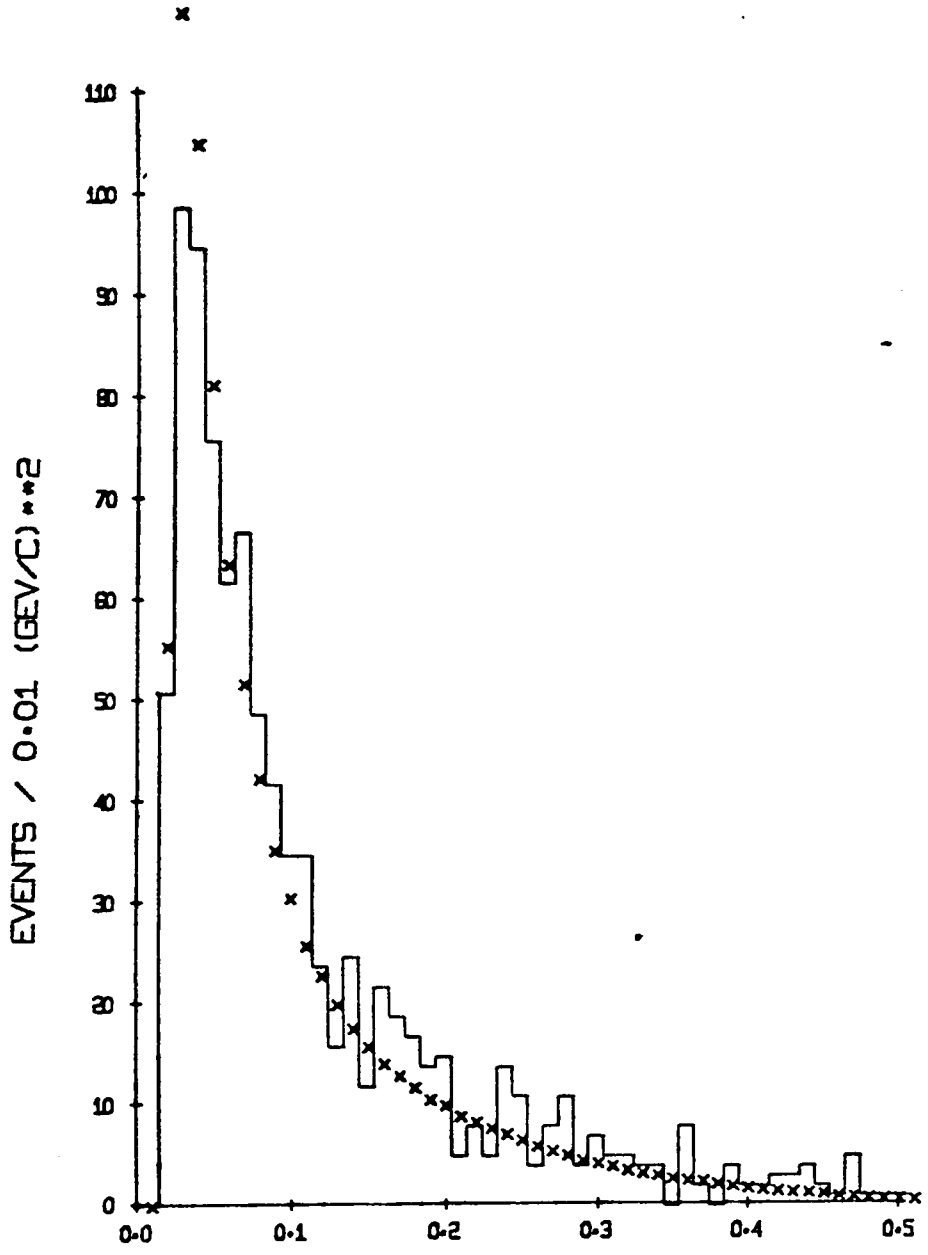

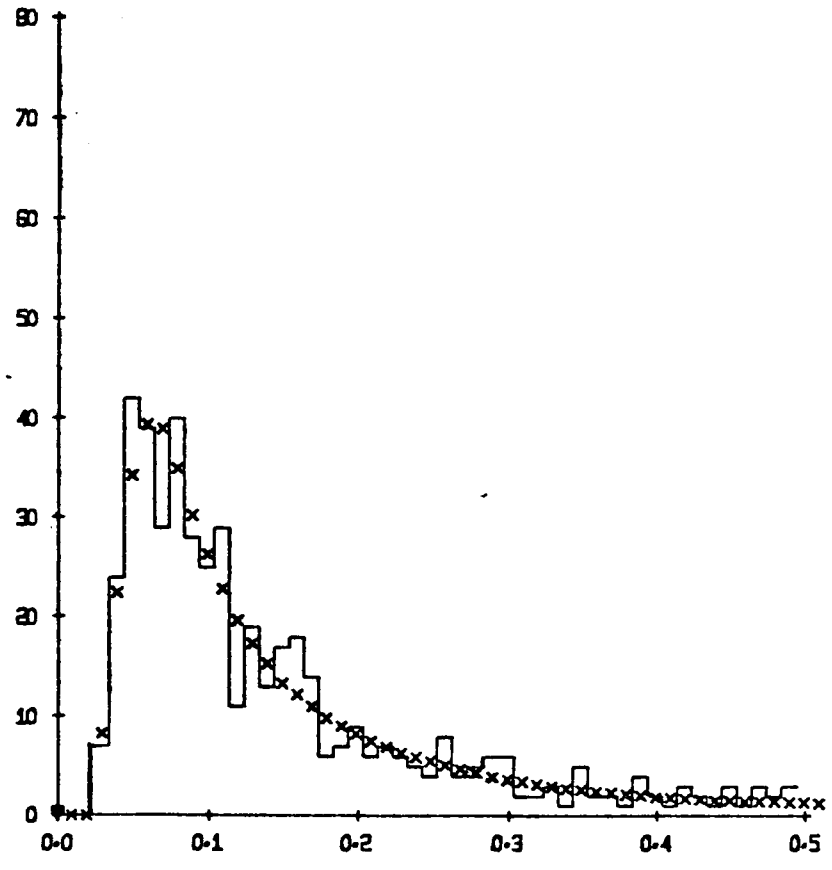

T TO (K+ PI-)

Fig. 2.8

cross-section but a characteristic of the model. However, all the fits in Figs. 2.7 and 2.8 are extremely good indicating the model has the necessary complexity to fit the data.

A similar analysis could not be carried out on the $K^o\pi^o\pi^+p$ final state. These events are one-constraint fits with a high laboratory π^o momentum. The mass resolution of these events is poor. The width of the $K^*(890)$ in the $K^o\pi^o$ mass projection (see Fig. 2.9) is significantly greater than 50 MeV/c^2 making any convenient parametrisation impracticable.

4 Kπ Scattering

In this section the scattering process at the meson vertex of Fig. 2.1 will be studied in detail. In a similar manner to Section 2, the angular distribution $w(\theta,\phi)$ of the outgoing kaon in the Kπ centre of mass is expanded in the form

$$w(\theta,\phi) = \sum_{l\,m} w_l^m \, Y_l^{m\,*}(\theta,\phi) \qquad (11)$$

with the z-axis as the incoming K^+ and the y-axis as the normal to the production plane. The moments w_1^0, w_2^0 and w_3^0, w_4^0 for both elastic ($\pi^-+K^+ \rightarrow \pi^-K^+$) and charge exchange ($\pi^-+K^+ \rightarrow \pi^oK^o$) processes are shown in Figs. 2.10 and 2.11, normalised to $w_0^0 = 1$. The same selections as applied in the fitting of Section 3, are applied here. These moments are independent of the Kπ cross-sections and are not, therefore particularly sensitive to the mass resolutions of the two

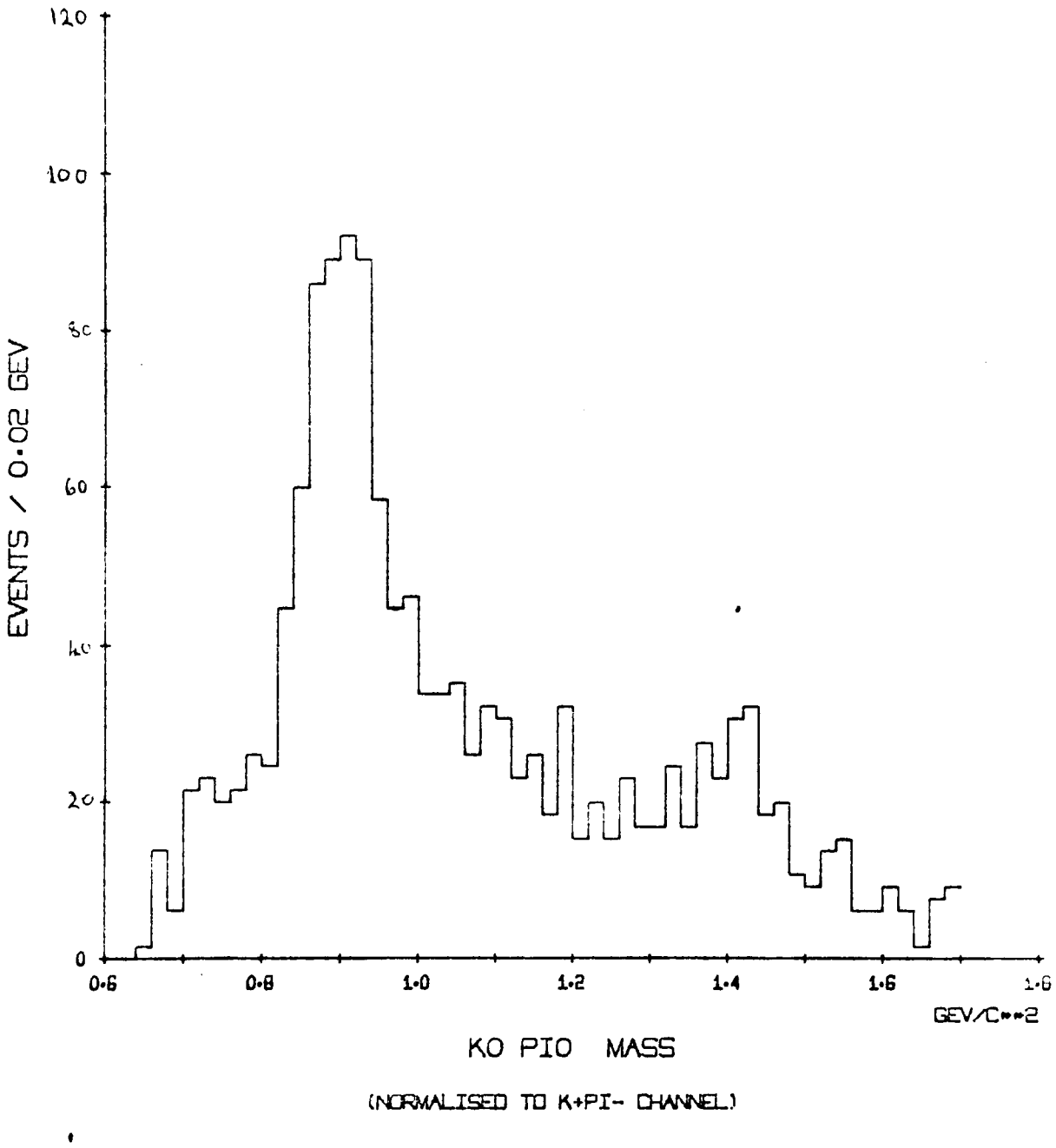
EVENTS / 0.02 GEV
120
100
80
60
40
20
0
0.6
0.8
1.0
1.2
1.4
1.6
1.8
GEV/C**2
KO PIO MASS
(NORMALISED TO K+PI- CHANNEL)

Fig. 2.9

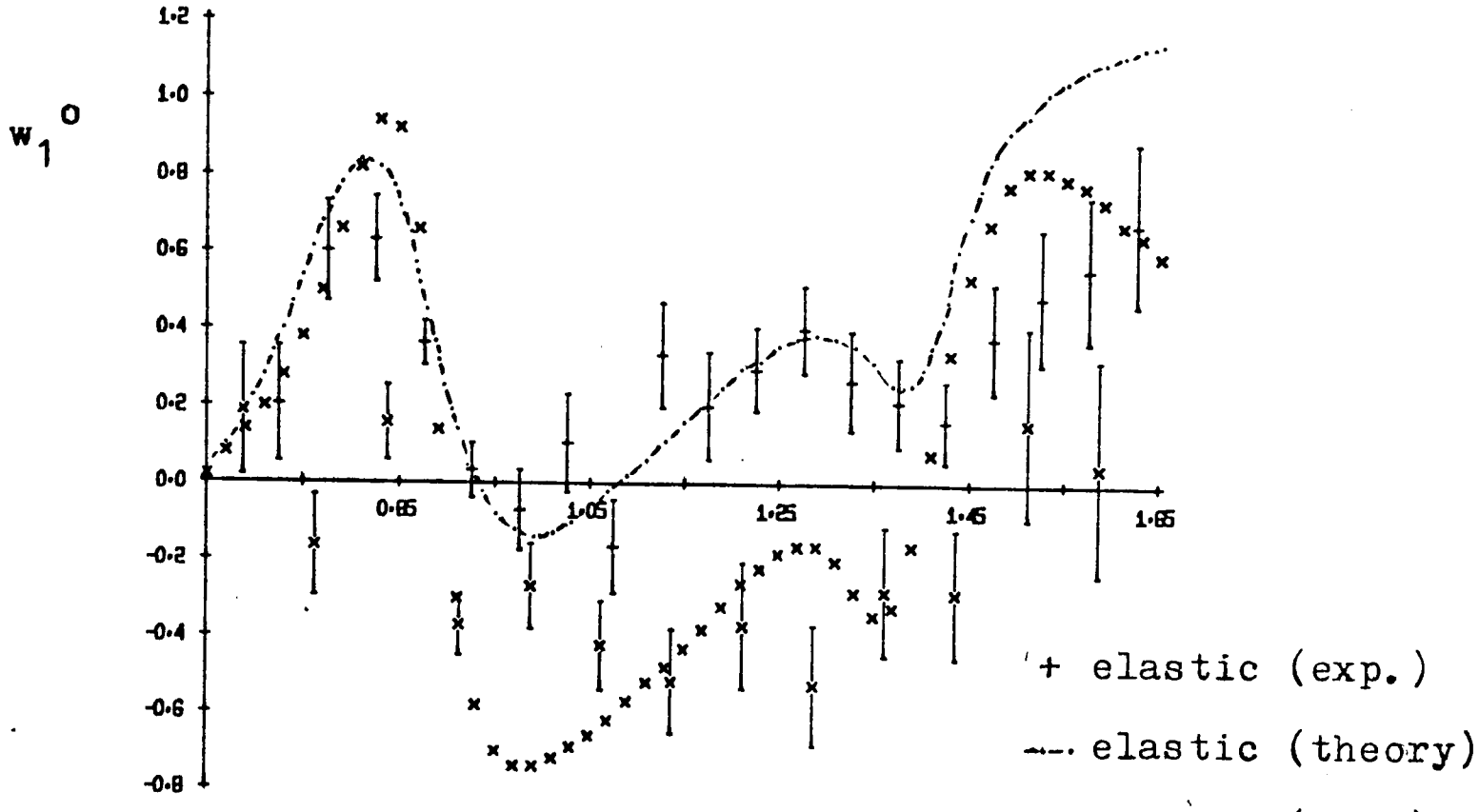

K PI MOMENTS

Fig. 2.10

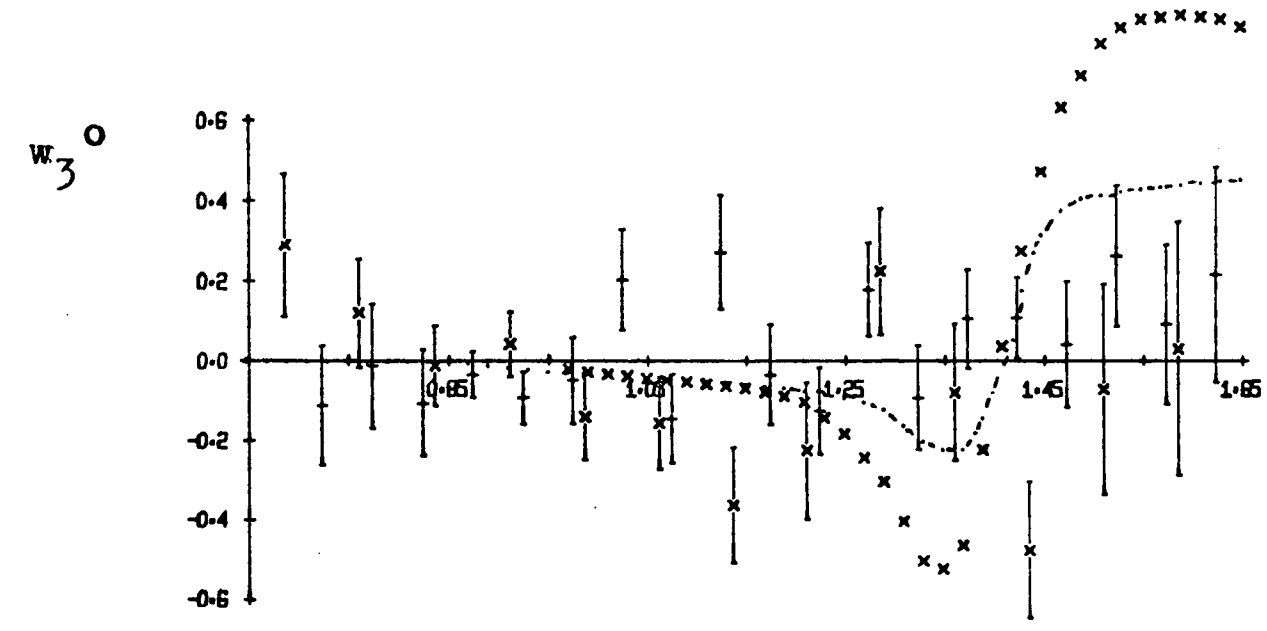

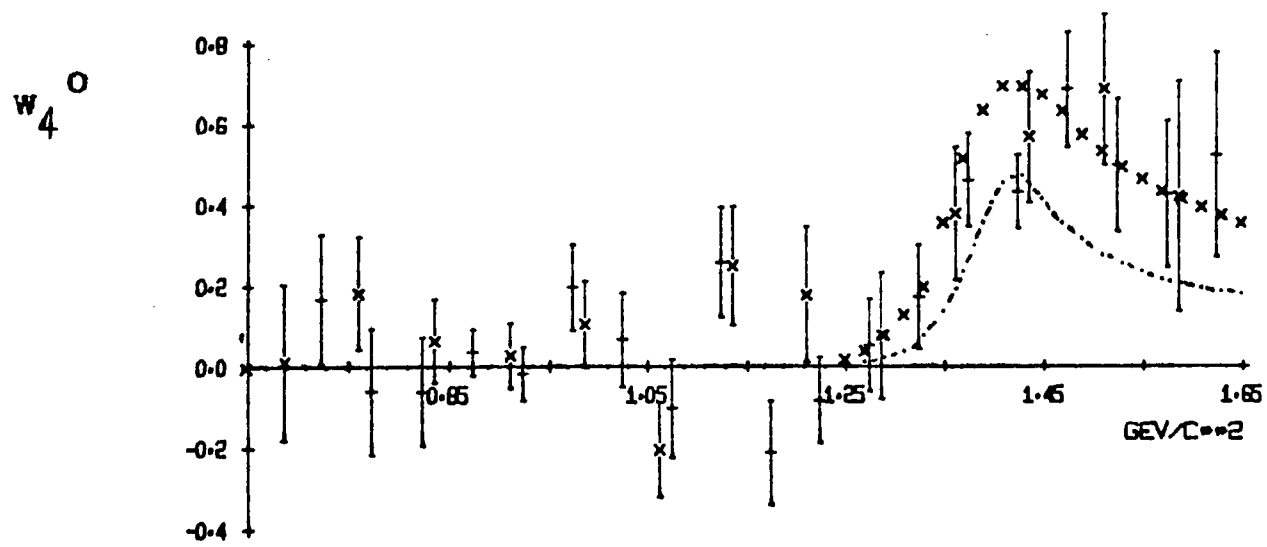

K PI MOMENTS

Fig. 2.11

final states. As expected the w_2^0 and w_4^0 moments peak in the p-wave $K^*(890)$ and d-wave $K^*(1420)$ mass regions respectively.

The isospin amplitudes for elastic and charge exchange scattering are given by

$$A_{elas.} = \frac{2}{3} A^{\frac{1}{2}} + \frac{1}{3} A^{3/2}$$

$$A_{c.e.} = \frac{\sqrt{2}}{3} (- A^{\frac{1}{2}} + A^{3/2}) \qquad (12)$$

If the $I = 3/2$ interaction were negligible, the ratio of the elastic to charge exchange cross-sections would be 2 : 1. Comparing the data in Figs. 2.7(a) and 2.9 where the latter has been normalised to the equivalent events per microbarn value of the former, the experimental ratio, for the entire range of $K\pi$ mass plotted, is found to be only $\sim$ 1.44 : 1, suggesting the presence of terms other than pure $I = 1/2$. The w_1^0 moments show strong indications of a significant $I = 3/2$ interaction. If this were negligible the w_1^0 moment would be identical for the elastic and charge exchange processes. However, the charge exchange moments (Fig. 2.10) are consistently lower than the elastic over the entire range of $K\pi$ mass.

The variation of the elastic w_1^0 moment with mass, falling through zero around 0.95 GeV/c^2 and rising again to a peak near 1.2 GeV/c^2 is very similar to the variation seen at 7.3 GeV/c, which led Trippe et al.[3] to postulate the existence of a broad ($\sim$ 400 MeV/c^2 wide) s-wave $K\pi$ resonance

around 1.1 GeV/c^2. They neglected any I = 3/2 interaction. If the I = 1/2 s-wave phase shift were large and positive, the separation in w_1^0 between the elastic and charge exchange processes could be explained by a negative I = 3/2 s-wave phase shift.

A modified form of the Dürr-Pilkuhn model used in Section 3 is developed here to test such hypotheses against the experimental Kπ moments and mass projections. The differential cross-section for the reaction fitted in Section 3 for Kπ scattering into an element of solid angle $d\Omega_{K\pi}$ we put equal to the right-hand side of formula (8), Section 3, with $\sigma(m)$ now replaced by $d\sigma(m)/d\Omega_{K\pi}$. For elastic scattering this is written as

$$\left.\frac{d\sigma(m)}{d\Omega}\right|_{K^+\pi^-} = 4\pi\lambda^2 \left| \frac{2}{3}\left[A_0\, Y_0^0(\theta,\phi) + \sqrt{3}\, A_1\, DP_{(1)}\, Y_1^0(\theta,\phi) + \sqrt{5}\, A_2\, DP_{(2)}\, Y_2^0(\theta,\phi)\right] + \frac{1}{3} A^{3/2}(\delta_s)\, Y_0^0(\theta,\phi) \right|^2 \tag{13}$$

and for charge exchange scattering as

$$\left.\frac{d\sigma(m)}{d\Omega}\right|_{K^0\pi^0} = 4\pi\lambda^2 \left| -\sqrt{\frac{2}{3}}\left[A_0\, Y_0^0(\theta,\phi) + \sqrt{3}\, A_1\, DP_{(1)}\, Y_1^0(\theta,\phi) + \sqrt{5}\, A_2\, DP_{(2)}\, Y_2^0(\theta,\phi)\right] + \sqrt{\frac{2}{3}} A^{3/2}(\delta_s)\, Y_0^0(\theta,\phi) \right|^2 \tag{14}$$

The A_ℓ are the Breit-Wigner functions of formula (10) and the $DP(\ell)$, the Dürr-Pilkuhn terms given in Table 2.1. The

$A^{3/2}(\delta_s)$ represents some $I = 3/2$ $K\pi$ interaction with an s-wave phase shift δ_s. The values used for c, R_1, R_2 and R_A were those obtained from the fits of Section 3 (Table 2.2). The normalisation factor 1.55 was also included. For each hypothesis tried, the differential cross-sections were numerically integrated over M and t. These off-shell corrections to the $K\pi$ amplitudes will hopefully provide a meaningful test of the data. However, it should be emphasised that the discussions in Section 2 on the uncertainties in both the definition of the off-mass-shell scattering angle and in Section 3 on the s-wave off-shell dependence, still apply.

Several hypotheses with an $I = \frac{1}{2}$, $J^P = 0^+$, resonant wave were tried. The best fits corresponded to a Breit-Wigner of mass 1.2 GeV/c^2 and width 0.4 GeV/c^2. Lovelace's $I = 3/2$ δ_s phase shift [2] was used in this fit. The form of δ_s is a phase shift which moves away from zero at threshold to -10^o around 0.75 GeV/c^2, -20^o around 0.9 GeV/c^2 and flattens off to a value of $\sim -33^o$ above 1.2 GeV/c^2. The moments predicted from this model are shown, normalised to $w_0^0 = 1$, as curves superimposed on the data of Figs. 2.10 and 2.11. The separation of the elastic and charge exchange moments are well fitted in the w_1^0 plot and, within quite large errors, the general trends of all moments are followed. The low experimental values of both the w_3^0 for the two processes and the w_1^0 under the $K^*(890)$ for the charge exchange process are the major disagreements. The w_3^0 moments show no indication of a possible p-wave daughter of the $K^*(1420)$ expected from the Veneziano model.

The predicted $K^+\pi^-$ and $K^0\pi^0$ mass projections for this model are shown in Figs. 2.12(a) and (b). Included for comparison are the corresponding projections using the hypothesis of Trippe et al. of an s-wave Breit-Wigner of mass 1.1 GeV/c^2 and with 0.4 GeV/c^2 with no I = 3/2 interaction. The charge-exchange projections of the two models almost coincide. The dip just below the $K^*(1420)$ is hinted at, in the experimental data (Fig. 2.9). The Trippe hypothesis though, fails to reproduce the flat nature of the $K^+\pi^-$ mass distribution between the $K^*(890)$ and $K^*(1420)$ peaks, (Fig. 2.7(a)). Better agreement with the general shape of the elastic data is obtained with the model suggested here, but the level of events predicted between the peaks is about 50% too high. This might have been expected from the results of Section 3, Fig. 2.6. It appears that with a Dürr-Pilkuhn model, there are an insufficient number of events between the two peaks in the $K^+\pi^-$ mass projection to allow a resonant s-wave interaction, interfering with a negative I = 3/2 s-wave phase shift.*

Some doubt has been cast as to the validity of using models such as these to interpret the s-wave phase shifts. Fu et al. [15] have suggested that these asymmetries may be due to overlap with a low mass $p\pi\pi$ enhancement. This seems unlikely - asymmetries are present in both the $K^0\pi^0$ as well as $K^+\pi^-$ angular distributions, but a low mass $p\pi\pi$ enhancement is present only in the latter final state (see Chapter 4).

---

* The possible contribution from $K\pi$ inelastic scattering can be estimated from the $K^0\pi^+\pi^-\Delta^{++}$ final state. The inelasticity appears negligible below 1.2 GeV/c^2 and small up to the $K^*(1420)$ region. However, any $K\pi\pi$ system cannot be in a 0^+ state.

(a)

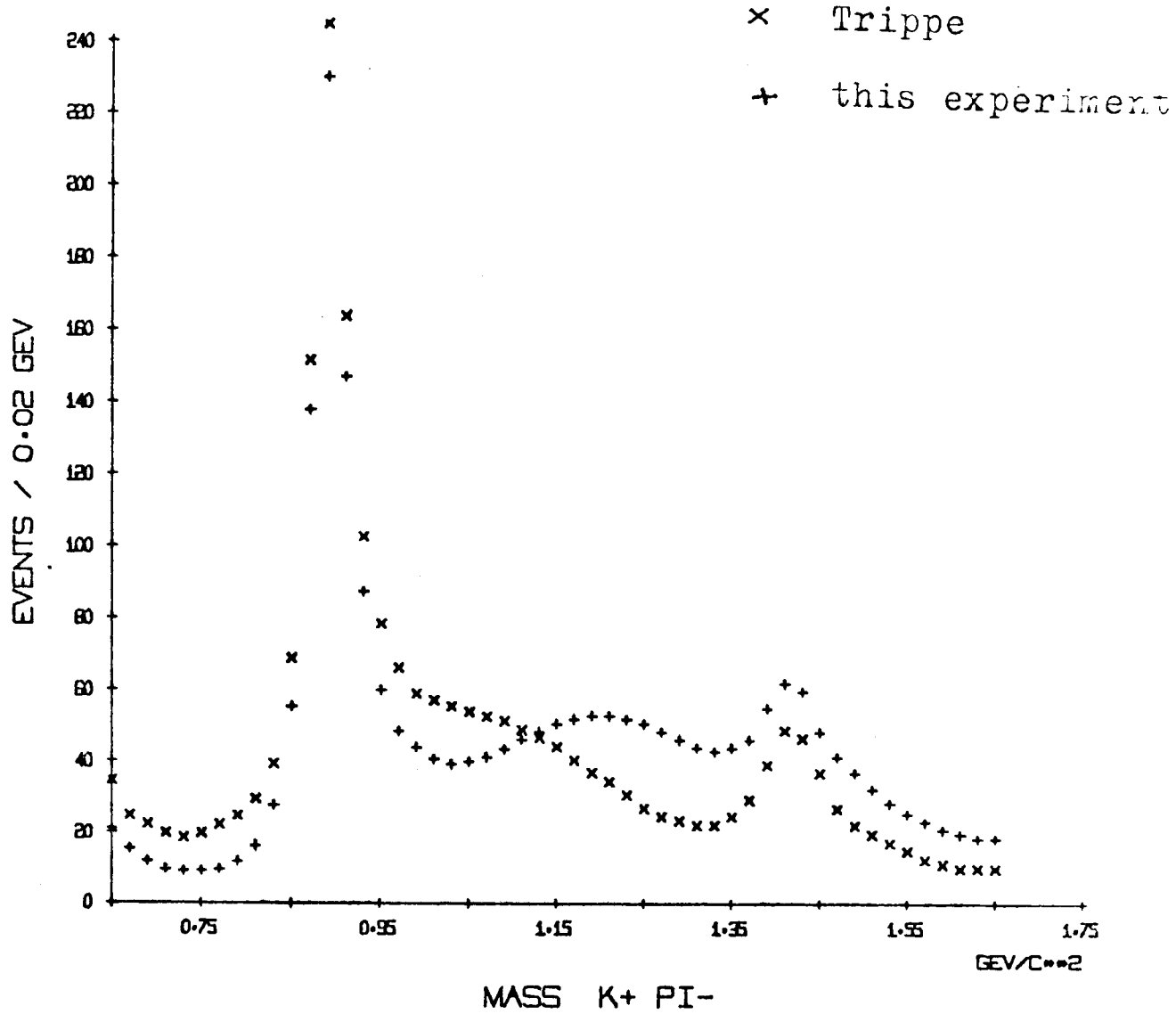

(b)

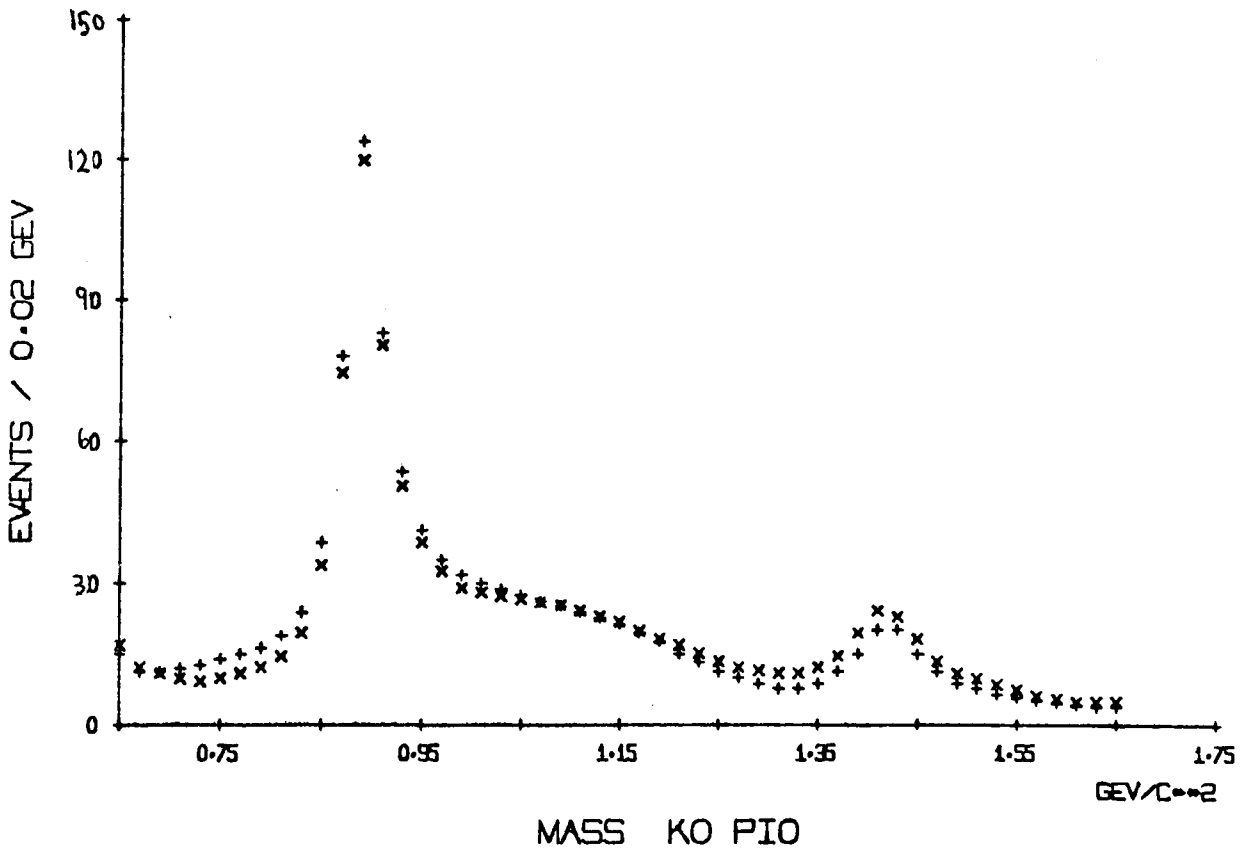

Kπ predicted cross-sections

Fig. 2.12

The excess of events between the $K^*(890)$ and $K^*(1420)$ in the elastic channel remains proportionally just as significant for those events where the low mass $p\pi^+\pi^-$ system has been anti-selected (not shown here). Similar elastic $K^+\pi^-$ moments to those seen here have been observed in reactions where no $p\pi\pi$ enhancement is present, e.g., $K^+n \rightarrow K^+\pi^-p$ (see reference [4]).

The possibility that the separation in the w_1^0 moments may be due to this effect must be considered. The overlap of the events studied here with the low mass $p\pi^+\pi^-$ system is small as can be seen in the Dalitz plot (Fig. 2.13) of $m^2(\Delta^{++}\pi^-)$ against $m^2(K^+\pi^-)$ for a sub-sample of events. The crowding at low $\Delta^{++}\pi^-$ mass for $m(K^+\pi^-) < 1.7$ GeV/c^2 represents a relatively small number of events, though their effect on the $K^+\pi^-$ angular distribution is uncertain. A qualitative estimate of this can be made by comparing this situation with that of the overlap of the Q and the $p\pi^+$ system. In the $K^+\pi^+\pi^-p$ channel there are about half as many events in the $p\pi^+\pi^-$ enhancement as in the Q. A comparison of the relative magnitude of the moments w_1^1, w_2^1, w_3^1 and w_4^1 shown in Fig. 2.14 with the corresponding moments of Fig. 2.5 for $p\pi^+$ scattering gives an estimate of the relative overlap of these enhancements with the data studied here. Although occasional values of the $K^+\pi^-$ moments are as large as the $p\pi^+$, they are not as consistently so. In particular, the w_1^1 moments are significantly smaller than the W_1^1 moments. Thus, as the effect of the Q in distorting the W_1^0 moments was small, it seems extremely unlikely that the comparatively weaker

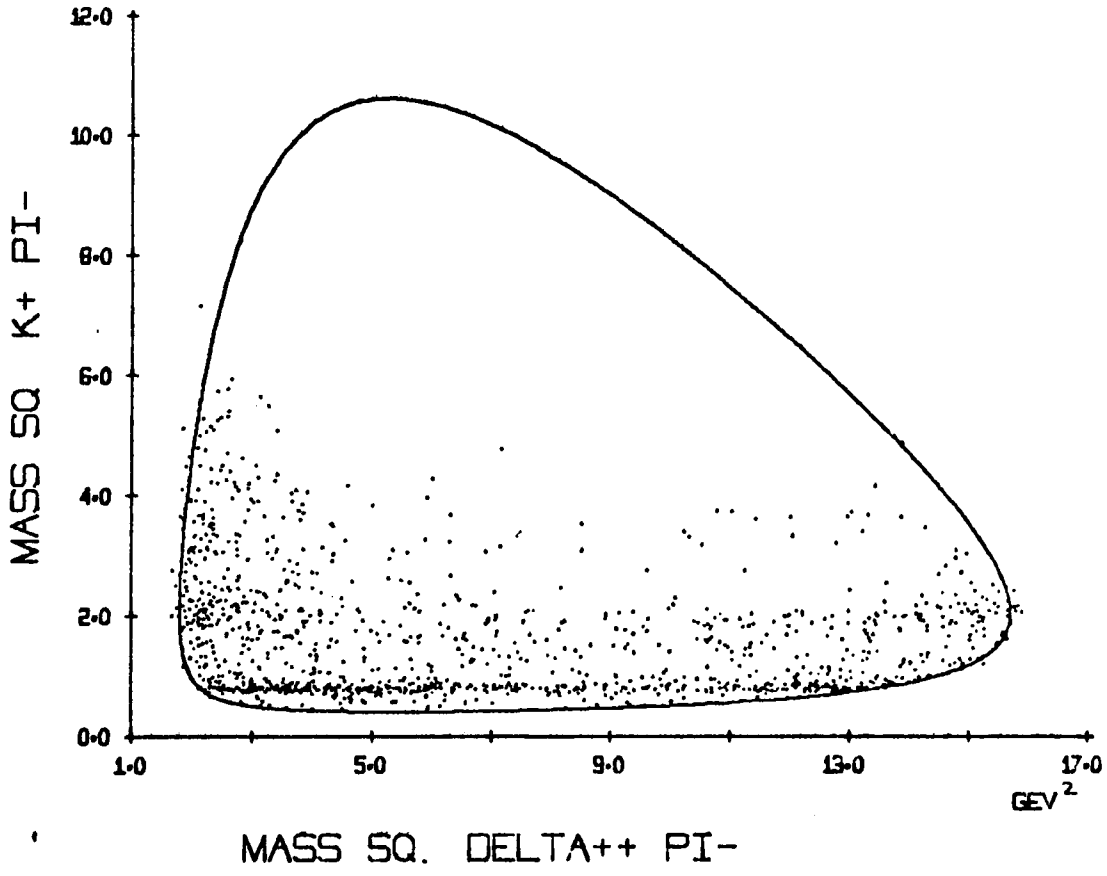
MASS SQ K+ PI-
12.0
10.0
8.0
6.0
4.0
2.0
0.0
1.0
5.0
9.0
13.0
17.0
GEV 2
MASS SQ. DELTA++ PI-

Fig. 2.13

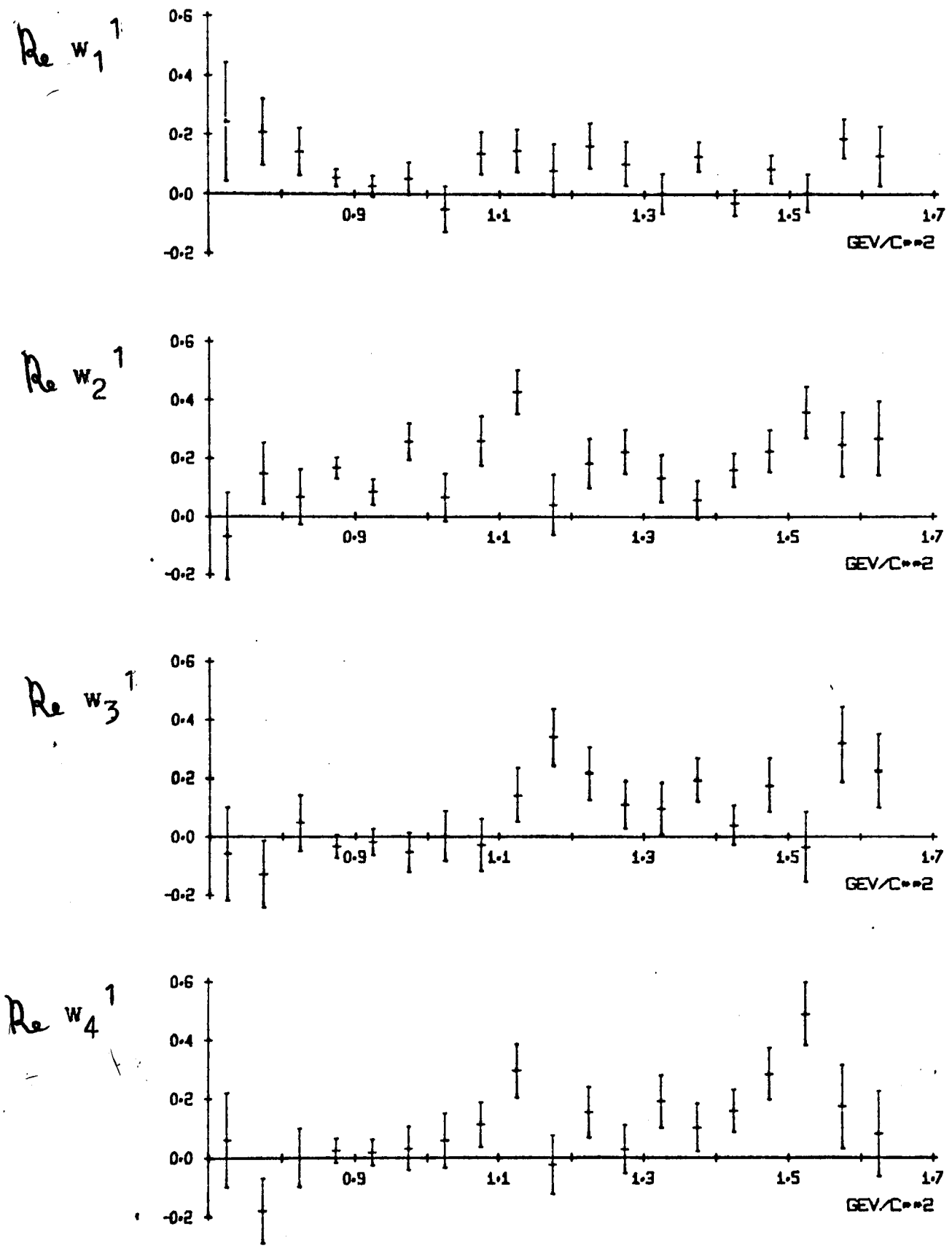
Re w1 1
0·6
0·4
0·2
0·0
-0·2
0·9
1·1
1·3
1·5
1·7
GEV/C**2
Re w2 1
0·6
0·4
0·2
0·0
-0·2
0·9
1·1
1·3
1·5
1·7
GEV/C**2
Re w3 1
0·6
0·4
0·2
0·0
-0·2
0·9
1·1
1·3
1·5
1·7
GEV/C**2
Re w4 1
0·6
0·4
0·2
0·0
-0·2
0·9
1·1
1·3
1·5
1·7
GEV/C**2
K+ PI- SCATTERING

Fig. 2.14

$p\pi^+\pi^-$ enhancement could be responsible for so large a separation in the w_1^0 moments between the two channels.

5 Conclusions

The validity of the models used in this chapter and the interpretation of the results are in most cases open to question. However, the analyses followed here indicate that there is a large positive $I = 1/2$ s-wave phase shift in the region of $K\pi$ mass between 0.8 and 1.3 GeV/c^2, but there is no evidence from this data that it is resonant. The separation in the w_1^0 moments between the two final states finds a natural interpretation with an $I = 3/2$ s-wave $K\pi$ phase shift of a similar form to that proposed by Lovelace.

Many of the inherent doubts of this chapter could be removed with a sample of data large enough to permit the $K\pi$ differential cross-sections to be measured over several ranges of t and subsequently extrapolated to the pion pole. Statistics this large are not likely to be available in the near future at one beam momentum, particularly for the $K^0\pi^0\pi^+p$ final state. In fact, from the results of the recent work of the C.E.R.N. group [5], using the combined data on the World Data Summary Tape, it appears that statistics, even there, are barely adequate to carry out a quadratic extrapolation of the $K^0\pi^0$ moments. The errors on their extrapolated moments are sufficiently large to allow several possible $K\pi$ phase shift solutions to exist.

REFERENCES

[1]	See M. Jacob	CERN/TH/1010 (unpublished)
[2]	C. Lovelace	Proceedings of the conference on $\pi\pi$ and $K\pi$ interactions, Argonne National Laboratory (1969), p. 562.
[3]	T.G. Trippe et al.	Phys Lett. 28B, 203, (1968).
[4]	See P.E. Schlein	Proceedings of the conference on $\pi\pi$ and $K\pi$ interactions, A.N.L. (1969), p. 446.
[5]	P. Herquit and T.G. Trippe	CERN/D.Ph II/Phys 70-29 (unpublished)
	and	
	R. Mercer et al.	'$K\pi$ scattering phase shifts', John Hopkins University preprint (1970).
[6]	E. Gellert et al.	Phys. Rev. Lett. 17, 844, (1966).
[7]	E.P. Colton and P.E. Schlein	Proceedings of the conference on $\pi\pi$ and $K\pi$ interactions A.N.L. (1969), p.1.
[8]	C.Y. Chien et al.	Phys. Lett. 29B 433 (1969).
[9]	R. Hagedorn	Relatistic Kinematics (W.A. Benjamin, Inc., N.Y. 1963), Sections 7.4 and 7.5.
[10]	H.P. Dürr and H. Pilkuhn	Nuovo Cimento 40, 899 (1965).
[11]	Ma et al.	Phys. Rev. Lett. 23, 342 (1969).
[12]	M.N. Focacci and G. Giacomelli	C.E.R.N. Report 66-18 (1966) unpublished.
[13]	G. Wolf	Phys. Rev. Lett. 19, 925 (1967).
[14]	T.G. Trippe et al.	UCLA-1024 (1967) unpublished.
[15]	C. Fu et al.	UCLRL - 18201 (1968) unpublished.

C H A P T E R 3

$K\pi\pi$ SYSTEMS

1 Introduction

This chapter will be devoted to a study of those events from both final states, lying on Face 1 of the cuboctahedron of Chapter 1. These events are dominated by production of the 'Q' enhancement, a broad peak in $K\pi\pi$ mass between 1.2 and 1.5 GeV/c^2. The unselected $K\pi\pi$ mass projections from the two reactions

$$K^+p \rightarrow K^+\pi^+\pi^-p \qquad (1)$$

and

$$K^+p \rightarrow K^0\pi^+\pi^0p \qquad (2)$$

at 10 GeV/c clearly display this enhancement (see Figs. 3.1(a) and 3.1(b)). A brief outline of the Quark Model for mesons which predicts interesting properties for this region is given below [1].

Mesons are regarded as bound states of quark-antiquark pairs where a quark is a fermion with spin $\frac{1}{2}$. The lowest bound states of this system would be* $^1S_0$ and $^3S_1$. For a fermion-antifermion pair the charge conjugation number C is equal to $(-1)^{L+S}$ and the parity P is equal to $(-1)^{L+1}$. Thus the lowest nonets have quantum numbers $J^{PC} = 0^{-+}$ and 1^{--},

---

* The notation $^{2S+1}L_J$ is used where S is the spin, L is the orbital angular momentum and J the total angular momentum of the system.

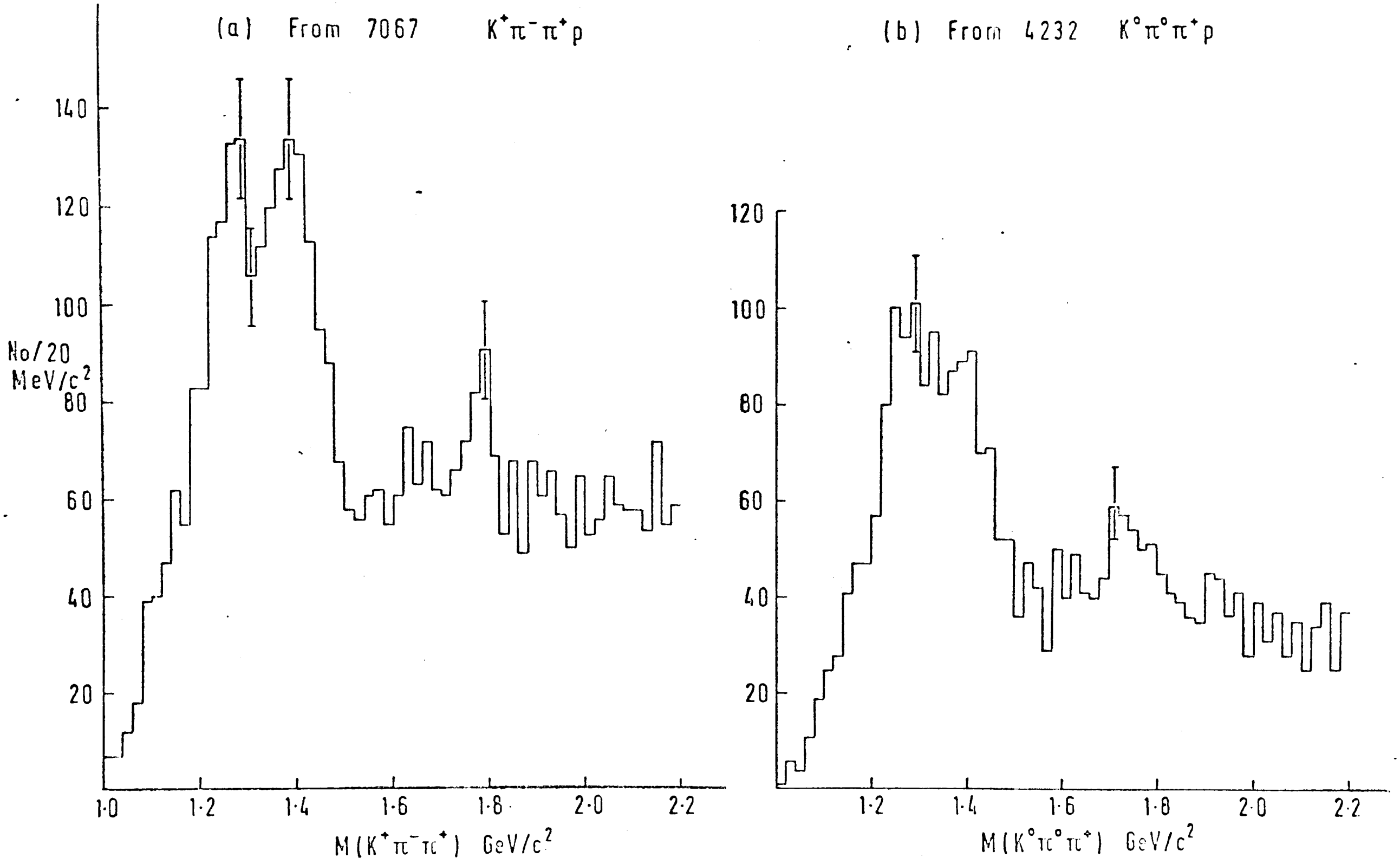
(a) From 7067 $K^+\pi^-\pi^+p$
(b) From 4232 $K^\circ\pi^\circ\pi^+p$
No/20 MeV/c²
140
120
100
80
60
40
20
1·0
1·2
1·4
1·6
1·8
2·0
2·2
M($K^+\pi^-\pi^+$) GeV/c²
M($K^\circ\pi^\circ\pi^+$) GeV/c²

Fig. 3.1

and may be identified with the well established pseudoscalar nonet of stable particles, and the vector nonet of K^*, ρ, ω and ϕ mesons, respectively.

The next states up in mass correspond to the first radial excitation of the quark-antiquark pair, i.e., the states $^3P_0$, $^3P_1$, $^3P_2$ and $^1P_1$. These have quantum numbers 0^{++}, 1^{++}, 2^{++} and 1^{+-} respectively. The 2^{++} nonet is well established ($K^*(1420)$, A_2, f and f'). Mesons associated with the scalar nonet are less clear, though the $K_N(1100)$, $\delta(960)$, $\epsilon(720)$ and $\pi_N(1016)$ are tentatively identified with this nonet [2]. The possible existence of the $K_N(1100)$ has been considered in detail in Chapter 2. Of the other two nonets the $A_1(1070)$ and D(1280) are associated with the 1^{++} and the B(1220) with the 1^{+-} nonet. There is therefore a strong suggestion of the existence of two K^* resonances both with J^P equal to 1^+ within the mass range 1.1 to 1.5 GeV/c^2.

Goldhaber [3] has pointed out that, as the strangeness non-zero mesons are not eigenstates of C (or G), possible mixing between these two K^* resonances could occur. If we denote them by K_+ and K_- where the suffix refers to the value of C characterising the nonet as a whole, then the physically observed mesons may be

$$K_I = K_+ \cos\alpha + K_- \sin\alpha$$

$$K_{II} = K_+ \sin\alpha - K_- \cos\alpha$$

where α is some mixing angle. Experimentally the Q appears to be produced by diffraction dissociation [4]. If this can

be represented by exchange of the vacuum quantum numbers 0^{++} (i.e., Pomeron exchange) then only the 1^{++} nonet members would be produced. For the C = + states this suggests the A_1 and not the B is produced diffractively. However, although only the K_+ would be produced by such a mechanism, both K_I and K_{II} could be observed in the mass projections. This possible mixing for the observed states would complicate any SU(3) predictions that may be made as to branching ratios etc..

Experimentally, over the past year or two, good statistics in the $K^+\pi^+\pi^-p$ final state (i.e., $\geq$ 6000 events) have been obtained by several groups [5] - [10] at incident K^+ momenta mainly in the range 5 GeV/c to 13 GeV/c. These groups all see a broad enhancement in the $K\pi\pi$ mass distribution which rises sharply around 1.2 GeV/c^2 and falls sharply near 1.45 GeV/c^2. The presence of structure in the intervening region is in doubt, but in all experiments the shape of the Q is inconsistent with a single Breit-Wigner hypothesis. A common feature to many of the distributions is a peak in the region 1.26 to 1.3 GeV/c^2 which has been associated with the C meson observed in $p\bar{p}$ annihilations [11] at a mass of 1.24 GeV/c^2.

No $K\pi$ decay mode of the Q has ever been observed, making any natural spin-parity assignment unlikely. The dominant decay mode is via $K^*(890)\pi$ with a $K\rho$ signal seen in practically every case, lying mainly in the overlap region with the K^* band in the Dalitz plot. There is some suggestion of a $K\epsilon$ decay mode [6]. For the spin-parity of the Q, 1^+ is

strongly favoured. Attempts have been made to interpret the enhancement as a kinematic effect of the Reggeised-Deck form [4],[12],[13]. These models predict a dominant spin parity for the Q of 1^+, and in some cases can reproduce the overall shape, though to a first approximation only.

The questions concerning the Q that still need to be answered are:

a) Is there present a resonance of another spin-parity (possibly 2^-) sitting on top of a predominantly 1^+ Deck background?

b) How large is the contribution from the $K^*(1420)$ to this region?

c) Is there any evidence for a $K\epsilon$ decay mode?

d) Are there properties which both change rapidly across the Q and are indicative of the presence of two resonances?

These problems will be considered below. The data available at 10 GeV/c, unlike most other experiments, are comparable for the two channels $K^+\pi^+\pi^-p$ and $K^o\pi^o\pi^+p$. This should be a distinct help when applying isospin arguments to question c).

2 The $K\pi\pi$ Mass Spectrum at 10 GeV/c

The two $K\pi\pi$ mass spectra of Fig. 3.1 are combined in Fig. 3.2. This is shown together with the result of removing

those events in which any πp combination lies in the $\Delta(1236)$ region, 1.12 - 1.34 GeV/c^2. These figures show the Q with the characteristic features discussed in Section 1. In addition there is evidence of splitting. In Fig. 3.1(a) and Fig. 3.2 two peaks are observed, centred at 1.27 and 1.39 GeV/c^2, separated by a dip at 1.31 GeV/c^2. The splitting is seen most strongly in events from reaction (1) where the mass resolution is the better (see Chapter 1). The dip is ~ 3 standard deviations below a line joining the peaks, but the data would adequately fit any hypothesis yielding a flat top to the Q. As mentioned, the lower peak is seen by several groups but the two peaked structure, seen here, is in remarkably good agreement with the results of Alexander et al. [6] from an experiment at 9 GeV/c. They report two peaks at 1.26 and 1.38 GeV/c^2 with a dip between them centred at 1.3 GeV/c^2. However, in contrast to their results the significance of the splitting at 10 GeV/c is not enhanced by $\Delta(1236)$ removal, vector meson selections or momentum transfer cuts. The effect of Δ removal is shown in Fig. 3.2, and all analyses of the production and decay of K$\pi\pi$ systems described below have been made on only those events remaining after this selection has been applied.

A fit to the widths of these peaks in the Q is sensitive to the level of background allowed. Alexander et al., fitting their lower peak with a background taken just below the position of the dip, obtained a value of 40 MeV/c^2 for the width, whereas Firestone who fitted a range of data, allowed no background and obtained a value nearer 200 MeV/c^2 [4].

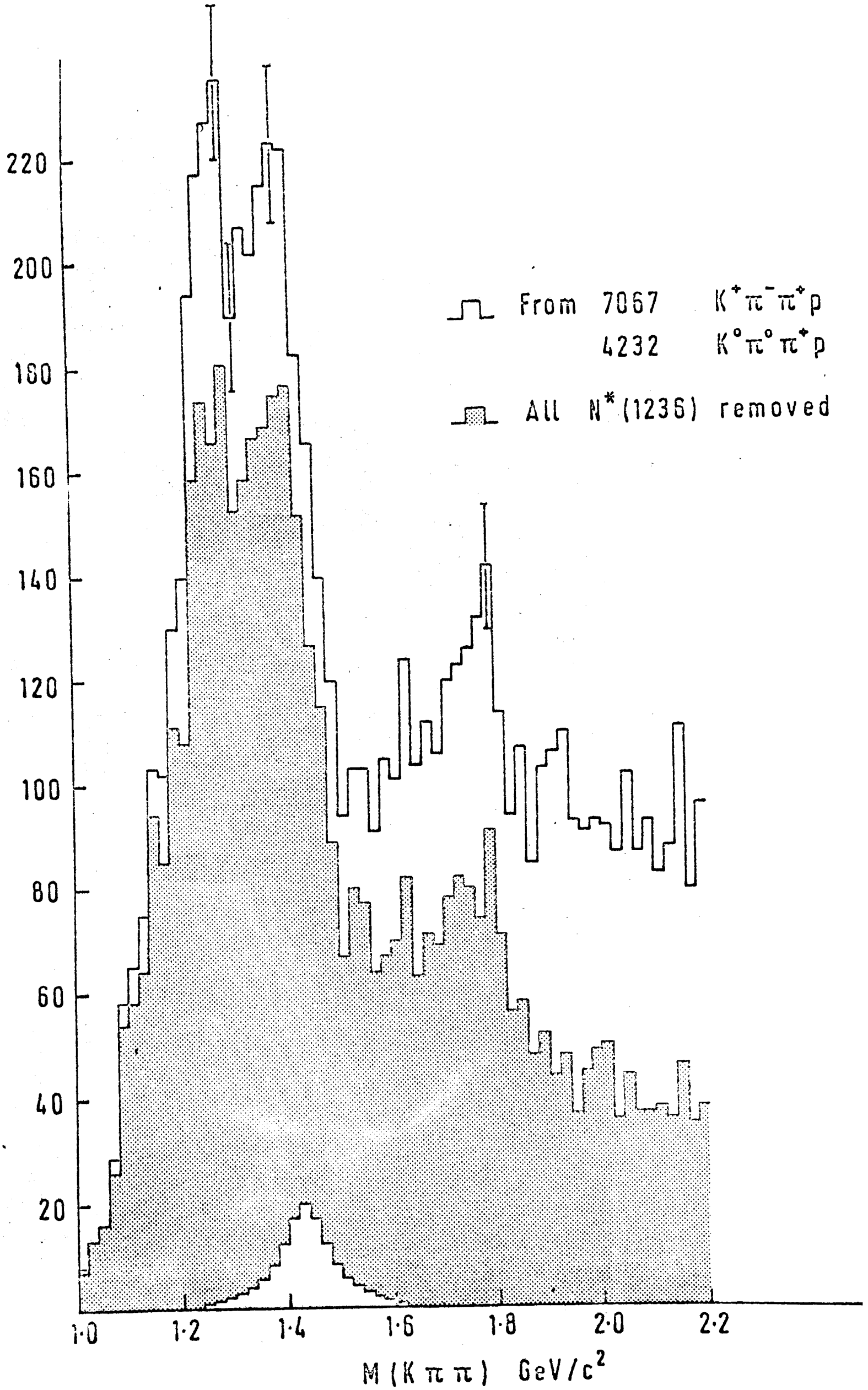
From 7067 $K^+\pi^-\pi^+p$
4232 $K^0\pi^0\pi^+p$
All $N^*(1236)$ removed
220
200
180
160
140
120
100
80
60
40
20
1·0
1·2
1·4
1·6
1·8
2·0
2·2
M (K π π) GeV/c²

Fig. 3.2

In this experiment a significant feature in the data is the shape of the leading edge of the Q. It is convex between 1.1 and 1.2 GeV/c^2 changing to concave above this mass. If the shoulder around 1.15 GeV/c^2 is used to locate the contribution of a Deck background, then over half the Q must be assigned to other causes, such as resonance production (assuming such a separation to be meaningful). Fits have been carried out at Oxford by A.W. Lowman to the mass distribution of Fig. 3.2 using the model of a Reggeised Deck background incoherent with two Breit-Wigners, with a variable degree of coherence between them superposed [14]. The results of the fits are reproduced in Fig. 3.3. The dotted line is the background used in the fits. As can be seen the leading edge of the enhancement is reproduced extremely well. With this level of background the width of the lower peak is fitted to $\sim$ 100 MeV/c^2. The upper peak was fitted to a width $\sim$ 140 MeV/c^2. The interesting feature, with coherence included in the fits, is that the mass of the first peak becomes 1.24 GeV/c^2, just the mass of the C meson.

A second enhancement occurs between 1.7 and 1.8 GeV/c^2, now called the L region, peaking at 1.79 GeV/c^2 in the combined data and the data from reaction (1), but at 1.71 GeV/c^2 in the data from reaction (2). It will not be considered in detail here as it is being studied by other members of the collaboration.

3 The Ambiguous Events

Attention has been dramatically drawn to the problem of

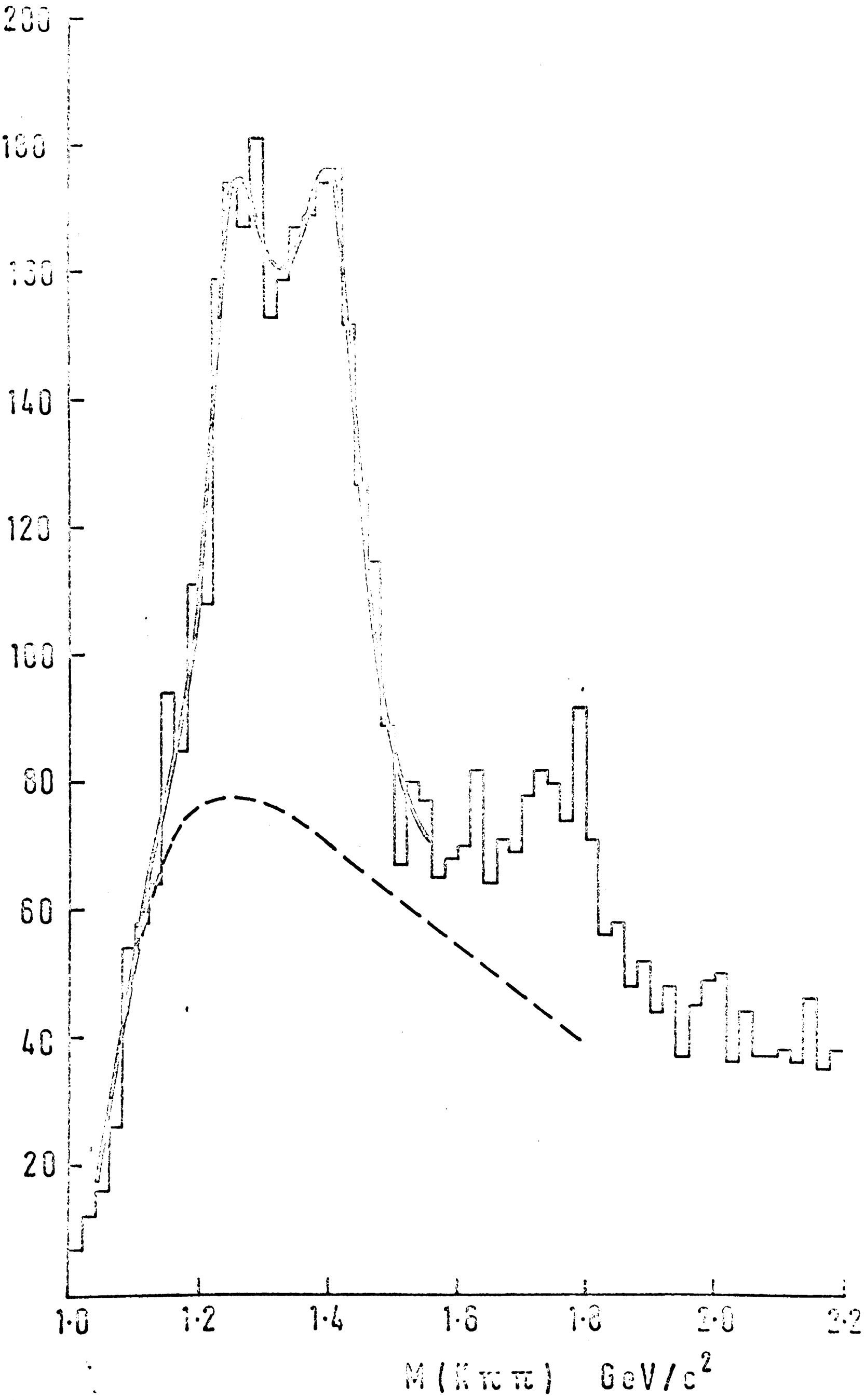

Fig. 3.3

the kinematic ambiguities in the $K^+\pi^+\pi^-$ system by the Van Hove Plots, Figs. 1.6 and 1.8 of Chapter 1. The events with the K^+-π^+ ambiguity contribute 30% of the events in the Q region from reaction (1). Furthermore, the whole of the ρ signal in the $\pi^+\pi^-$ projection of the $K^+\pi^+\pi^-$ Dalitz Plot (Fig. 3.12) is constituted by these ambiguous events: their omission would seriously bias the data. In subsequent analyses the higher probability fit has been selected. The effect of this procedure is discussed in Appendix A. The conclusion drawn is that the misidentified events selected by this procedure have not significantly biased the data.

4 Production Characteristics of the Q Enhancement

The production of the Q is highly peripheral, most events having a 4-momentum transfer squared, t, of modulus less than 0.3 $(GeV/c)^2$. On fitting an exponential e^{at} to the t distribution for those events with $K\pi\pi$ mass between 1.2 and 1.4 GeV/c^2, the value of a was found to be 7.1 ± 0.2 $(GeV/c)^{-2}$, in the range appropriate to diffractive scattering. There is no significant variation of the parameter a with increasing $K\pi\pi$ mass below 1.4 GeV/c^2, but between 1.4 and 1.5 GeV/c^2 the value of a is 5.8 ± 0.3 $(GeV/c)^{-2}$. Distributions of t in the mass range 1.2 - 1.5 GeV/c^2 are shown in Fig. 3.4.

Further evidence for diffractive production is found in the angular properties of the $K\pi\pi$ system. The angular distribution in space of the normal to the $K\pi\pi$ decay plane, in the $K\pi\pi$ centre of mass, contains only moments of the

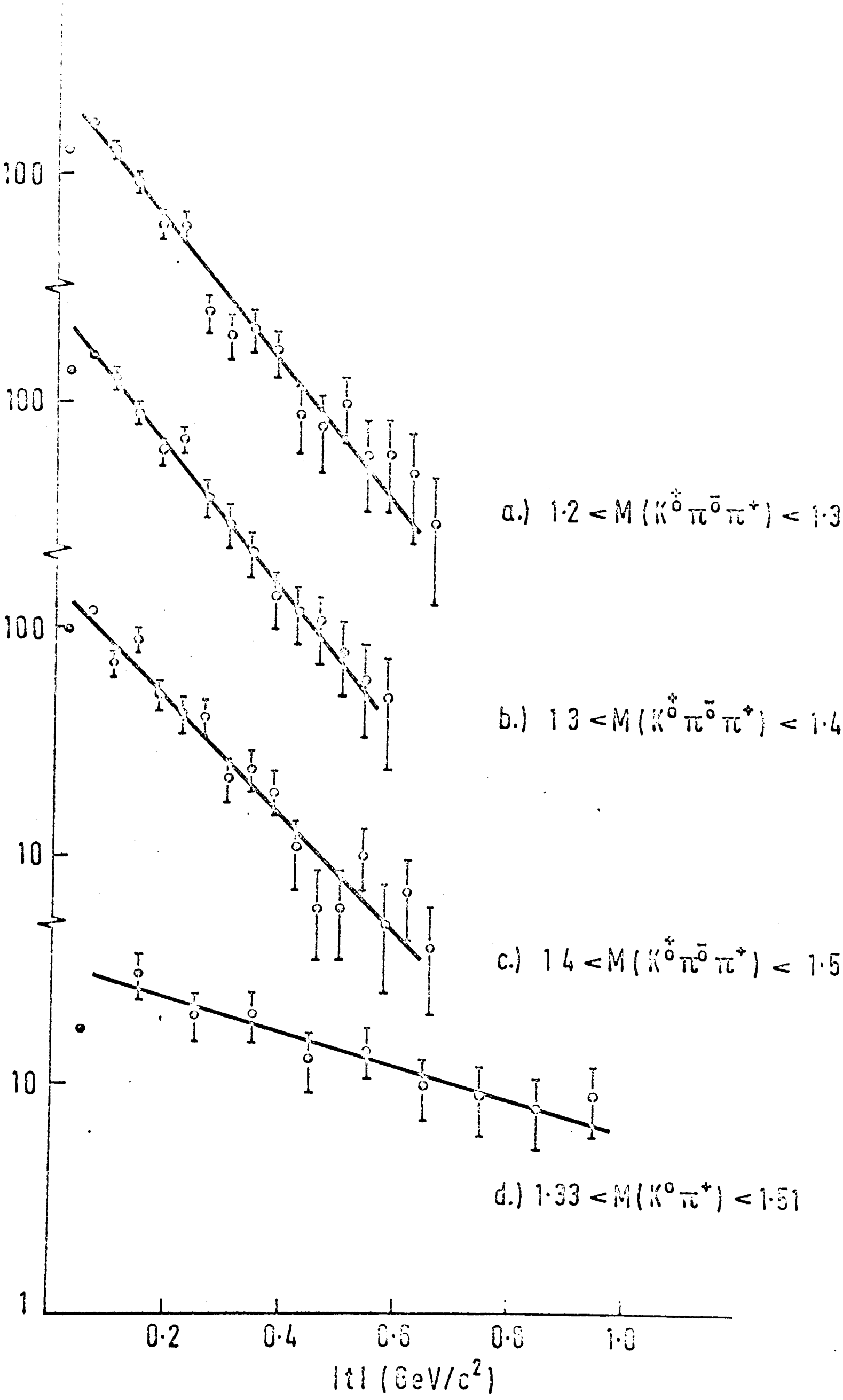
100
100
100
10
10
1
a.) 1·2 < M (K°π⁻π⁺) < 1·3
b.) 1·3 < M (K°π⁻π⁺) < 1·4
c.) 1·4 < M (K°π⁻π⁺) < 1·5
d.) 1·33 < M (K°π⁺) < 1·51
0·2
0·4
0·6
0·8
1·0
|t| (GeV/c²)

Fig. 3.4

spherical harmonics Y_J^M with M = 0, with respect to the incoming K^+, again as expected for diffractive production (see Section 6).

5 Contribution of the $K^*(1420)$ to the Q Region

The decay of $K^*(1420)$ into $K\pi\pi$ could affect strongly the interpretation of the Q enhancement, and the characteristics of $K^*(1420)$ production in the reaction

$$K^+p \rightarrow K^o \pi^+ p \qquad (3)$$

have been used to estimate the contribution to the Q. If the $K\pi\pi$ decay mode of the $K^*(1420)$ is dominated by $K^*(890)\pi$ and the branching ratio $K\pi/K\pi\pi$ is ~ 1 as quoted by the Particle Data Group, then the estimated maximum contribution is 40 events per 20 MeV/c^2 bin in Fig. 3.2 at the peak of the $K^*(1420)$. This occurs at a mass of 1.43 GeV/c^2 in the data on reaction (3). Removal of this $K^*(1420)$ contribution would reduce the upper peak at 1.39 GeV/c^2 to a shoulder, but would not remove it. However, a comparison of the t distribution to the proton in the $K^*(1420)$ region, of reactions (1), (2) and (3), sets a more stringent limit on the possible contribution of $K^*(1420)$ to the Q. The t distribution to the $K^*(1420)$ for reaction (3) is compared in Fig. 3.4 with the t distribution for the Q and is very flat, having a parameter a of 1.7 ± 0.3. Approximately half the $K^*(1420)$ events in reaction (3) are produced with $|t| > 0.4$ and in Fig. 3.5 the mass spectra of $K^o\pi^+$ from reaction (3) and $K^{\pm o}\pi^{\mp o}\pi^+$ from

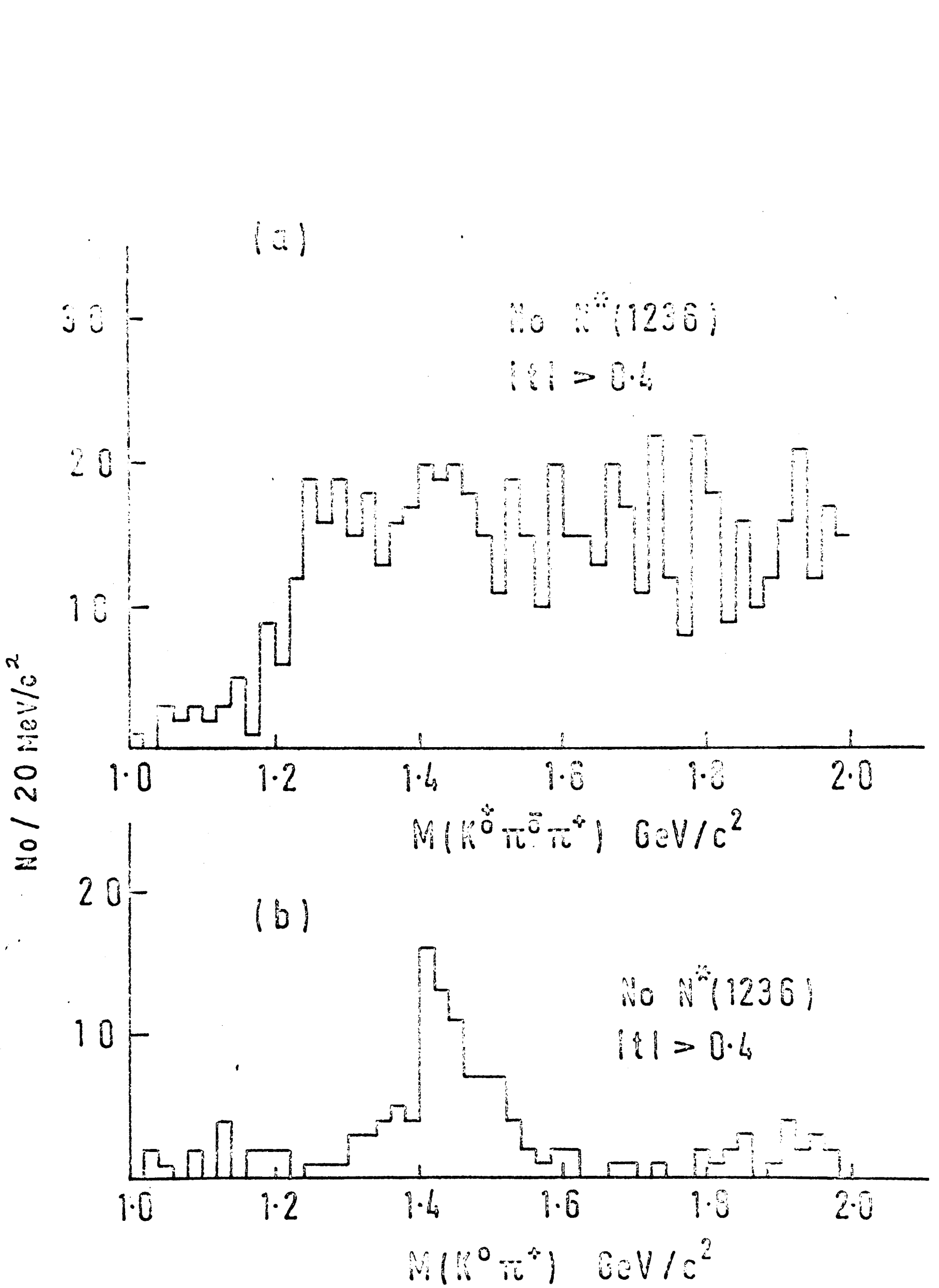
No / 20
MeV/c²
(a)
No N*(1236)
|t| > 0·4
1·0
1·2
1·4
1·6
1·8
2·0
M(K°π⁻π⁺) GeV/c²
(b)
No N*(1236)
|t| > 0·4
M(K°π⁺) GeV/c²

Fig. 3.5

reactions (1) and (2) are compared for $|t| > 0.4$. No visible $K^*(1420)$ signal is observed in the $K\pi\pi$ spectrum, nor for any other t cut, and this allows us to conclude that the maximum contribution of the $K^*(1420)$ to the data of Fig. 3.2 is $\sim$ 20 events per 20 MeV/c^2 bin at peak, corresponding to a branching ratio $K\pi\pi/K\pi$ of less than 1/2 for the $K^*(1420)$. The shape of the Q enhancement thus remains essentially unchanged by removal of the possible $K^*(1420)$ contribution.

6 Angular Properties of the $K\pi\pi$ System

The discussion, Section 4, suggests the production of the $K\pi\pi$ system may be well represented by the Feynman diagram of Fig. 3.6(a). The interaction at the $K\pi\pi$ vertex is then essentially the 2- to 3-body scattering process

$$K^+ + e \rightarrow K + \pi + \pi \qquad (4)$$

To study the angular properties of this process two sets of axes may be set up in the $K\pi\pi$ centre of mass. They are illustrated in Fig. 3.6(b). The set OX, OY, OZ are fixed with respect to the final state particles with

OZ as the normal to the $K\pi\pi$ decay plane

OX as a vector within the plane (e.g. the π^+ momentum vector is used here)

and OY as $\overrightarrow{OZ} \wedge \overrightarrow{OX}$.

The set Ox, Oy, Oz are fixed with respect to the production process with

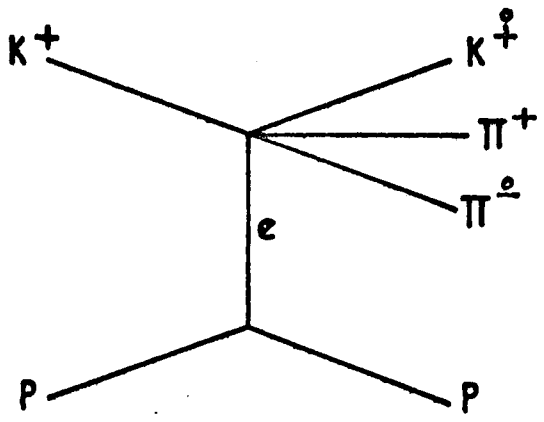

a) Diagram For Q Production

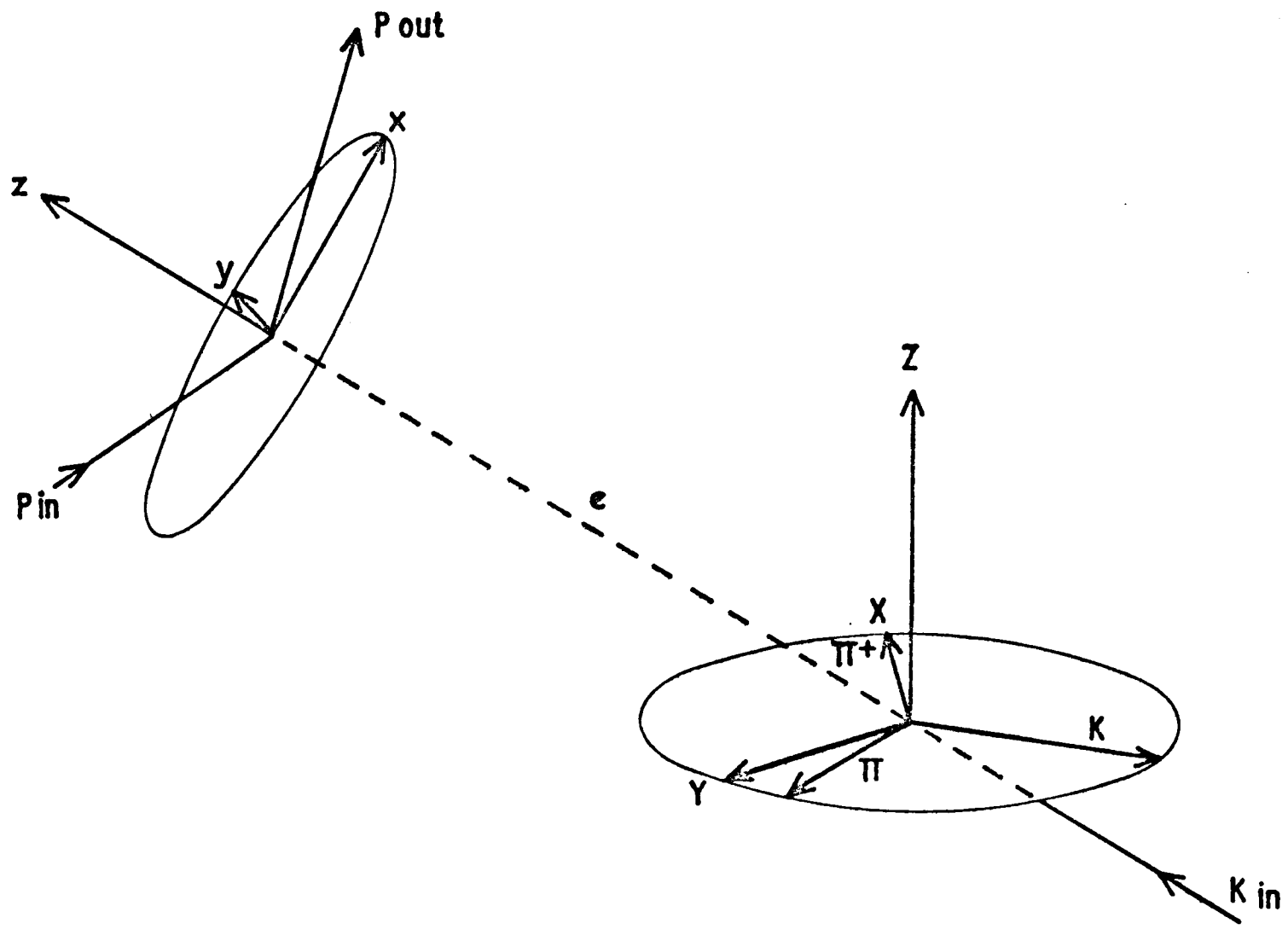

b) Axes Used For K π π Calculations

FIG. 3.6

Oz as the incoming K^+

Oy as the normal to the production plane

(i.e. $p_{in} \wedge p_{out}$)

Ox as $\overrightarrow{Oy} \wedge \overrightarrow{Oz}$

The system is then specified by a set of 3 Euler angles (Φ , Θ , Ψ) which transform one system of axes into the other. The angles Θ and Φ may represent the polar and azimuthal angles of the decay plane normal referred to the Oxyz axes. Ψ is then essentially a measure of the rotation of the decay plane about the normal.

Following Berman and Jacob [15] the angular distribution $W(\Theta, \Phi)$ of the normal to the $K\pi\pi$ decay plane with respect to the axes Oxyz was expanded as

$$W(\Theta, \Phi) = \sum_{LM} W_L^M \; Y_L^{M\,*}(\Theta, \Phi) \qquad (5)$$

Both the real and imaginary parts of W_L^M were evaluated for every 50 MeV/c^2 mass bin between 1.1 and 2.0 GeV/c^2. Of the many moments that are allowed with $M \neq 0$, none showed any systematic trends and they were all consistent with zero. This strongly suggests that the production of the Q is due to exchange of a spin zero object. It does not require it, but implies only that the Q is produced with a diagonal density matrix.

The moments W_2^0 and W_4^0 are displayed in Fig. 3.7 for the two final states. They are consistent with each other. The absence of any significant W_4^0 moment below 1.5 GeV/c^2

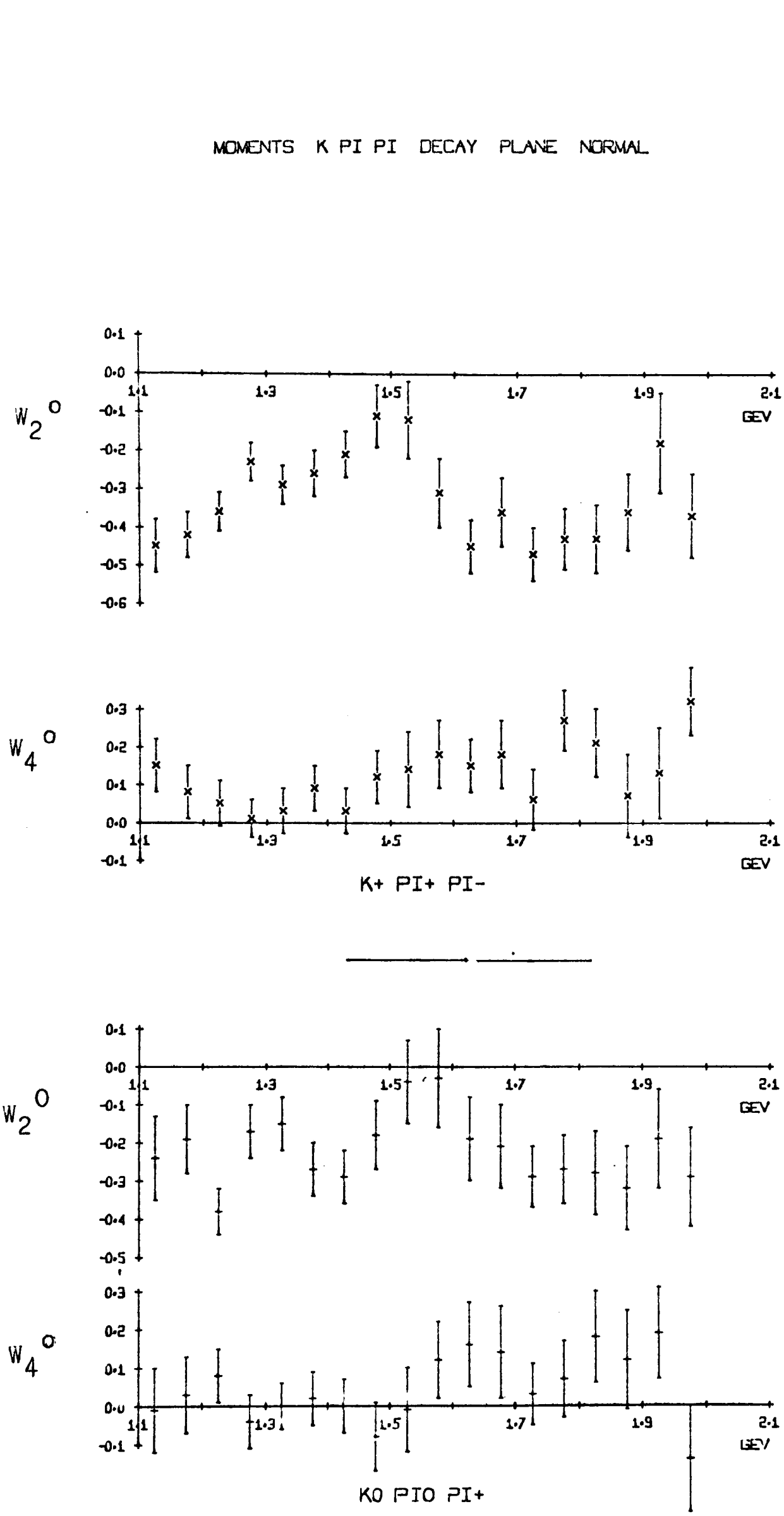
MOMENTS K PI PI DECAY PLANE NORMAL
W2 O
W4 O
0·1
0·0
-0·1
-0·2
-0·3
-0·4
-0·5
-0·6
1·1
1·3
1·5
1·7
1·9
2·1
GEV
0·3
0·2
0·1
0·0
-0·1
K+ PI+ PI-
W2 O
W4 O
0·1
0·0
-0·1
-0·2
-0·3
-0·4
-0·5
1·1
1·3
1·5
1·7
1·9
2·1
GEV
0·3
0·2
0·1
0·0
-0·1
K0 PI0 PI+

Fig. 3.7

suggests that spin 2 contributions are not appreciable below this mass, but become significant above it. The predictions of Berman and Jacob for $W(\Theta, I)$ for various J^P states when produced by spin zero exchange may be summarised as follows :-

$$\begin{array}{ll} 0^- & \text{Isotropic} \\ 1^+ & \sin^2\Theta \\ 2^- & (\frac{9}{4} + K)\sin^4\Theta - 3\sin^2\Theta + 1 \end{array} \qquad (6)$$

where K is a real positive number depending on the decay mechanism. The 1^+ distribution corresponds to a value of W_2^0 of -0.447. This is inconsistent with the experimentally observed values in the region 1.25 to 1.6 GeV/c^2. These could be due to a large 0^- contribution, a small 2^- contribution (if K is treated as a free parameter) or production of a 1^+ state by the exchange of a particle with spin $\neq 0$. The last possibility is acceptable for diffractive production if a Regge model, with exchange of the Pomeron trajectory, is used. This trajectory is usually regarded as having a small slope with an intercept, $\alpha(o)$, of one, and hence possesses spin. The possible production mechanisms of the Q will be considered further below.

The angular distributions studied so far have an implied integration over Ψ. Thus information contained in this angle which is particularly sensitive to interference between different spin-parities is lost. To gain further information, the angular distribution $w(\Theta, \psi)$ of the incoming K^+ referred to the OXYZ set of axes was expanded in a similar manner to

(5), i.e., as

$$w(\Theta, \psi) = \sum_{Im} w_L^m Y_L^{m*}(\Theta, \psi) \qquad (7)$$

The moments w_L^0 are of course equal to W_L^0. The variations of some of the other more significant moments are shown in Fig. 3.8. Appendix B contains an outline of the theory [16] and the variations expected for these moments for various hypotheses. It is shown that the moments w_1^1 and w_3^1 are characteristic of interference between 1^+ and 2^- states. These moments are small in the Q region (see Fig. 3.8) but become significant at higher masses. The moments w_1^0, w_3^0 and w_3^2 are characteristic of 1^+ and 2^+ interference. They are consistent with zero throughout the $K^*(1420)$ region suggesting no coherent production of this resonance.

Constrained fits to the moments w_L^m can be carried out for certain hypotheses if the exchange particle e (Fig. 3.6(a)) is assumed to have spin zero. Details of the theory are given in Appendix B. Fits were carried out to the two channels $K^+\pi^+\pi^-$ and $K^0\pi^0\pi^+$ independently in 50 MeV/c^2 wide bins. The hypotheses tried were: 1^+ and 2^-, 1^+ and 0^-, and for comparison 1^- and 2^+. Table 3.1 gives the χ^2 for the fits tried. All moments up to w_4^4 were included in the evaluation of the χ^2. The natural spin-parity states give very poor fits. The 1^+ and 2^-, and 1^+ and 0^- fits are of comparable quality below 1.5 GeV/c^2 but above this region where L = 4 moments become appreciable the 1^+ and 2^- are relatively better. The hypothesis of 1^+ and 2^- gives acceptable χ^2

× Real

\+ Imag.

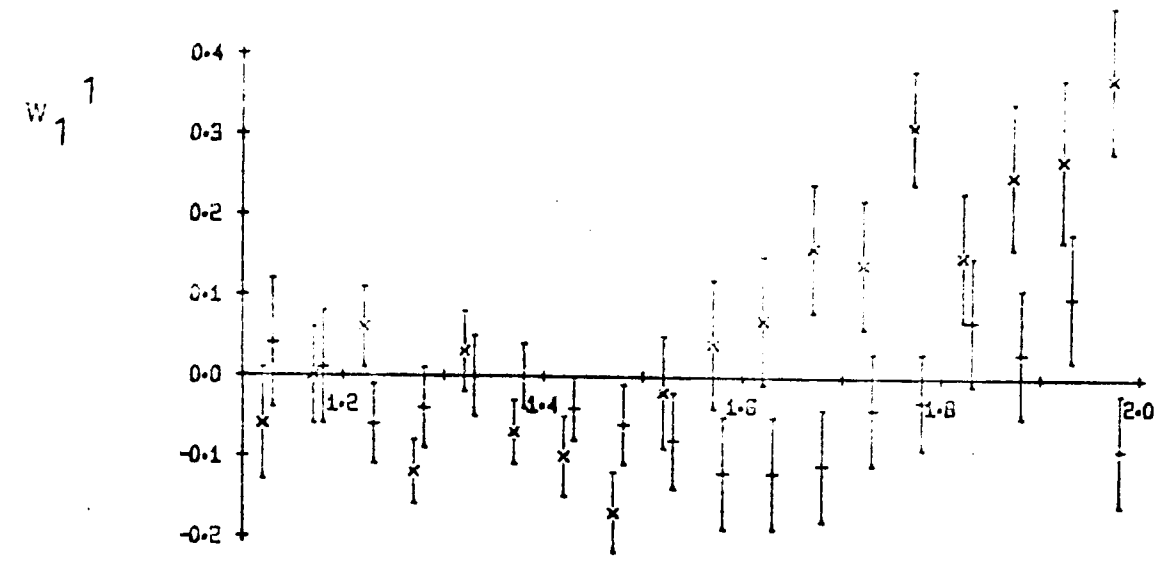

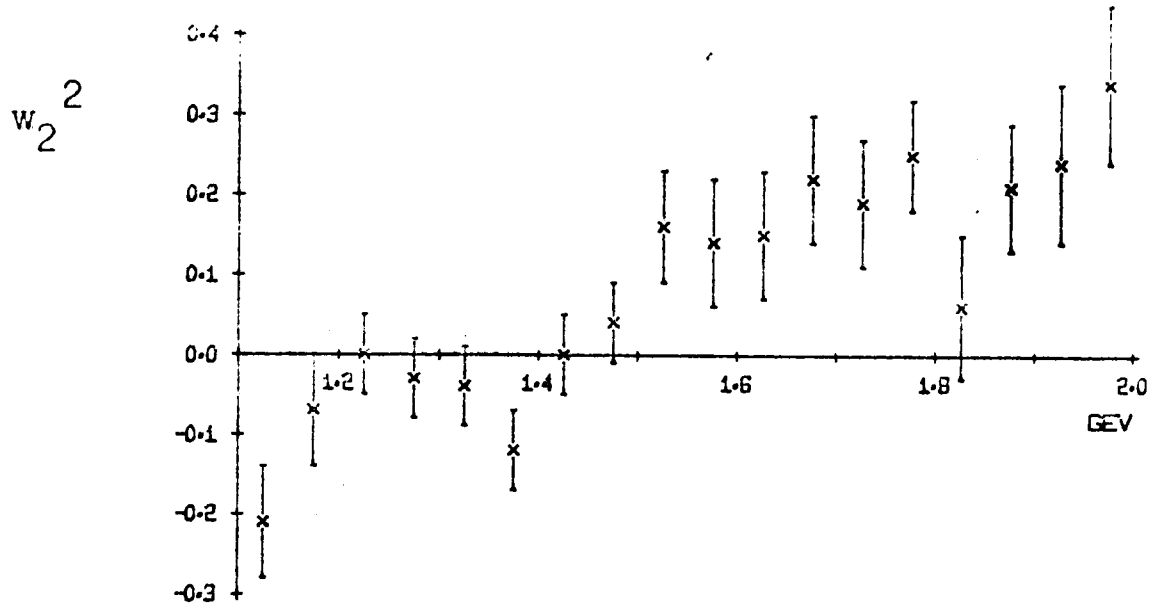

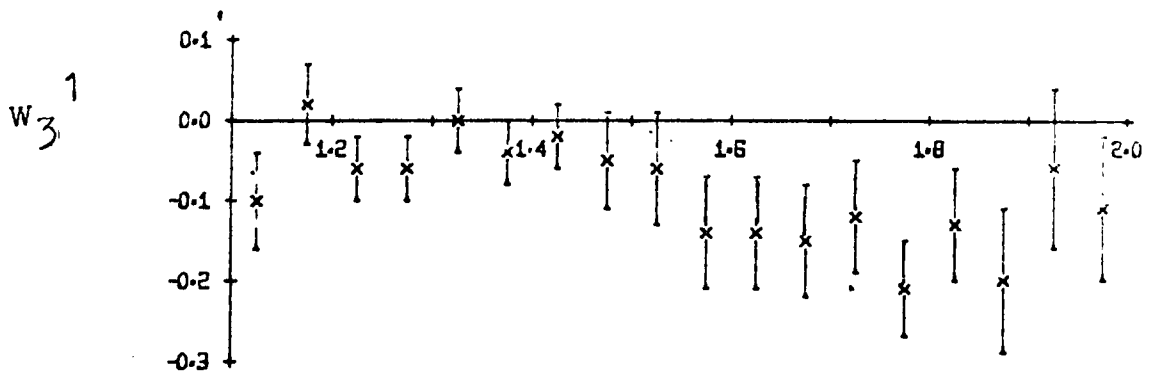

K+ PI+ PI- MOMENTS

Fig. 3.8

Table 3.1

χ^2 values for fitting to the moments w_J^m

Region GeV/c^2	$K^+\pi^+\pi^-$ Final State			$K^0\pi^0\pi^+$ Final State	
	$\chi^2(1^+2^-)$	$\chi^2(1^+0^-)$	$\chi^2(1^-2^+)$	$\chi^2(1^+2^-)$	$\chi^2(1^+0^-)$
1.1-1.15	12	19	200	11	17
1.15-1.2	17	26	233	10	13
1.2-1.25	31	61	263	12	14
1.25-1.3	21	24	206	26	14
1.3-1.35	23	30	219	21	13
1.35-1.4	16	18	236	18	18
1.4-1.45	28	22	197	29	30
1.45-1.5	13	15	139	21	22
1.5-1.55	20	20	96	20	21
1.55-1.6	16	30	147	23	21
1.6-1.65	24	32	217	16	31
1.65-1.7	12	25	161	14	23
1.7-1.75	15	19	194	19	24
1.75-1.8	9	40	313	13	17
1.8-1.85	12	34	176	14	24
1.85-1.9	13	25	121	12	20
Number of constraints in fit	15	19	20	15	19

values in most bins. The fraction of 2^- for these fits is displayed in Fig. 3.9. In the Q region it is small ($\sim 10\%$) but larger although poorly determined above this region. The large peak in the 2^- contribution in the L region (1.75 to 1.8 GeV/c^2) for the $K^+\pi^+\pi^-$ system cannot be regarded as significant as it is not reproduced in the fits to $K^0\pi^0\pi^+$.

It is apparent from these fits that although the moments W_2^0 are not consistent with the production of a pure 1^+ state by spin zero exchange, the distributions are consistent with this hypothesis if a small proportion of 2^- is included and K is allowed to be free.

7 Dalitz Plot Analysis of the Q

The discussions of the previous sections were concerned with the production mechanisms of the Q. Models for its subsequent decay were not considered. The population distribution of the Dalitz plot on the other hand depends on the spin-parity J^P of the system and the mechanism by which it decays. It is independent of the magnetic substate in which the system is produced and does not contain interference between states of different J^P. The analyses carried out here on the Dalitz plot population are thus essentially independent of the previous considerations.

Figures 3.10 and 3.11 show the Dalitz plot distributions of the two final states for three 100 MeV/c^2 wide regions in $K\pi\pi$ mass between 1.2 and 1.5 GeV/c^2. A dominant $K^*(890)$ band is seen. A ρ signal is also indicated, particularly in the $K^0\pi^0\pi^+$ channel. The model used here assumes the

× $K^+ \pi^+ \pi^-$

\+ $K^0 \pi^+ \pi^0$

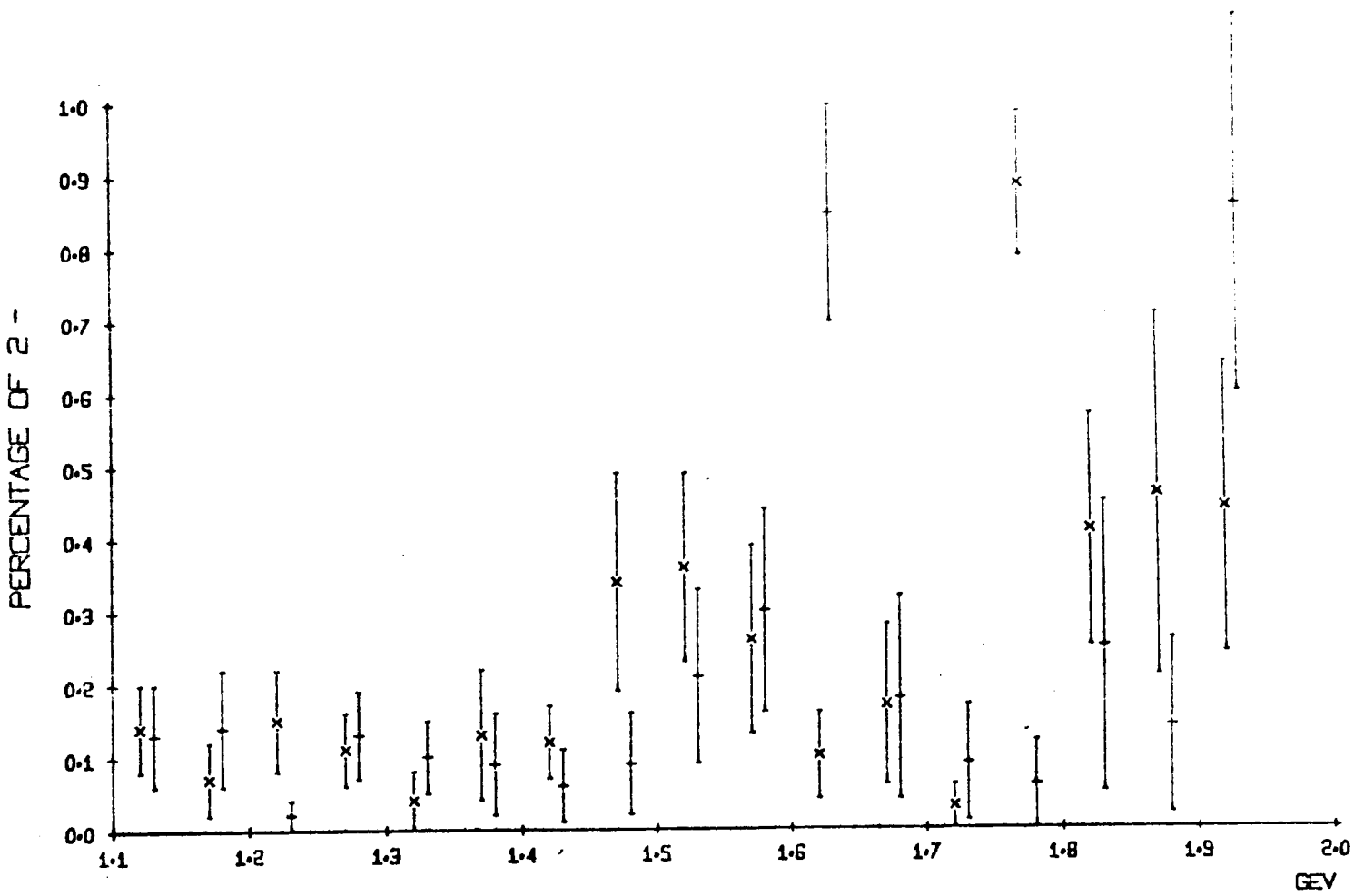

Fig. 3.9

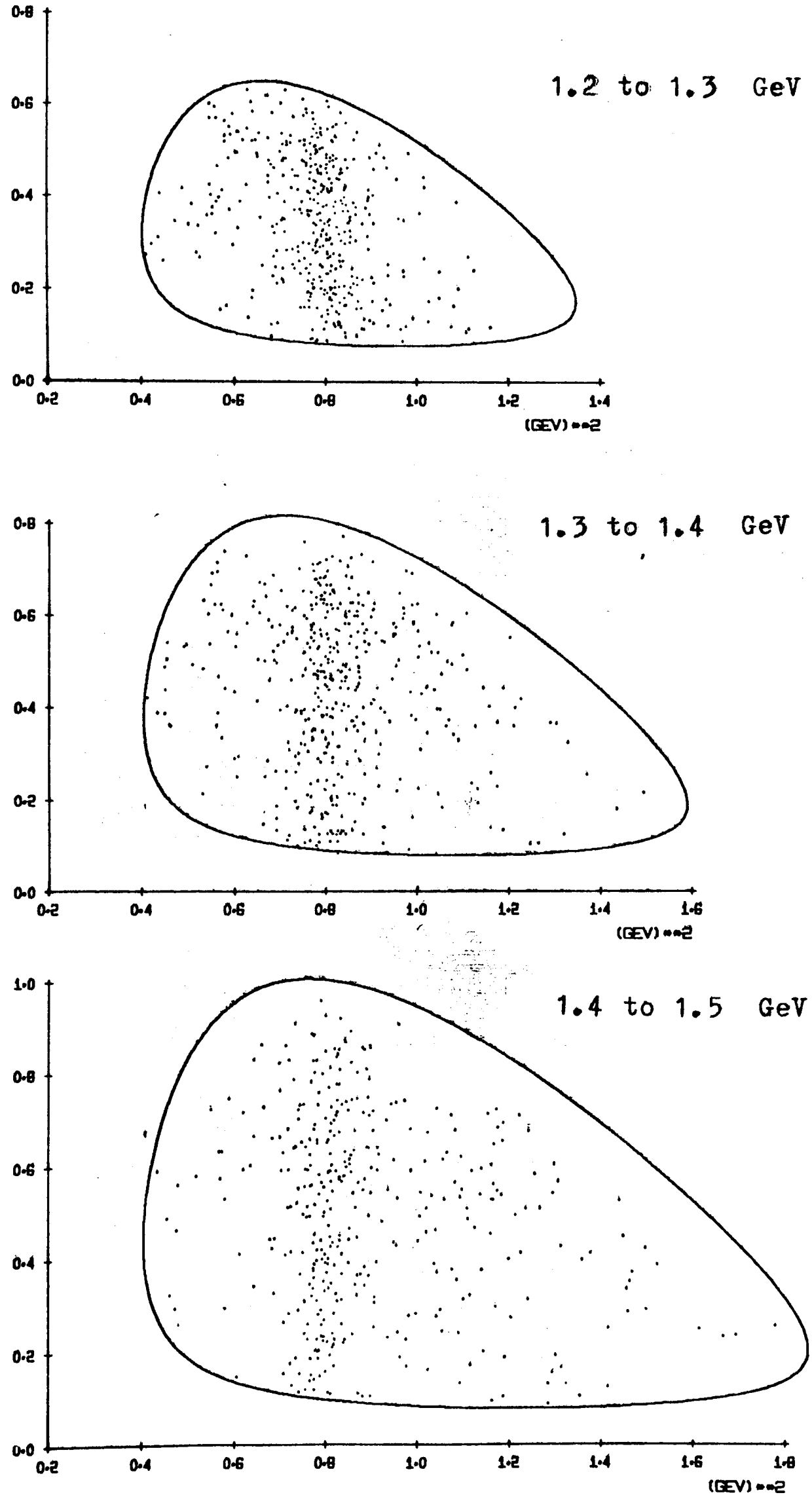

$K^+\pi^+\pi^-$ final state

Fig. 3.10

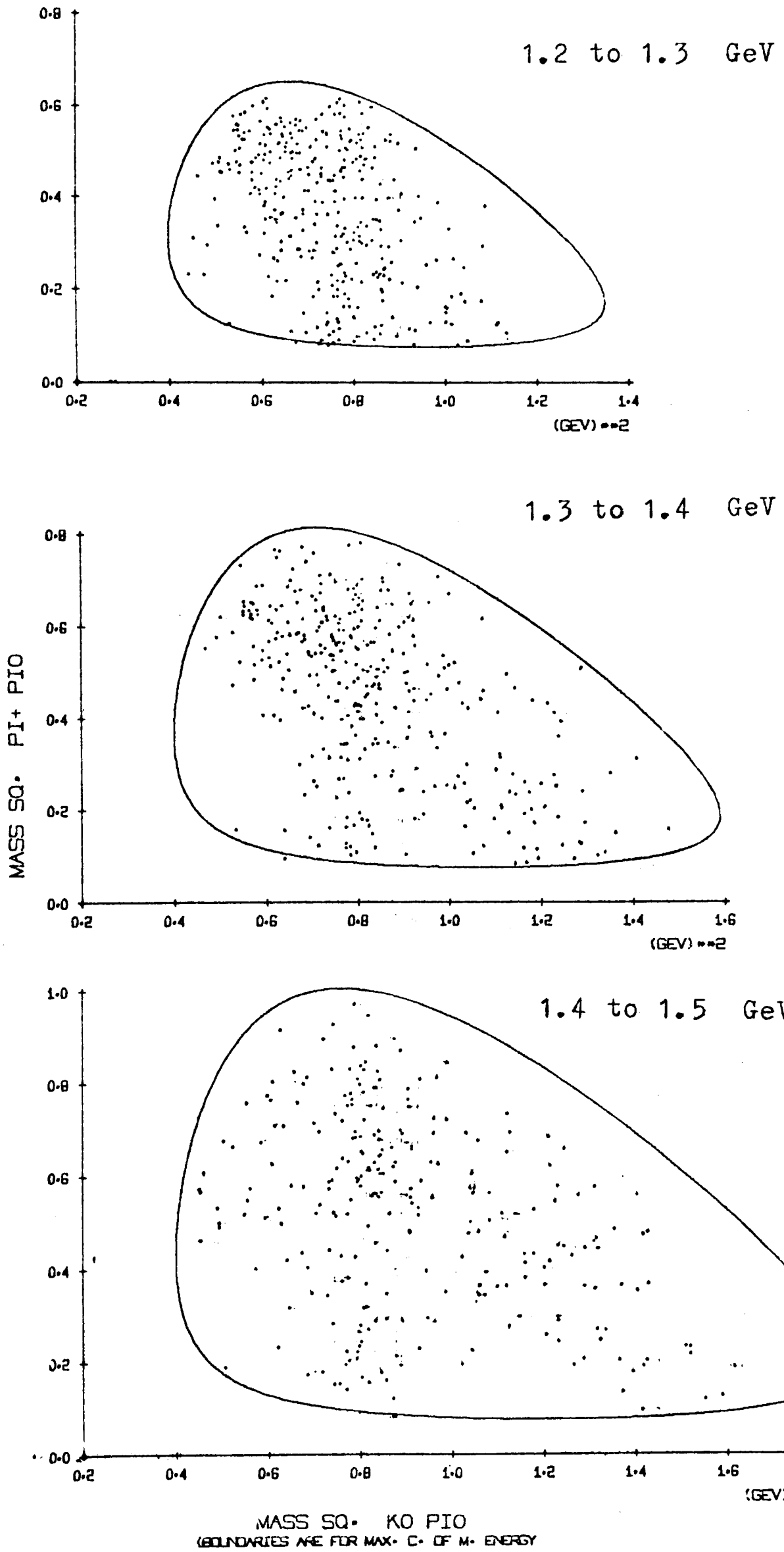

$K^0 \pi^+ \pi^0$ final state

Fig. 3.11

dominant decay processes are:

$$Q \rightarrow K^{*} \pi \quad , \quad K^{*} \hookrightarrow K \pi \tag{8}$$

and

$$Q \rightarrow K \rho \quad , \quad \rho \hookrightarrow \pi \pi \tag{9}$$

Non-relativistic angular momentum theory is used throughout. All details of the calculations and fitting procedures are given in Appendix C. The model will be described in outline only here.

The Q has never been observed in the reaction $K^{+}p \rightarrow K^{o}\pi^{+}\pi^{+}n$ so it is assumed to have isospin $I = 1/2$. The intensities in the two channels $K^{+}\pi^{-}\pi^{+}$ and $K^{o}\pi^{o}\pi^{+}$ may then be written as

$$\left| \langle K^{+}\pi^{+}\pi^{-} \mid T \mid Q \rangle \right|^{2} = 2 \left| \frac{\sqrt{2}}{3} A\left(\underline{p}_{\pi^{+}}, \underline{q}_{K^{+}}\right) BW(K^{+}, \pi^{-}) + \sqrt{\frac{1}{6}}\, a\, e^{i\beta} A\left(\underline{p}_{K^{+}}, \underline{q}_{\pi^{+}}\right) BW(\pi^{+}\pi^{-}) \right|^{2} \tag{10}$$

$$\left| \langle K^{o}\pi^{o}\pi^{+} \mid T \mid Q \rangle \right|^{2} = 2 \left| \frac{1}{3}\left(A\left(\underline{p}_{\pi^{+}}, \underline{q}_{K^{o}}\right) BW(K^{o}, \pi^{o}) - A\left(\underline{p}_{\pi^{o}}, \underline{q}_{K^{o}}\right) BW(K^{o}, \pi^{+})\right) + \sqrt{\frac{1}{3}}\, a\, e^{i\beta} A\left(\underline{p}_{K^{o}}, \underline{q}_{\pi^{+}}\right) BW(\pi^{+}, \pi^{o}) \right|^{2} \tag{11}$$

The factors $a\, e^{i\beta}$ are the relative amplitude and phase to be

determined in the fitting of the $|K\rho\rangle$ mode relative to the $|K^{*}\pi\rangle$ mode. The term $A(\underline{p},\underline{q})$ contains the angular dependence of the decay chain and the centrifugal barrier for the decay of the Q into vector and pseudoscalar. The vector $\underline{p}$ is that of the pseudoscalar recoiling against the vector in the overall centre of mass and $\underline{q}$ is the momentum in the vector centre of mass of one of the decay products. For states of natural spin-parity ($J^P = 1^-, 2^+$) the vector meson and pseudoscalar have a unique orbital angular momentum L between them, while two values of L are possible for states in the unnatural series, $1^+, 2^-$. In the latter case only the lower L value was used.

The function BW(a,b) is a p-wave Breit-Wigner amplitude for vector mesons decaying to particles a and b, and is taken to be

$$BW = \frac{\sqrt{\Gamma_r \frac{M_r}{q_r} \frac{q}{q_r}}}{(M-M_r) + i\frac{\Gamma}{2}} \qquad \text{with } \Gamma = \Gamma_r \left(\frac{q}{q_r}\right)^3 \frac{M_r}{M} \tag{12}$$

Here, M is the mass of the vector meson and $\Gamma = \Gamma_r$, $q = q_r$ when $M = M_r$.* Fitting was carried out by a maximum likelihood procedure for six 50 MeV/c^2 wide mass bins from 1.2 to 1.5 GeV/c^2.

The ideal approach to follow would be to allow all spin-parity terms and all possible decay modes to be present with

---

* The values used for the K^* were $M_r = 0.89$ and $\Gamma_r = 0.05$, and for the ρ, $M_r = 0.765$ and $\Gamma_r = 0.12$.

various degrees of coherence between the modes. This would require numerous parameters. Enormous statistics would be necessary in order to have confidence that the fits were measuring something meaningful. The approach followed here is to apply the simplest models first and only add extra terms when the previous fits prove inadequate.

a) Unique Spin-Parity

The first fits were carried out with the assumption that the events in each bin corresponded to a state of unique J^P of either 1^+, 2^-, 1^- or 2^+. The assumption that the Q region is of pure isospin relates the two final states uniquely and so fits were carried out simultaneously in both of the channels $K^+\pi^-\pi^+$ and $K^o\pi^o\pi^+$. The resulting values of $\mathcal{L}$, the logarithm of the likelihood function, are given in Table 3.2. The relative probability in favour of 1^+ over 2^- is nominally $\gtrsim 10^3$: 1 in all six bins. As expected from the production characteristics 2^+ and 1^- are excluded, the corresponding values of $\mathcal{L}$ being smaller than the values for either 1^+ or 2^- by > 100. It should be emphasised that no simple comparison between the quality of the fits in different bins can be deduced from the $\mathcal{L}$ values. Only fits made with the same sample of data can be compared.

The quality of these fits is illustrated in Fig. 3.12, which shows the experimental projections of the Dalitz plot for bins 1-4, 1.2 - 1.4 GeV/c^2, together with the sums of the four fits for the assumption of $J^P = 1^+$. It is clear that the addition of some relatively isotropic background would improve the agreement between theory and experiment in

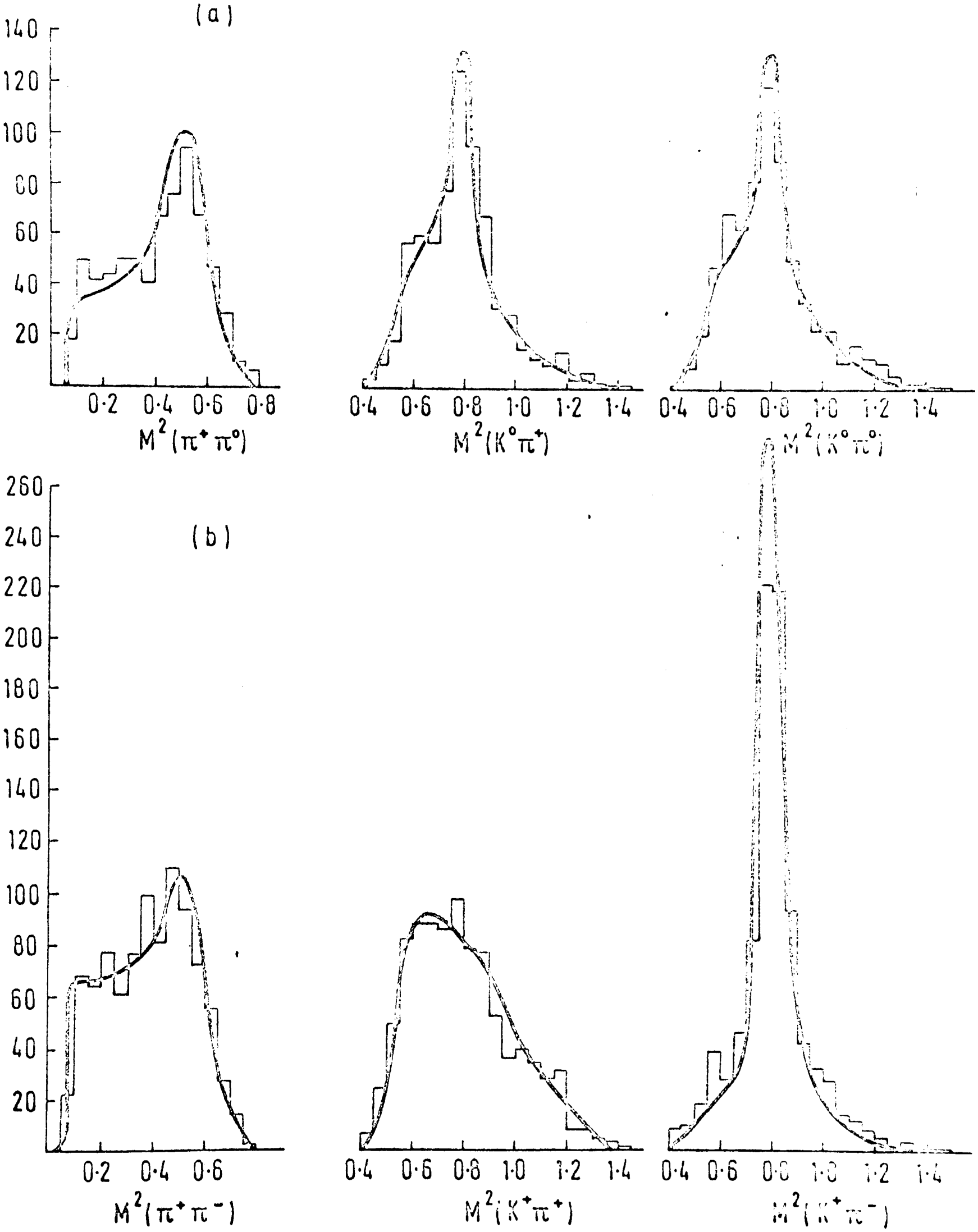

Fitting to 1^+ , no ϵ

Fig. 3.12

Table 3.2

Log. likelihood values for various Dalitz plot fits

Region GeV/c^2	1^+ no ϵ	1^+ with ϵ	1^+ partial coherence	$1^+ 2^-$	$1^+ 0^-$	2^- no ϵ	2^- with ϵ
1. 1.2-1.25	379	383	385	386	385	359	359
2. 1.25-1.3	396	399	405	411	404	389	390
3. 1.3-1.35	248	255	257	261	260	235	236
4. 1.35-1.4	121	140	133	144	147	111	111
5. 1.4-1.45	30	40	37	43	42	9	9
6. 1.45-1.5	-58	-54	-55	-45	-47	-75	-72

the $K^+\pi^-$ mass distribution, and that the ρ signal appearing in the $\pi^+\pi^o$ mass distribution is overestimated. The latter effect was enhanced when subsequently each final state was fitted separately. Table 3.3 contains the values of the parameter a for 1^+ fits to both channels simultaneously and to the two final states separately. The magnitude a of the ρ amplitude is systematically larger in the fits to $K^+\pi^-\pi^+$ than in the fits to $K^o\pi^o\pi^+$, and it is not possible to choose the phase β to suppress the ρ signal in $\pi^+\pi^o$ relative to $\pi^+\pi^-$. This discrepancy could have a number of sources.

It is possible that a residuum of misidentified ambiguous events in the $K^+\pi^-\pi^+$ channel might be responsible for the discrepancy, although there appears to be no evidence for such an effect in the studies of these ambiguities. If the discrepancy is real, however, there are a number of other factors that could be responsible. If the systems have some admixture of $I = 3/2$ the ratio between the ρ signals in the two final states would be freed. While there is no evidence for a significant $I = 3/2$ contribution in $K^+p \rightarrow K^o\pi^+\pi^+n$, this channel cannot contain Kρ. The discrepancy could reflect the inadequacy of the assumption that each bin has unique spin-parity, and finally it is possible that a decay mode $Q \rightarrow K\epsilon$ could increase the apparent ρ signal in $\pi^+\pi^-$, as suggested by Alexander and his collaborators who have observed the same effect [6].

b) Inclusion of an ϵ Term

To try and explain this discrepancy, amplitudes for decay of the Q into $K^+\epsilon$ were included, where the ϵ was taken to be

Table 3.3.i.

$J^P = 1^+$ ρ amplitudes from various fits

Region GeV/c^2	a					
	$K^0\pi^0\pi^+$	$K^+\pi^+\pi^-$	Both channels			
	1^+	1^+ no ϵ	1^+ no ϵ	1^+ with ϵ	1^+2^-	1^+0^-
1. 1.2-1.25	0.81±0.2	1.53±0.2	1.08±0.2	0.94±0.2	0.77±0.1	0.80±0.1
2. 1.25-1.3	1.15±0.2	1.62±0.2	1.32±0.1	1.44±0.2	1.04±0.1	1.09±0.1
3. 1.3-1.35	0.80±0.1	1.01±0.2	0.90±0.1	0.97±0.1	0.71±0.1	0.81±0.1
4. 1.35-1.4	0.42±0.08	1.04±0.1	0.74±0.07	0.68±0.1	0.48±0.1	0.48±0.1
5. 1.4-1.45	0.47±0.08	0.71±0.1	0.58±0.06	0.59±0.1	0.33±0.1	0.50±0.1
6. 1.45-1.5	0.74±0.1	0.71±0.1	0.67±0.07	0.63±0.1	0.64±0.1	0.62±0.1

- continued -

Table 3.3 continued

Table 3.3.ii

$J^P = 1^+$ ρ phases for various fits

Region	β (radians)					
	$K^o\pi^o\pi^+$	$K^+\pi^+\pi^-$	Both channels			
	1^+	1^+ no ϵ	1^+ no ϵ	1^+ with ϵ	1^+2^-	1^+0^-
1.	0.01±0.4	1.4±0.4	0.7±0.3	0.06±0.4	-0.64±0.4	0.06±0.3
2.	0.24±0.2	0.42±0.1	0.29±0.1	0.11±0.2	-0.49±0.3	-0.05±0.3
3.	0.26±0.2	0.25±0.1	0.23±0.1	0.05±0.1	-0.34±0.3	0.15±0.2
4.	0.11±0.3	1.7±0.2	0.77±0.2	0.03±0.2	-0.16±0.3	0.45±0.3
5.	0.91±0.3	1.6±0.3	1.21±0.3	0.69±0.3	0.21±0.4	0.75±0.3
6.	1.10±0.3	2.2±0.2	1.82±0.2	1.52±0.3	1.20±0.6	1.20±0.3

Table 3.4

$J^P = 1^+$ ϵ terms for various fits

Region	Both channels		
	Amplitude γ		
	1^+	$1^+ 2^-$	$1^+ 0^-$
1.	1.17±0.25	1.01±0.2	1.0±0.5
2.	1.23±0.3	0.81±0.2	0.56±0.5
3.	0.98±0.2	0.67±0.2	0.98±0.3
4.	1.36±0.2	1.47±0.2	0.47±0.3
5.	0.84±0.2	0.71±0.2	0.61±0.2
6.	0.75±0.2	0.31±0.1	0.53±0.3
	Phase δ (radians)		
1.	0.27±0.5	-0.6±0.7	0.0±0.6
2.	-1.67±0.5	2.0±0.7	0.7±1.3
3.	-1.39±0.6	-0.25±0.8	0.4±0.5
4.	-1.62±0.3	-1.7±0.3	-0.8±0.9
5.	-0.23±0.4	-0.9±0.5	-0.2±0.6
6.	-0.29±0.4	-2.2±2.0	0.2±0.9

Table 3.5

Percentage contributions from fitting to pairs of angular momenta

Region	% of 2^- from $1^+ + 2^-$	% of 0^- from $1^+ + 0^-$	% of pure s-wave from 1^+ s + d-wave
1.	23	11	84
2.	27	10	93
3.	29	12	84
4.	28	23	84
5.	20	8	99
6.	45	25	84

Table 3.6

Values of $\frac{d\sigma}{dm}(K^+\pi^+\pi^-)/\frac{d\sigma}{dm}(K^0\pi^0\pi^+)$,

theory and experiment

Region	Experimental (Errors are statistical)	1^+ fits no ϵ	1^+ fits with ϵ
1.	0.86±0.09	0.85	0.86
2.	0.87±0.08	0.77	0.88
3.	0.80±0.08	0.82	0.91
4.	0.95±0.08	0.84	1.11
5.	0.91±0.08	0.89	0.90
6.	1.08±0.09	0.88	0.96

an s-wave $\pi\pi$ interaction with I = 0, represented by a Breit-Wigner of mass 720 MeV/c^2 and width 250 MeV/c^2. (Other values of the ϵ parameters were tried but the fits proved insensitive to the values used).

The fitting was repeated for the two channels simultaneously for the hypotheses 1^+ and 2^- with the ϵ terms included in the $K^+\pi^+\pi^-$ final state. The amplitudes and phases of both ρ and ϵ relative to the K^* amplitude were variables. Significantly larger values of $\mathcal{L}$ were obtained for the 1^+ hypothesis, but not for 2^- (see Table 3.2). However, comparing in Table 3.3 the ρ amplitudes for the joint fits to 1^+ both with and without ϵ, there appears to be essentially no change in these amplitudes. The discrepancy remains.

One of the arguments Alexander et al. gave for the need to include an ϵ decay mode was that in their data the ratio of the cross-sections for Q production in the two channels was ~ 1. This is in agreement with the isospin predictions for a $K^*\pi$ decay mode but for $K\rho$ decay the ratio $\sigma(K^+)/\sigma(K^o)$ should be $\frac{1}{2}$. An extra mode contributing to the $\sigma(K^+)$ term would permit the ratio to remain near unity with still appreciable $K\rho$ decay. To test these arguments on this data, the predicted $K^+\pi^+\pi^-$ to $K^o\pi^o\pi^+$ relative cross-sections were calculated from the results of the fits to 1^+ both with and without ϵ terms and compared with experiment (see Table 3.6). The experimental ratios here are mostly slightly below unity. The fits with $K^+\epsilon$ give predicted ratios only slightly higher than those without. Both are consistent within errors with the data, though the fits with ϵ are marginally better.

The cross-section estimates do not appear to be sensitive tests of the presence of the ϵ mode, as its major influence in the fits appears to be from the $K^{*}-\epsilon$ and $\rho-\epsilon$ interference terms.

c) Fits to pairs of spin-parity states

The discrepancy in the ρ amplitudes, as suggested, may be a manifestation of the inadequacy of a model of a pure spin-parity state. Consequently fitting was carried out on pairs of angular momenta to both final states simultaneously. As the unnatural spin-parity series appears the most likely, the pairs tried were 1^{+} and 2^{-}, and 1^{+} and 0^{-}, all states containing an ϵ term in the $K^{+}\pi^{+}\pi^{-}$ channel. The variables were the ρ and ϵ amplitudes and phases which were independent for each spin parity and the amounts of 2^{-} or 0^{-} relative to 1^{+}. The resulting values of ℓ are given in Table 3.2 and the fraction of each state in Table 3.5. A mixture of 1^{+} and 2^{-} is slightly favoured over 1^{+} and 0^{-}, but in both cases 1^{+} is dominant. The contribution of 2^{-} is less than 30% in the first five bins and of 0^{-} is $\sim$ 15% in these bins. The sums of the fitted projections for bins 1-4, under the assumption of 1^{+} and 2^{-} is shown in Fig. 3.13. All projections are well fitted and no discrepancy remains among the ρ signals; a combination of 1^{+} and 2^{-} $K\pi\pi$ states with $I = 1/2$ provides an extremely good representation of the Dalitz plot in the Q region.

d) Other hypotheses

The assumption of complete coherence between the $|K^{*}\pi>$

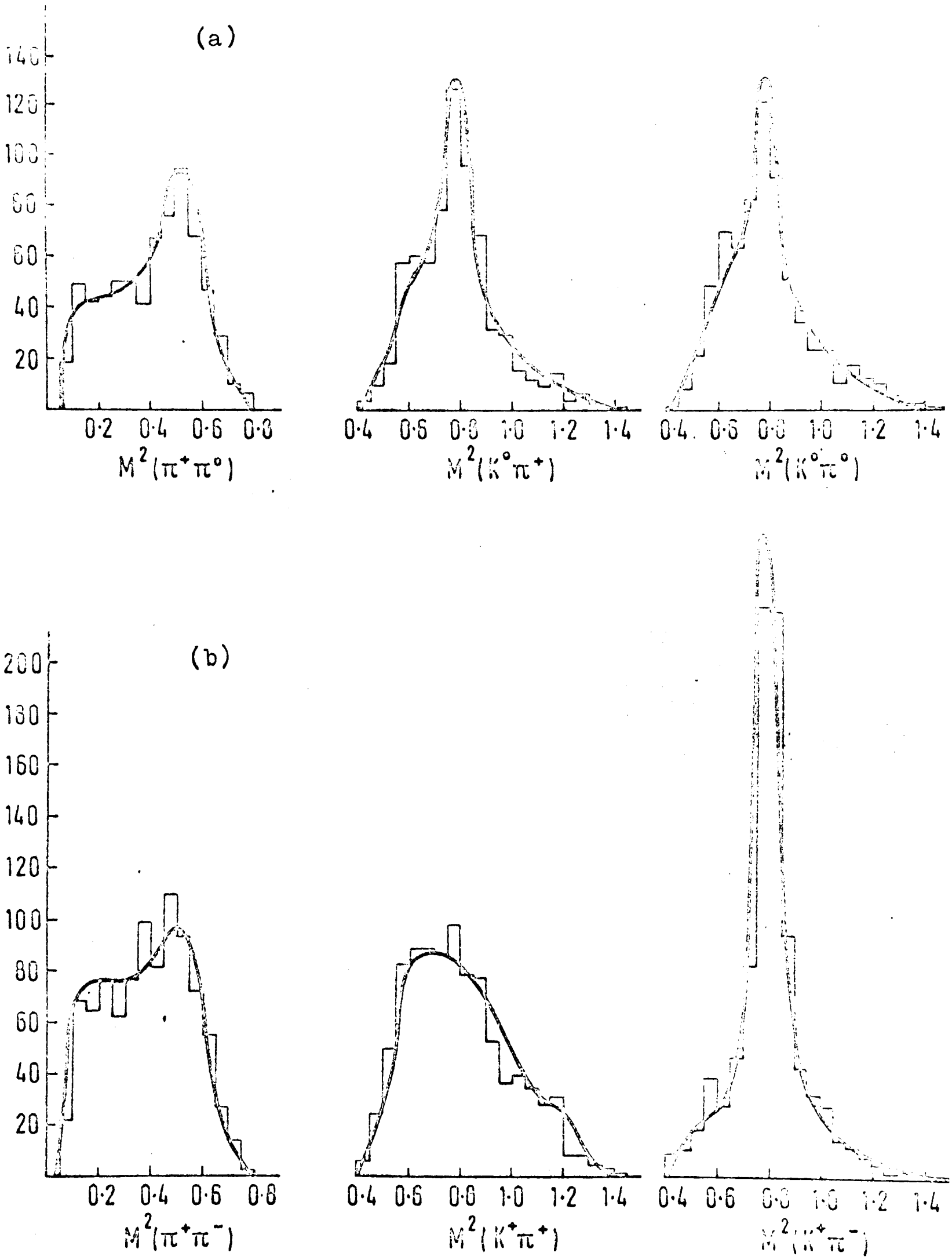

Fitting to $1^+$and 2^-

Fig. 3.13

and $|K\rho\rangle$ modes is implicit in the model used. If, however, the 1^+ $K\pi\pi$ system has structure in the Q region, coherence between the $K\rho$ and $K^*\pi$ final states could be destroyed in integration over the variable t, in integration over the orientation of the normal to the decay plane and in integration over the 50 MeV/c^2 mass bins. In the subsequent fitting the amount of interference between these two modes was allowed to vary. The two channels $K^+\pi^+\pi^-$ and $K^0\pi^0\pi^+$ were then fitted to the 1^+ amplitudes with α, β and ξ as variables, where ξ was a coherence factor constrained to be between 0 and 1 which multiplied the interference terms. No ϵ amplitudes were included. The resulting ℓ values (see Table 3.2) are comparable to those fits with an ϵ mode. The variation of α is essentially unchanged, though ξ is only $\sim$ 0.3 in most bins (see Fig. 3.14).

Because of a possible d-wave decay of a 1^+ state into a pseudoscalar and vector meson, fitting was carried out for both channels simultaneously to a coherent superposition of s- and d-wave 1^+ amplitudes. No ϵ amplitudes were present. The results were generally worse than pure s-wave fits with an ϵ amplitude and the contribution of pure s-wave to the total intensity was $\geq$ 84% in all bins (see Table 3.5). There is no indication in the data of any significant d-wave decay.

The possible presence of $K^*(1420)$ in the Q was tested by applying fits to the data in this region with the pair of waves 1^+ and 2^+. The percentage of 2^+ in the last 4 bins was 22%, 23%, 7% and 16% respectively. Thus in bin 5 (1.4 to

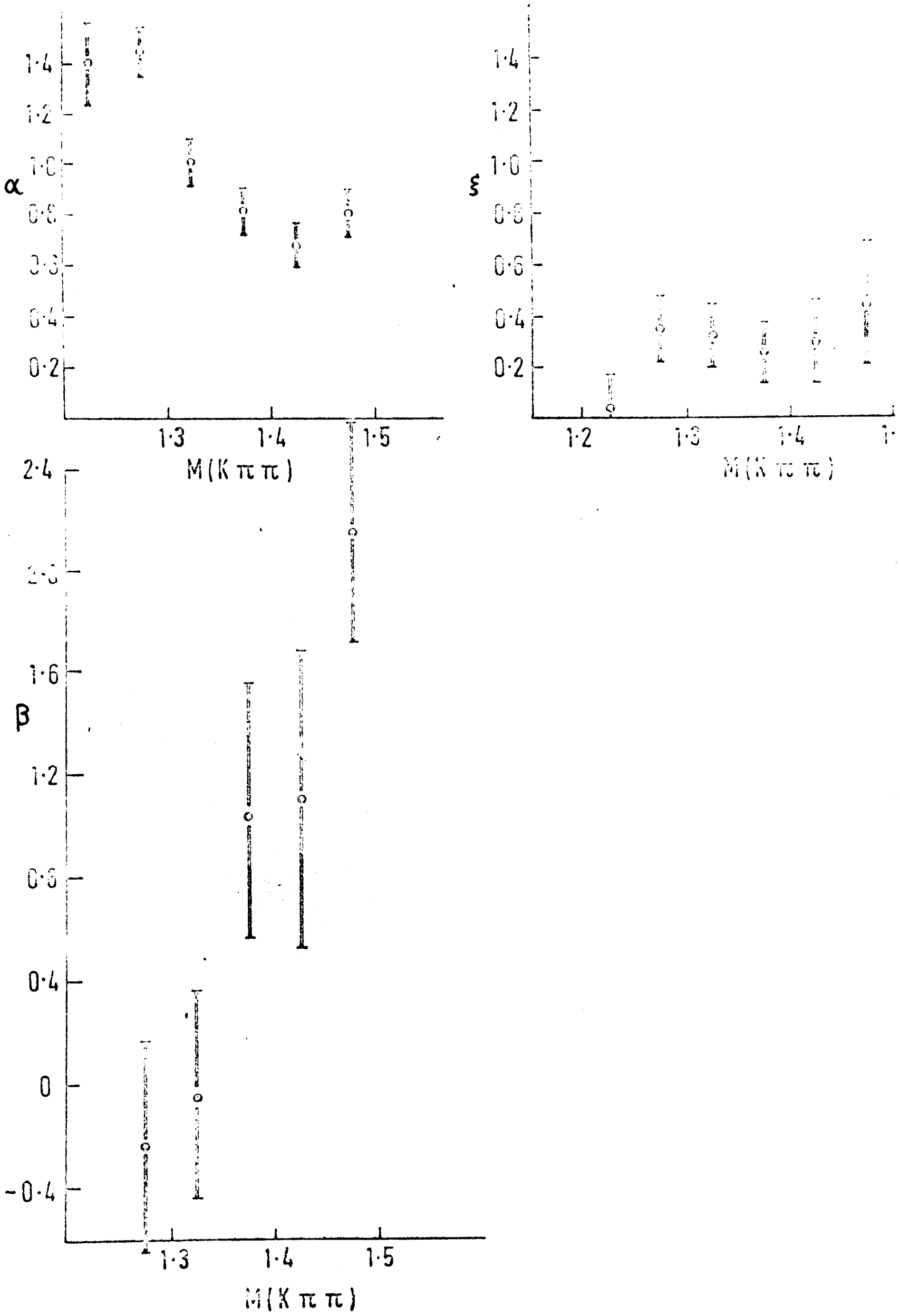

Fitting to 1^+ with partial coherence factor

Fig. 3.14

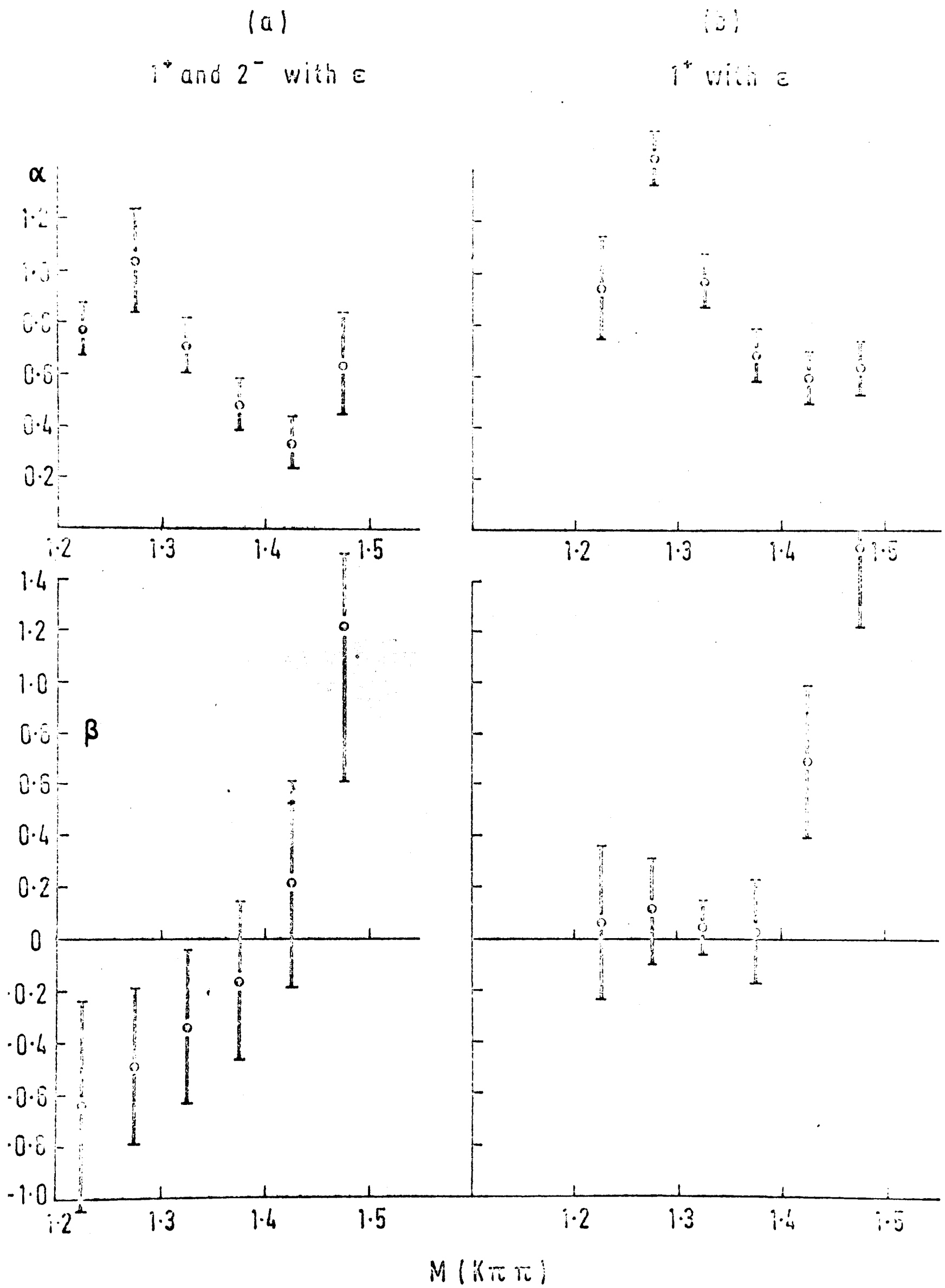
(a)
1⁺ and 2⁻ with ε
(b)
1⁺ with ε
α
β
1·2
1·3
1·4
1·5
1·0
0·8
0·6
0·4
0·2
0
-0·2
-0·4
-0·6
-0·8
-1·0
M (Kπ π)

Fig. 3.15

1.45 GeV/c^2) where the contribution is expected to be greatest, it in facts dips down to 7%; again suggesting no appreciable $K\pi\pi$ decay mode of the $K^*(1420)$.

e) Discussion of results

In Tables 3.3(i) & 3.3(ii) the amplitudes and phases of the 1^+ $|K\rho>$ term may be compared for the several hypotheses tried. For most of them especially (i) Pure 1^+, (ii) 1^+ and 2^-, (iii) 1^+ and 0^-, and (iv) 1^+ with partial coherence very similar variations in α and β are observed. Indeed, the values obtained from fitting hypotheses (ii) and (iii) to both final states simultaneously are in excellent agreement with the results of fitting hypothesis (i) to $K^0\pi^0\pi^+$ alone where neither ϵ amplitudes nor misidentified $K^+\pi^-\pi^+$ events can contribute. This internal consistency among the variables in the 1^+ amplitude encourages the belief that the variations of both magnitude and phase of the ρ are physically significant. The values of α and β for some hypotheses are displayed in Figs. 3.14 and 3.15 for ease of comparison, and the effect on the $\pi\pi$ Dalitz plot projections of these variations together with the fits to 1^+ and 2^- are shown in Fig. 3.16. The variation in both magnitude and phase of the ρ amplitude could be produced by interference between a single resonance and an appropriate background. However, taken in conjunction with the mass distribution it finds a more natural interpretation in terms of interference between two 1^+ resonances with different signs between the amplitudes for decay into $K^*\pi$ and $K\rho$, essentially the hypothesis put forward by Goldhaber. The small value of ξ in the fits with a partial coherence

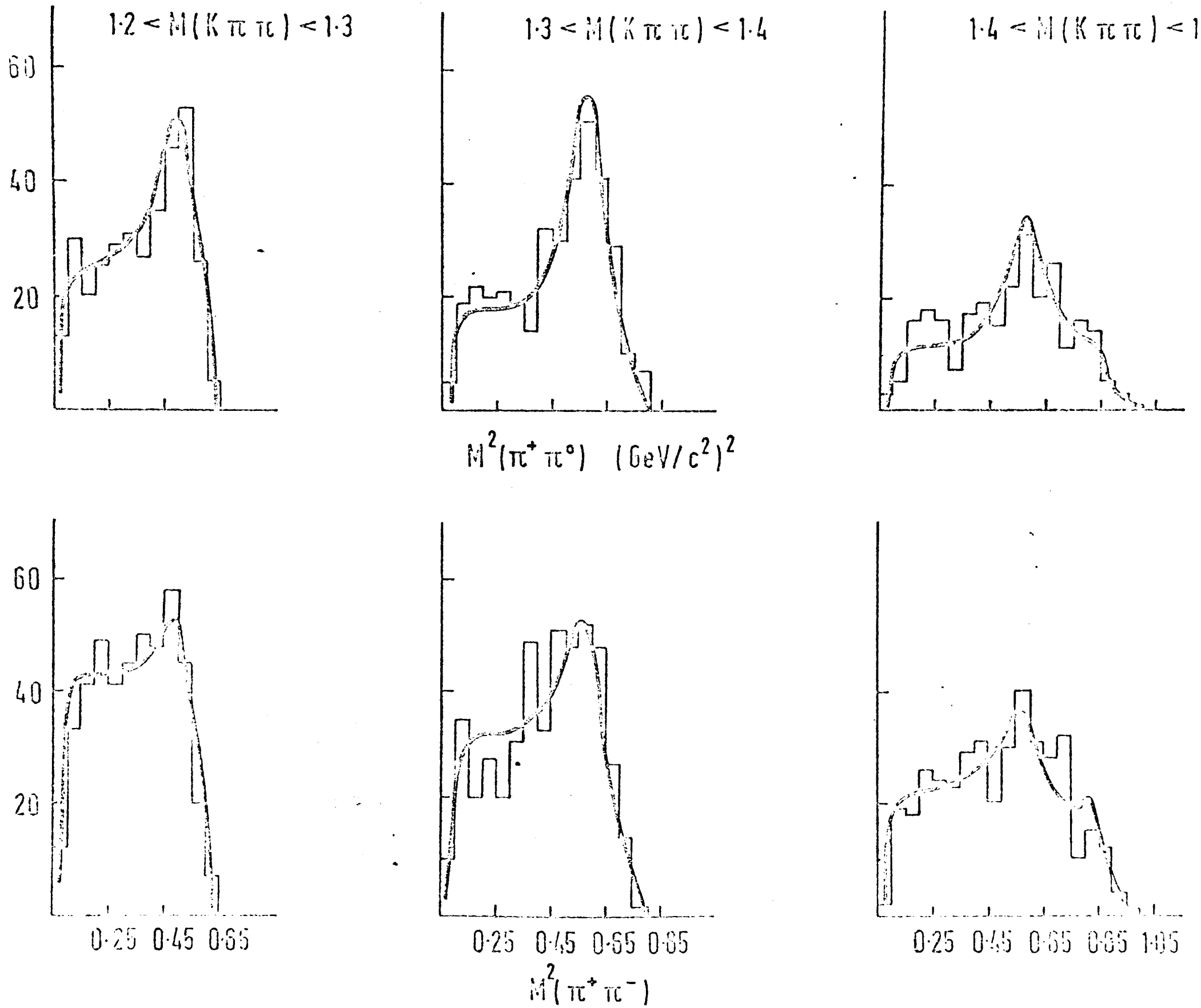
1·2 < M (K π π) < 1·3
1·3 < M (K π π) < 1·4
1·4 < M (K π π) < 1·5
60
40
20
M²(π⁺ π°) (GeV/c²)²
60
40
20
0·25 0·45 0·65
0·25 0·45 0·55 0·65
0·25 0·45 0·65 0·85 1·05
M²(π⁺ π⁻)

Fig. 3.16

factor may only reflect on the inadequacy of fitting a single angular momentum state to the Dalitz plot, but the results of this fit in no way weaken the evidence for structure in the 1^+ amplitude, in that the variation of β is enhanced by relaxing the constraints in the interference term.

The background terms (i.e., all other terms than $K^*\pi$ or $K\rho$ in a 1^+ state) have not been so well determined. The $K\epsilon$ relative amplitude and phase for 1^+ is not as independent of other terms present as the $K\rho$ (see Table 3.4) and in view of the uncertainty in the effect of a small residuum of misidentified $K^+\pi^+\pi^-$ events the quantitative estimates of the ϵ cannot be regarded as reliable.

In connection with the 2^- contribution, the quantity K appearing in expression (6) may be calculated from the 2^- ρ and ϵ amplitudes resulting from the joint 1^+ and 2^- fits. This has been done. The value of K was ~ 3 in all bins corresponding to values around -0.5 for W_2^0 and +0.2 for W_4^0, for the 2^- contribution. Thus production of 1^+ and 2^- by spin zero exchange and decay structure determined by the Dalitz plot fits will not reproduce the experimental values of W_2^0 and W_4^0 in the region 1.3 - 1.5 GeV/c^2.

8 Conclusions

The analyses of this chapter indicate that in the region 1.2 to 1.45 GeV/c^2, the contribution of states with $J^P \neq 1^+$ is $\lesssim 25\%$ of the total intensity and the hypothesis that the Q enhancement consists of two 1^+ resonances is supported by

the variations in the $|K^*\pi\rangle$ and $|K\rho\rangle$ relative amplitudes.

Even in those experiments where no splitting is observed, the general shape of the Q is suggestive of two unresolved resonances superimposed on a slowly varying background. The splitting observed in this data, and at 9 GeV/c [6] reinforces such a model.

REFERENCES

[1] See R.H. Dalitz — High Energy Physics, Les Houches, 1965 (Gordon+Breach) for further details.

[2] See O.W. Greenberg — Proceedings of the Lund International Conference on Elementary Particles (1969), p. 387 for a discussion on these assignments.

[3] G. Goldhaber — Phys. Rev. Lett. 19, 976 (1967).

[4] A. Firestone — Talk presented at the 1970 Conference on Meson Spectroscopy, Philadelphia. UCRL-19846 (1970) preprint.

[5] G. Bassompierre et al. — Phys. Lett. 26B, 30 (1967).

[6] G. Alexander et al. — Nuc. Phys., B13, 503 (1969).

[7] F. Bomse et al. — Phys. Rev. Lett. 20, 1519 (1968).

[8] C.Y. Chien et al. — Phys. Lett. 28B, 143 (1968).

[9] A. Barbaro-Galtieri et al. — Phys. Rev. Lett. 22, 1207 (1969).

[10] M.S. Farber et al. — Phys. Rev., D1, 78 (1970).

[11] Astier et al. — Nuc.Phys., B10, 65 (1969).

[12] C.Y. Chien et al. — Phys. Lett. 29B 433 (1969).

[13] M.S. Farber et al. — Phys. Rev. Lett. 22, 1394 (1969).

[14] K. Barnham et al. — Submitted to Nuclear Physics.

[15] S.M. Berman, M. Jacob — Phys. Rev. 139B, 1023 (1965).

[16] See D. Branson, P.V. Landshoff and J.C. Taylor — Phys. Rev. 132, 902 (1963) for further details.

CHAPTER 4

THE $p\pi\pi$ SYSTEM

1 Introduction

In recent years several methods have been used to gain information on $p\pi\pi$ systems. Elastic scattering π-p phase shift analyses have been carried out by several groups. Using this technique numerous N^* resonances have been found in both the $I = 1/2$ and $I = 3/2$ isospin states [1]. Many of these are predicted to be highly inelastic and so should probably be seen in $\pi\pi N$ final states as well. Bubble Chamber experiments have been performed to study the inelastic processes $\pi p \rightarrow \pi\pi N$ directly. Detailed studies of the pure $I = 3/2$ channel [2] ($\pi^+ p$ scattering experiments) and mixtures of the $I = 3/2$ and $I = 1/2$ channels [3] (e.g. $\pi^- p$ scattering experiments) have been carried out particularly for low N^* masses ($\lesssim 1.6$ GeV/c^2). More general fitting [4] has also been done for a larger range of $\pi\pi N$ masses. These analyses have in many cases confirmed the qualitative features predicted by the elastic scattering experiments.

The study of N^* systems has also been followed in production experiments. Counter and spectrometer methods have been used for pp [5] and πp [6] scattering processes, where the N^* is measured only as missing mass (M). These techniques provide data with good statistics in the distributions of M and t (the momentum transfer to the N^* system) but do not allow a study of the internal properties of the N^*.

Bubble Chamber experiments, on the other hand have provided relatively meagre statistics with p-p [7], π-p [8] and K-p [9] interactions but they allow the possible measurement of the internal quantum numbers of the N^* system.

In this experiment production of low mass N^* systems corresponds to those events lying on Face 2 of the cub-octahedron of Chapter 1, mainly in the $K^+\pi^+\pi^-p$ final state. From production experiments very little has been firmly established as to the properties of this $p\pi^+\pi^-$ system. It is predominantly $I = 1/2$ (see Section 3) and appears to have two mass peaks. The first is generally found in the range 1.45 - 1.5 GeV/c^2 in bubble chambers and the second between 1.68 and 1.72 GeV/c^2. The lower peak has been tentatively identified with the Roper $P_{11}(1470)$ and the upper peak [7] with the $F_{15}(1688)$ of phase-shift analyses. However, the spin-parity analyses of the $p\pi^+\pi^-$ system are generally inconclusive. Models of non-interfering resonances and background subtraction procedures have been used. Both methods appear dangerous according to the data available here.

There exists some disagreement between the results of spectrometer and bubble chamber experiments which has yet to be reconciled. The lower peak in spectrometer experiments appears at a mass near 1.4 GeV/c^2 produced with a very sharp momentum transfer distribution of $\sim e^{20t}$, though the peak in some cases [5] is seen to move to a mass near 1.52 GeV/c^2 at higher values of t. This effect is not generally apparent in chamber experiments, including this one described below.

2 The $p\pi^+\pi^-$ Mass Spectrum at 10 GeV/c

The $p\pi^+\pi^-$ invariant mass distribution for all unique events from the reaction $K^+p \rightarrow K^+\pi^+\pi^-p$ is shown in Fig. 4.1. (The ambiguous events contribute a negligible proportion of the total to the region of interest here and have been neglected in all subsequent analyses.) A clear peak is visible in the data centred at a mass of 1.7 GeV/c^2 with a width $\sim$120 MeV/c^2. No other peak is resolved, though a shoulder is apparent in the distribution below 1.5 GeV/c^2. The unshaded histogram of Fig. 4.2(a) shows the same distribution for those events produced with a momentum transfer squared to the K^+ of $|t| < 0.5$ (GeV/c)^2 after antiselection of the $K^{*o}(890)$ defined by $0.83 < M(K^+\pi^-) < 0.95$ GeV/c^2. Two peaks are now clearly visible, one centred at 1.48 GeV/c^2 and the other at 1.69 GeV/c^2. The shaded histogram of Fig. 4.2(a) has the additional selection of $p\pi^+$ mass in a narrow band in the $\Delta^{++}(1236)$ region (1.15 to 1.30 GeV/c^2). There appears to be a rapid fall off in the proportion of events decaying via the Δ^{++} above a mass of 1.75 GeV/c^2. At low masses it is not clear that Δ^{++} is necessarily dominant in the decay, as phase space restricts $p\pi^+$ mass to this region anyway. Though from Figs. 4.3 (a),(b) and (c) of the Dalitz plot distributions for 100 MeV/c^2 wide mass regions centred at 1.48, 1.58 and 1.68 GeV/c^2, the Δ signal clearly shows up in the first and third regions.

3 Production Characteristics

The data show features characteristic of diffractive

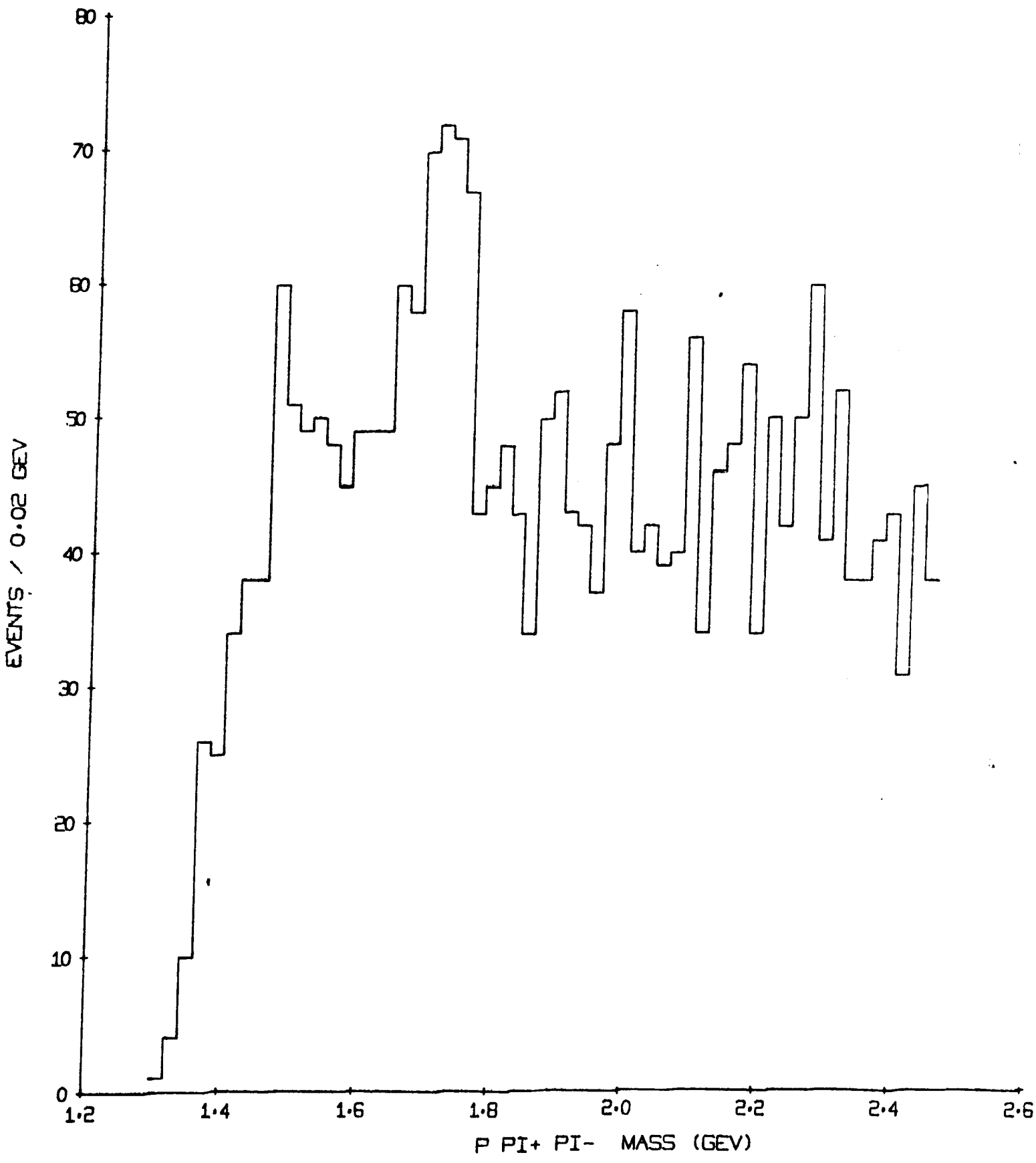
80
70
60
50
40
30
20
10
0
EVENTS / 0.02 GEV
1.2
1.4
1.6
1.8
2.0
2.2
2.4
2.6
P PI+ PI- MASS (GEV)

Fig. 4.1

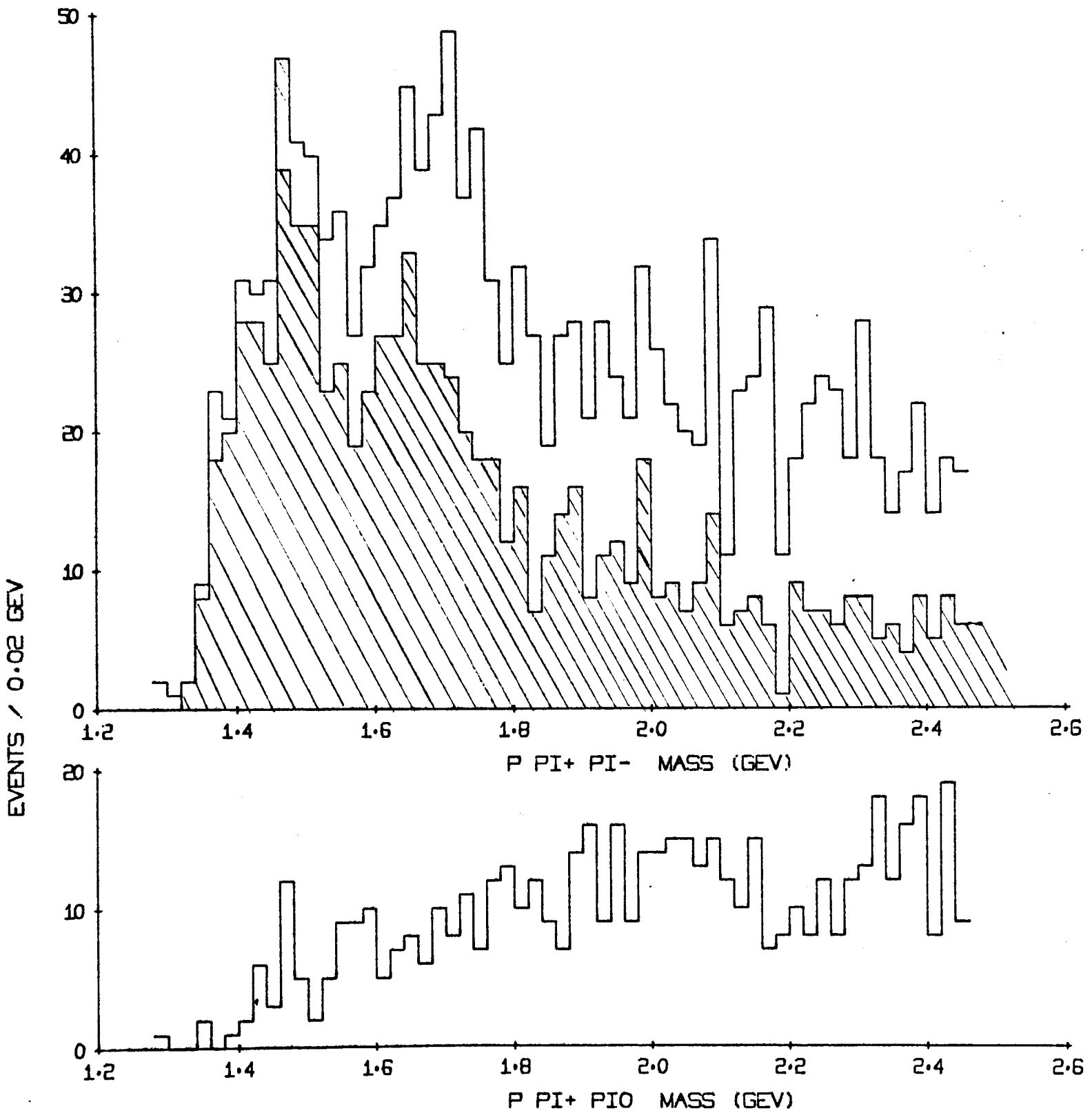
EVENTS / 0.02 GEV
50
40
30
20
10
0
1.2
1.4
1.6
1.8
2.0
2.2
2.4
2.6
P PI+ PI- MASS (GEV)
20
10
0
1.2
1.4
1.6
1.8
2.0
2.2
2.4
2.6
P PI+ PIO MASS (GEV)

Fig. 4.2

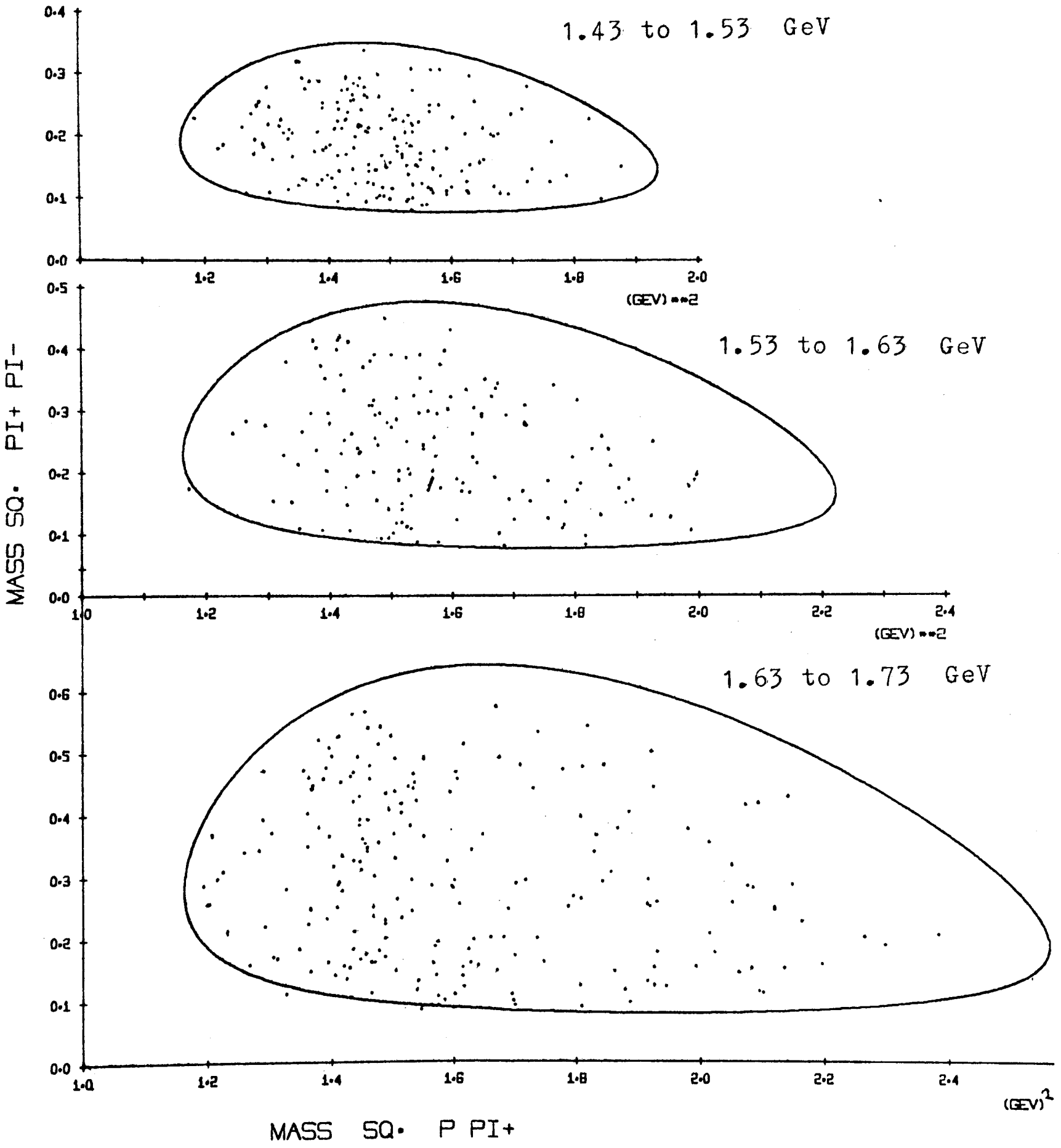
1.43 to 1.53 GeV
1.53 to 1.63 GeV
1.63 to 1.73 GeV
MASS SQ. PI+ PI-
(GEV)**2
MASS SQ. P PI+
(GEV)^2

Fig. 4.3

production of the $p\pi^+\pi^-$ system. This system is produced peripherally, most events having $|t| < 0.4$ (GeV/c)^2. Figure 4.4 shows the $|t|$ distributions for 100 MeV/c^2 mass regions centred at 1.48, 1.58 and 1.68 GeV/c^2. The lines are a fit to the data of an exponential e^{at} out to $|t| = 0.4$ (GeV/c)^2. The values obtained for a are 7.3 ± 0.7, 6.8 ± 0.8 and 4.8 ± 0.8 respectively. The last two values are consistent with other experiments both spectrometer and bubble chamber but the first slope disagrees with the characteristic sharp forward peak observed in spectrometer experiments. The data are consistent with a larger value of a (~ 10) below 0.2 (GeV/c)^2 in the first region but the statistics are too poor to draw any further conclusions.

Production appears to be dominated by I = 0 exchange which leaves the N^* system in an I = 1/2 state. An estimate of the I = 3/2 contribution to these data can be obtained from the reaction $K^+p \rightarrow K^0\pi^0\pi^+p$. Here the $p\pi^+\pi^0$ system is in a pure I = 3/2 state. Figure 4.2(b) shows the $p\pi^+\pi^0$ mass distribution from this reaction for those events satisfying the same selection criteria as applied to the unshaded histogram of Fig. 4.2(a). No low mass $p\pi^+\pi^0$ enhancement is observed. If it is assumed that the I = 3/2 state couples to $\Delta\pi$ only, then by conservation of isospin the ratio of production of $\Delta^{++}\pi^0$ to $\Delta^{++}\pi^-$ for these two reactions is predicted to be 9 : 2. This would put an upper limit to the I = 3/2 intensity of 8 ± 3% of the $p\pi^+\pi^-$ final state at a mass of 1.75 GeV/c^2 and less than this value at lower masses.

The distribution of the Treiman-Yang angle of the normal

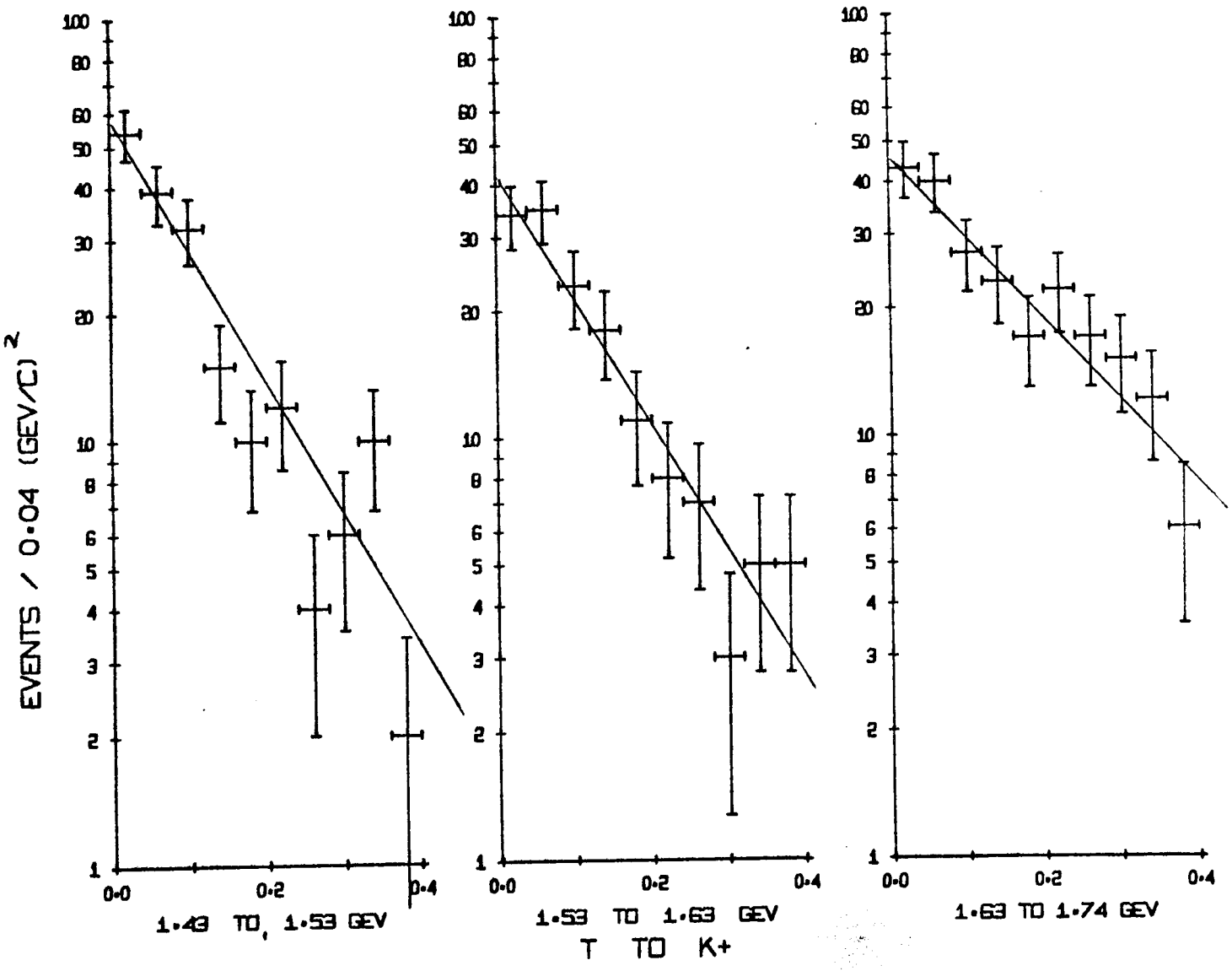
EVENTS / 0·04 (GEV/C)²
1·43 TO 1·53 GEV
1·53 TO 1·63 GEV
1·63 TO 1·74 GEV
T TO K+

Fig. 4.4

to the $p\pi^+\pi^-$ decay plane is isotropic, consistent with production by spin zero exchange. This will be discussed further in the next section.

4 Angular Properties

The angles of interest in the reaction $p + e \rightarrow p + \pi^+ + \pi^-$ where e is the virtual exchange particle, are exactly akin to those studied in Chapter 3, Section 6, for the $K\pi\pi$ system. The only change is that the kaon is now replaced by the proton and the X axis is conveniently taken to be in the direction of the π^- within the $p\pi\pi$ decay plane.

The angular distribution $W(\Theta, \phi)$ of the normal to the $p\pi\pi$ decay plane referred to the Oxyz set of axes was expanded into moments W_L^M. No sign of any ϕ dependence was detected, i.e., all W_L^M with $M \neq 0$ were consistent with zero. This is indicative of spin zero exchange.

Following Chapter 3, the alternative approach of expanding the distribution $w(\Theta, \psi)$ of the incoming proton referred to the OXYZ axes into moments w_L^m was followed. The results of this procedure for the more significant w_L^m's between 1.35 and 2.0 GeV/c^2 are shown in Fig. 4.5. Unfortunately, unlike the $K\pi\pi$ system, in this case no quantitative fitting can be carried out on the moments w_L^m for any spin-parity hypotheses. The essential difference between this case and that of Chapter 3 is that the proton spin introduces an extra degree of freedom. This problem has been considered in detail by Cashmore [10]. His main conclusion was that, although spin-flip and non spin-flip terms for each value of J and Λ

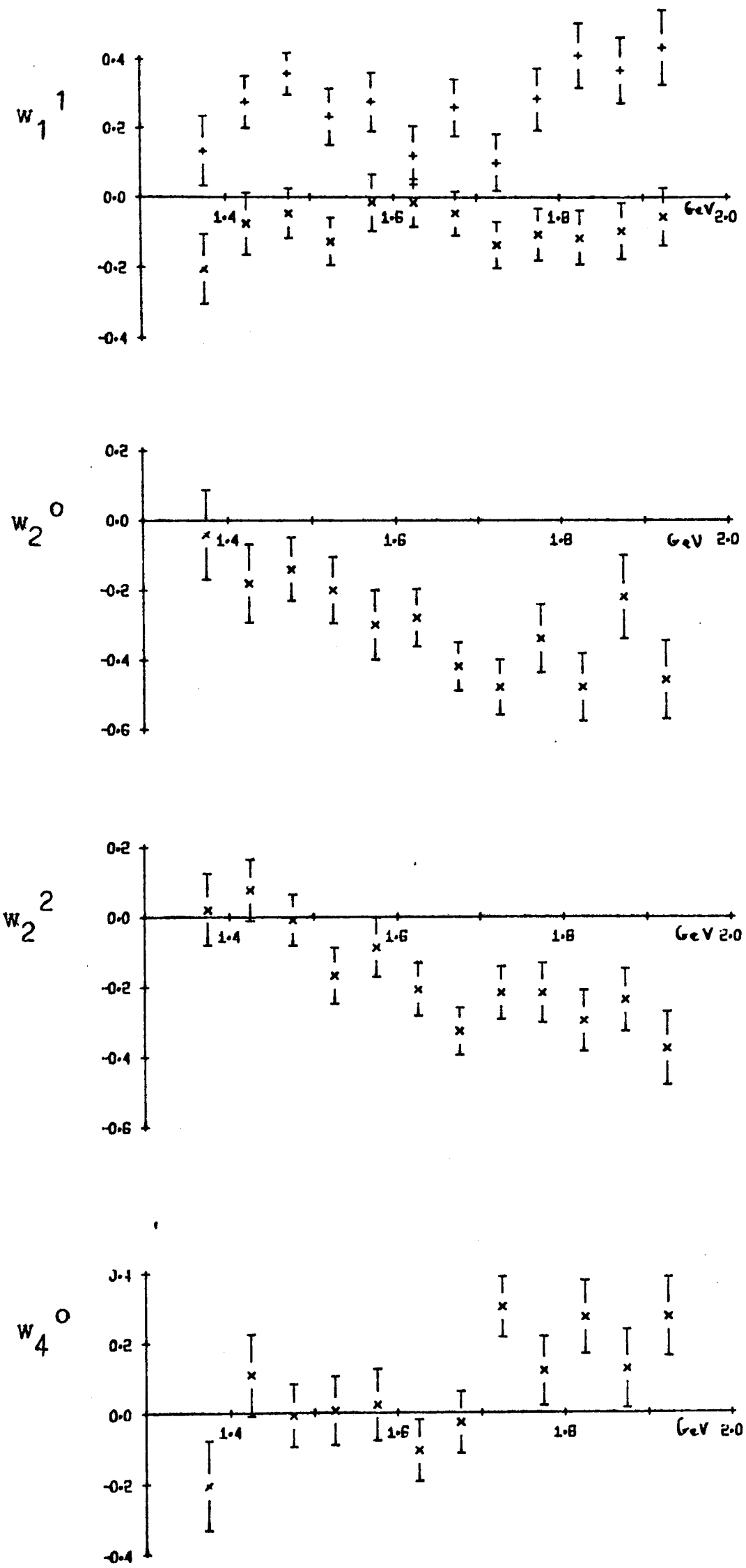

VARIATION OF MOMENTS WITH P PI+ PI- MASS

Fig. 4.5

lead to identical angular distributions, they correspond to states of opposite parity, and without measurement of the final proton spin, constrained fits are impossible. However, qualitative conclusions can be drawn from the moments in Fig. 4.5. The imaginary part of w_1^1 is seen to be large and positive throughout the entire mass region considered, requiring interference between at least two waves of different spin-parity throughout the region. The w_2^0 moment is non – zero above 1.4 GeV/c^2, indicating the presence of some spin $J \geqslant 3/2$ even in the 1.48 region. Like the w_2^0, the w_2^2 moment becomes more dominant above 1.5 GeV/c^2. The w_4^0 moment is non zero above 1.7 GeV/c^2 implying the presence of spin $J \geqslant 5/2$ at these higher masses.

No moments with L + m odd are significant, suggesting there is no interference between exchange particles of natural and unnatural parities.

5 Model Dependent Fits

In order to determine the spin-parity states present in the $p\pi^+\pi^-$ system below 1.75 GeV/c^2, certain assumptions have to be made. The discussions of the previous sections make certain things apparent. The $p\pi^+\pi^-$ system is predominantly $I = 1/2$ and couples strongly to $\Delta(1236)\pi$. Its production is characteristic of diffraction dissociation so exchange of a particle with the quantum numbers $IJ^P = 0^+$ is indicated. ($J^P = 0^-$ exchange is forbidden by parity conservation at the meson vertex.) There is strong interference between waves of different J^P throughout this region. All these properties

have been included in the model outlined below. The events used were those with the selection of $|t| < 0.5$ (GeV/c)^2 and antiselection of the $K^{*o}(890)$.

A $\Delta\pi$ decay mode was assumed to be the dominant process for all J^P waves, except $J^P = \frac{1}{2}^+$ where in addition a $p\epsilon$ decay mode was included. The ϵ was an s-wave π-π interaction, taken from the Lovelace-Veneziano model phase shifts [11]. The motivation for this was that its inclusion was found necessary in a high statistics low energy $\pi^- p \to \pi\pi N$ experiment [12] where the Lovelace form gave adequate fits. The statistics available here are insufficient to be sensitive to the form of ϵ taken.

The decay of the N^{*+} into $\Delta\pi$ and $p\epsilon$ for a given J^P may be written as

$$N^{*+} = a_{J^P} \langle \Delta\pi | + b_{J^P} \langle p\epsilon | \qquad (1)$$

where a_{J^P} and b_{J^P} are complex amplitudes to be determined by the fits, with b_{JP} non zero for $J^P = \frac{1}{2}^+$ only. On labelling the charge states and including isospin factors for decay of the intermediate states to $p\pi^+\pi^-$, the transition amplitude T becomes

$$T^{J^P}_{\lambda m_s} = a_{J^P}\left[A^{J^P}_{\lambda m_s}(\underline{p}_{\Delta^{++}}, \underline{q}_p)\, BW(\Delta^{++}) + \frac{1}{3} A^{J^P}_{\lambda m_s}(\underline{p}_{\Delta^o}, \underline{q}_p)\, BW(\Delta^o) \right]$$

$$+ \frac{2}{\sqrt{3}}\, b_{J^P}\, B_\epsilon(\pi^+, \pi^-) \qquad (2)$$

where λ and m_s are the initial and final proton spin

projections. The function BW(Δ) is a p-wave Breit-Wigner for the Δ defined to be

$$BW = \frac{\sqrt{\Gamma_r \frac{M_r}{q_r} \frac{q}{q_r}}}{(M - M_r) + i \frac{\Gamma}{2}} \quad \text{with} \quad \Gamma = \Gamma_r \left(\frac{q}{q_r} \right)^3 \frac{M_r}{M} \qquad (3)$$

with $M_r = 1.236$ and $\Gamma_r = 0.12$ GeV/c^2. The variable q is the 3-momentum of the proton in the Δ centre of mass. The term A($\underline{p}$,$\underline{q}$) contains the angular dependence of the decay chain and the centrifugal barrier for the decay of the N^* into Δ and π. The angular dependence of the p ϵ mode is just unity. The B_ϵ represents the Lovelace-Veneziano amplitudes.

To calculate the terms A($\underline{p}$,$\underline{q}$) production was assumed to be in the magnetic substate M = λ only, with respect to the incoming proton as z-axis. Written explicitly it takes the form

$$A^{J^P}_{\lambda m_s} = \sum_{m\, m_s'\, m_L} \left(\begin{matrix} 3/2 & L & J \\ m_s' & m_L & \lambda \end{matrix} \right) Y^{m_L}_L(\underline{p}) \left(\begin{matrix} 1/2 & 1 & 3/2 \\ m_s & m & m_s' \end{matrix} \right) Y^m_1(\underline{q})\, p^L \qquad (4)$$

where the arguments $\underline{p}$ and $\underline{q}$ of the spherical harmonics are the polar and azimuthal angles of the Δ momentum vector in the N^{*+} centre of mass and the final proton momentum vector in the Δ centre of mass respectively. The angles are referred to a set of axes taken in the N^* centre of mass

with the incoming proton as z-axis and the plane of the incoming and outgoing protons as x-axis. The term p^L is the angular momentum barrier factor for $N^* \rightarrow \Delta\pi$. Specific forms of the $A(\underline{p},\underline{q})$'s for various spin-parities are given in Table 4.1.

The total intensity is then given by

$$I = \frac{1}{2} \sum_{\lambda, m_s} \left| \left(\sum_{J^P} T^{J^P}_{\lambda m_s} \right) \right|^2 \qquad (5)$$

Fitting to the data was carried out by maximising the sum $\mathcal{L} = \sum_i \ln I_i$ with respect to the variables a_{J^P} and b_{J^P}, the intensities I_i being normalised by Monte-Carlo integration over phase-space. The data is therefore fitted to the entire decay characteristics of the $p\pi\pi$ system (except, of course, for the proton polarisation) i.e., the intensity is a function of both the Dalitz plot population and its orientation in space. This in fact reduces the work involved, compared with that of the Q analysis, since the terms in Table 4.1 can be calculated directly for each event without having to do a partial integration over some of the variables. Fitting was carried out to seven 50 MeV/c^2 wide bins from 1.4 to 1.75 GeV/c^2 in $p\pi^+\pi^-$ mass.

Morrison [13] has indicated that, in diffraction dissociation, the spin-parity series $1/2^+$, $3/2^-$, $5/2^+$ should dominate. The justification for this is meagre; however, it was taken as a suitable starting assumption in the fitting. The results of these fits are summarised in Table 4.2. The $1/2^+$

Table 4.1

Angular Terms for decay of the N^* via $\Delta\pi$

Spin-Parity State	$A(p,q) \times (4\pi)$ for $\lambda = +\frac{1}{2}$	
	Non Spin Flip	Spin Flip
$1/2^+$	$-\sqrt{2}[\underline{p}\cdot\underline{q}+\frac{i}{2}(\underline{p}\wedge\underline{q})_z]$	$\frac{1}{\sqrt{2}}[(\underline{p}\wedge\underline{q})_y - i(\underline{p}\wedge\underline{q})_x]$
$3/2^-$	$\sqrt{2}\,q_z$	$-\frac{\sqrt{2}}{2}[q_x - iq_y]$
$5/2^+$	$-\frac{3}{\sqrt{10}}[\underline{p}\cdot\underline{q}-3p_zq_z]$	$-\frac{3}{\sqrt{10}}[(p_zq_x+p_xq_z)+i(p_zq_y+p_yq_z)]$
$1/2^-$	$-\frac{1}{\sqrt{2}}[3(\underline{p}\cdot\underline{q})p_z-q_z]$	$\frac{1}{\sqrt{2}}[q_x - 3p_x(\underline{p}\cdot\underline{q}))+i(q_y-3p_y(\underline{p}\cdot\underline{q}))]$
$5/2^-$	$\frac{\sqrt{3}}{14}[2p_z(\underline{p}\cdot\underline{q})$ $+(1-5p_z^2)q_z$ $+7i\,p_z(\underline{p}\wedge\underline{q})_z]$	$-\frac{\sqrt{3}}{14}[q_x+3p_y(\underline{p}\wedge\underline{q})_z - 5p_xp_zq_z$ $+i[q_y-3p_x(\underline{p}\wedge\underline{q})_z - 5p_yp_zq_z]$

Barrier factors have been neglected in this table. The vector $\underline{p}$ is a unit vector specifying the direction of the Δ in the N^* centre of mass and $\underline{q}$ is a unit vector specifying the direction of the proton in the Δ centre of mass. The opposite helicity terms were calculated using the relation

$$A^{J^P}_{-\frac{1}{2}-\frac{1}{2}} = A^{J^P\,*}_{\frac{1}{2}\,\frac{1}{2}} \quad \text{and} \quad A^{J^P}_{-\frac{1}{2}\frac{1}{2}} = -A^{J^P\,*}_{\frac{1}{2}-\frac{1}{2}}.$$

Table 4.2

Fits with $1/2^+$, $3/2^-$ and $5/2^+$ amplitudes

Intensities are normalised to the number of experimental events. The pure $\Delta\pi$ and $p\epsilon$ fractions do not add up to unity because of interference between them.

$p\pi^+\pi^-$ Mass Region GeV/c^2		$1/2^+$ Fraction of		$3/2^-$	$5/2^+$	Log-likelihood change when $p\epsilon$ excluded
	Inten.	$\Delta\pi$	$p\epsilon$	Inten.	Inten.	
1 1.4-1.45	14	.61	.46	54	5	-1.3
2 1.45-1.50	41	.51	.35	55	10	-6.2
3 1.50-1.55	60	.08	.84	16	12	-25.5
4 1.55-1.60	7	.67	.19	59	11	-0.7
5 1.60-1.65	51	.45	.41	1	41	-7.8
6 1.65-1.70	52	.61	.47	4	50	-1.7
7 1.70-1.75	57	.21	.58	8	40	-13.1

Table 4.3

Contributions of $\frac{1}{2}^-$ and $\frac{5}{2}^-$ terms from fits to all waves

$P\pi\pi$ Mass Region GeV/c^2	Percentage of $\frac{1}{2}^-$	Percentage of $\frac{5}{2}^-$
1. 1.4-1.45	0	10
2. 1.45-1.5	24	5
3. 1.5-1.55	2	20
4. 1.55-1.6	13	6
5. 1.6-1.65	1	19
6. 1.65-1.7	2	9
7. 1.7-1.75	1	5

component is seen to be large throughout most of the region dipping only in the bin 1.55 - 1.6 GeV/c^2, whereas the $3/2^-$ contribution is large up to 1.6 GeV/c^2 and small above. The proportion attributed to $5/2^+$ rises steadily with increasing $p\pi^+\pi^-$ mass reaching a peak in the region 1.65 - 1.7 GeV/c^2. These trends are consistent with the production and decay to $p\pi^+\pi^-$ of the $P_{11}(1470)$, $D_{13}(1520)$ and $F_{15}(1688)$ pion-nucleon resonances predicted by phase shift analyses. The low proportion of $3/2^-$ in the region 1.5 - 1.55 GeV/c^2 is the only significant discrepancy.

In Figs. 4.6(a), 4.7(a) and 4.8(a) the invariant mass projections of the data are shown as histograms with the distributions calculated from the fits superimposed as crosses. The variation in shape of the data from bin to bin is quite pronounced and is followed closely by the fits, suggesting the rapid variations indicated in the fits are present in the data. The similarity of the two distributions adds to ones confidence in the validity of the model as the projections were fitted only in a very indirect way.

Questions which arise from this analysis are :

a) How necessary is the p ϵ term?

b) Are both the $P_{11}(1470)$ and $P_{11}(1780)$ resonances produced?

c) Is there any indication of the presence of $1/2^-$ or $5/2^-$ $p\pi^+\pi^-$ states?

These questions are discussed below.

a) The fitting was repeated as above but with no p ϵ term

$\pi^+\pi^-$ mass projections

(a) with ϵ

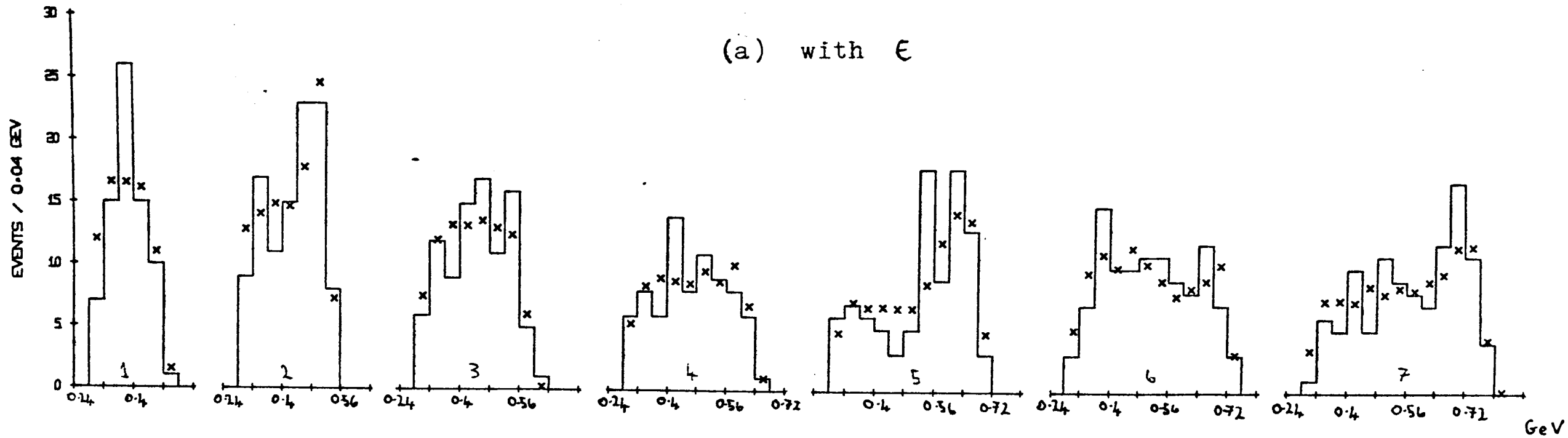

(b) without ϵ

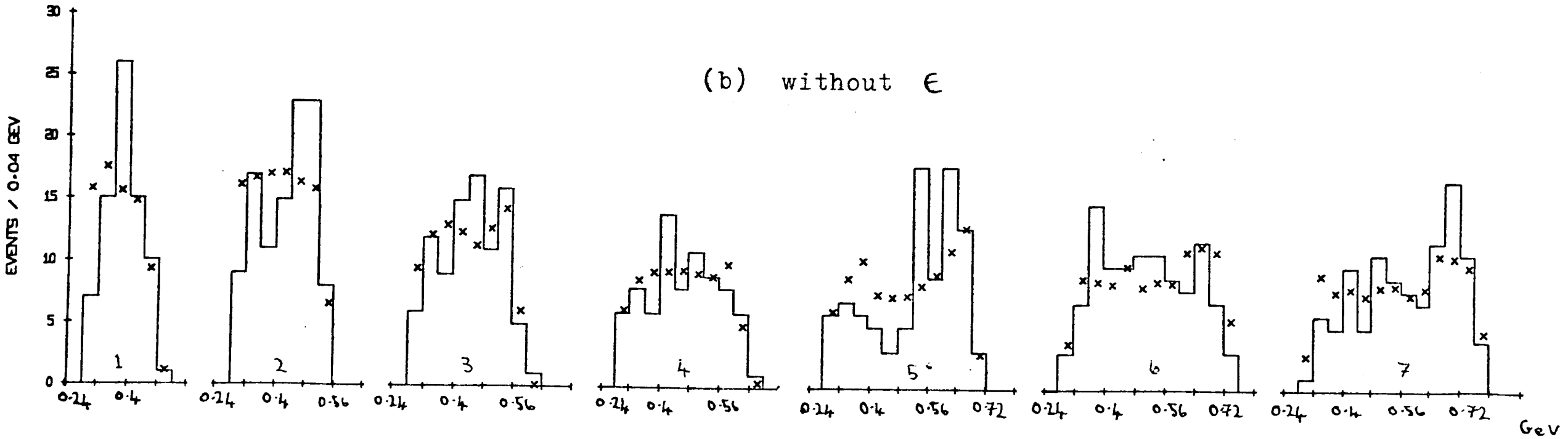

Fig. 4.6

$p\pi^+$ mass projections

(a) With ϵ

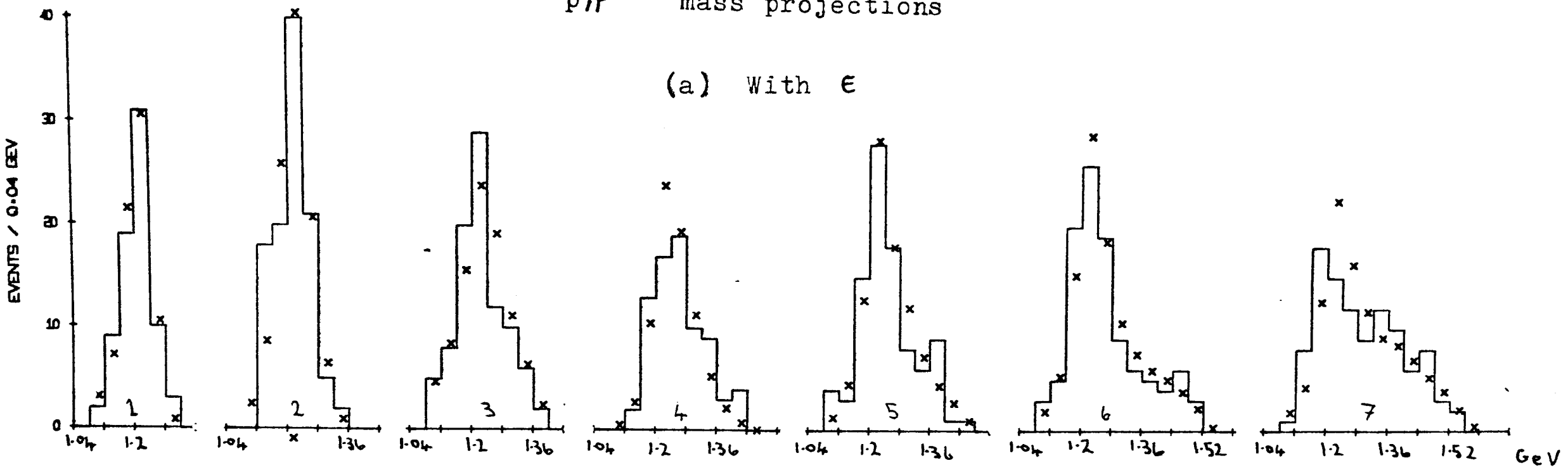

(b) Without ϵ

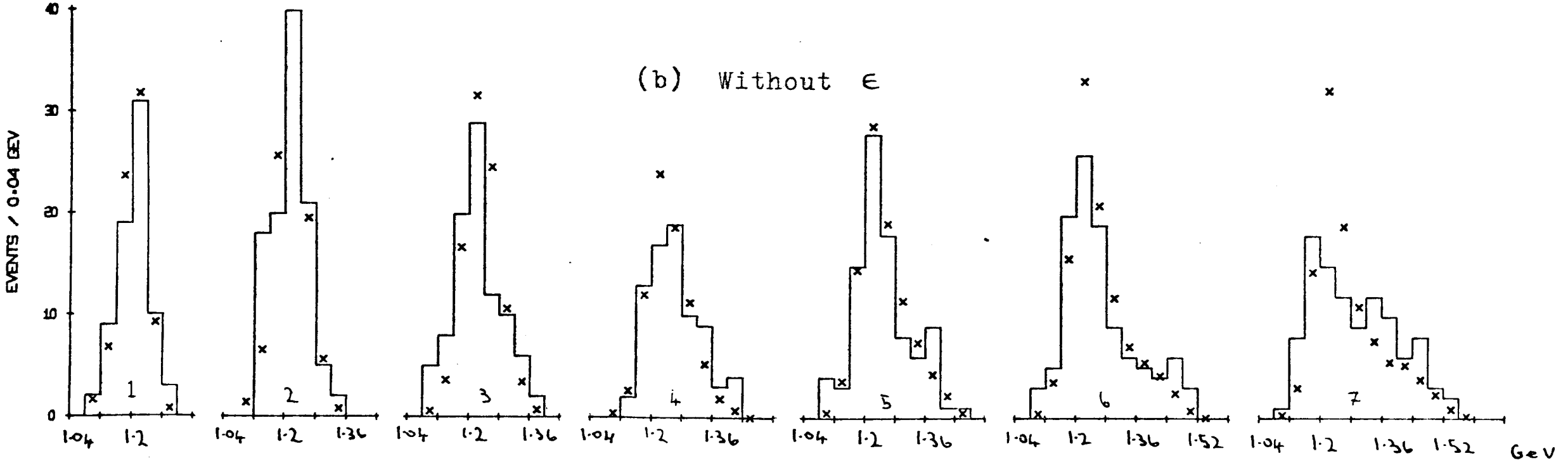

Fig. 4.7

$p\pi^-$ mass projections

(a) With ϵ

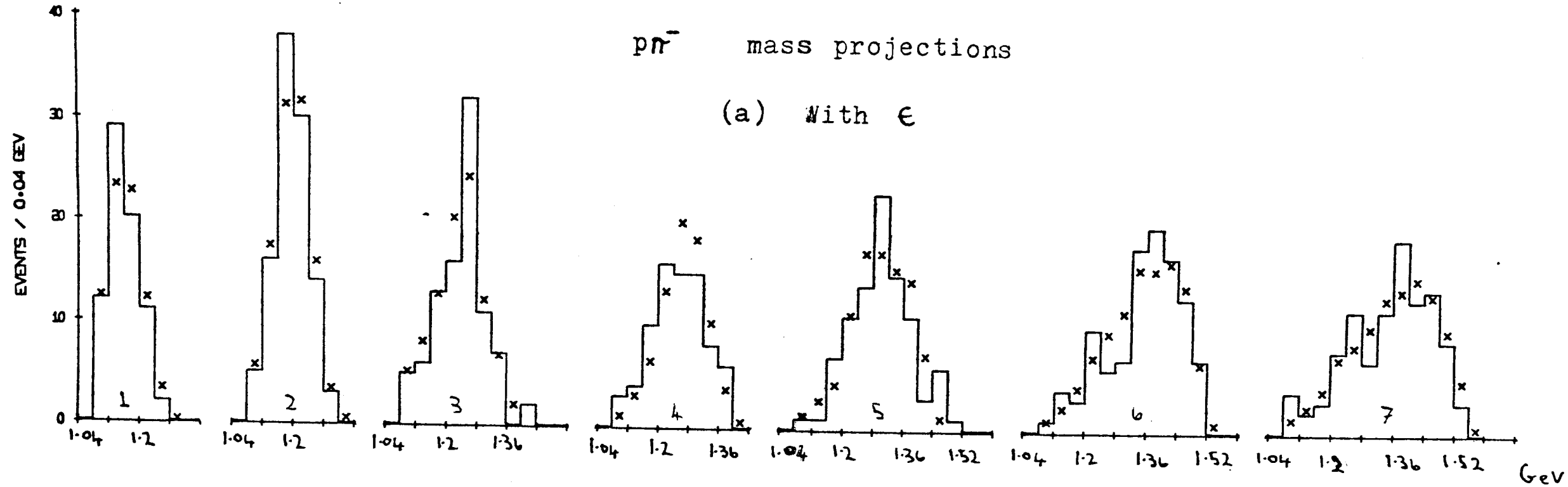

(b) Without ϵ

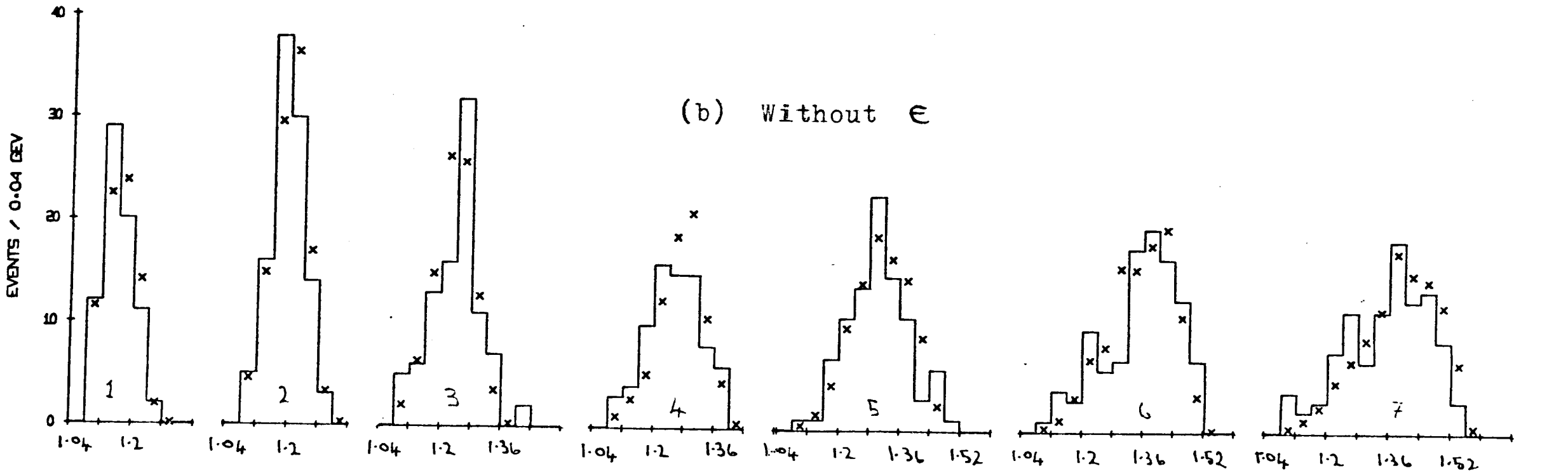

Fig. 4.8

present. The projections resulting from these fits are shown in Figs. 4.6(b), 4.7(b) and 4.8(b) superimposed on the data. The $\pi^+\pi^-$ and $p\pi^+$ predicted mass spectra are generally in worse agreement with the data than the fits with $p\epsilon$ present and in four of the regions fitted (bins 2,3,5 and 7) the log-likelihood function was lower by 6 or more than in the fits with $p\epsilon$ (see Table 4.2). There is therefore some evidence for a $\pi\pi$ interaction in the data.

b) The intensity of $^1/_2{}^+$ is low in region 4 (1.55 to 1.6 GeV/c^2) and the coupling of $^1/_2{}^+$ to $\Delta\pi$ is low in both of the regions 3 and 4 in fits both with and without a $p\epsilon$ coupling. There is therefore some indication of production of two $^1/_2{}^+$ states which may be tentatively identified with the $P_{11}(1470)$ and $P_{11}(1780)$ of phase shift analyses. The data is meagre, though, and the errors in the fits are large. The low $^3/_2{}^-$ contribution in region 3 may reflect on the reliability of this dip in the $^1/_2{}^+$ amplitude. Also the $^1/_2{}^+$ was the only wave with a term other than $\Delta\pi$, included. The contribution by the fits to the $^1/_2{}^+$ $p\epsilon$ mode at high $p\pi^+\pi^-$ masses may not be real but only a reflection of the presence of a non-$\Delta\pi$ 'background' in the data of the upper peak.

c) Fits were carried out with both $^1/_2{}^-$ and $^5/_2{}^-$ states decaying via $\Delta\pi$, included in the hypotheses. The validity of fitting a relatively small sample of data with so many parameters is questionable. The log-likelihoods did not however, indicate a significant improvement with the inclusion

of these extra waves. In each region they increased by ~ 5 for four extra parameters and the proportions attributed to each wave were erratic but generally small (see Table 4.3). In particular there was no increase in the regions of the $1/2^-(1535)$ or $5/2^-(1670)$ isobars for the two waves. Although it is not conclusive, there appears no evidence in the data for the production of $1/2^-$ or $5/2^-$ states in any part of the region studied.

6 Summary of Conclusions

The $p\pi^+\pi^-$ system shows features characteristic of diffractive production of the $I = 1/2$ nucleon isobars in the spin-parity series $1/2^+$, $3/2^-$ and $5/2^+$. Although statistics are inadequate to draw quantitative conclusions, two observations are clear. Firstly, there is strong interference between states of different J^P throughout the region studied which makes any analysis with a unique spin parity hypothesis highly questionable. Secondly, the $p\pi^+\pi^-$ system has properties which vary considerably from one region to the next. This casts doubt on those analyses which use a background subtraction procedure to extract the properties of a particular region.

REFERENCES

[1]	A. Donnachie	Proceedings of the XIVth International Conference on High Energy Physics, Vienna (1968), p. 139.
[2]	M.G. Bowler, R.J. Cashmore and M. De Beer et al.	Nucl. Phys., B17 331 (1970). Nucl. Phys. B12, 617 (1969).
[3]	D.H. Saxon et al.	O.N.P.L. 3/70 preprint
[4]	D. Morgan	Phys. Rev., 165, 1699 (1968).
[5]	E.W. Anderson	Phys.Rev.Lett., 16, 855 (1966).
[6]	K.J. Foley	Phys.Rev.Lett., 19, 397 (1967).
[7]	J.I. Rhode et al.	Phys.Rev., 187, 1844 (1969).
[8]	D.J. Crennell et al.	Phys. Rev. Lett. 25, 187 (1970).
[9]	P. Antlich et al.	Phys. Rev. Lett. 22, 39 (1969).
[10]	R.J. Cashmore	D.Phil. Thesis, Oxford (1969) unpublished.
[11]	C. Lovelace	Proceedings of the Conference on $\pi\pi$ and $K\pi$ Interactions, A.N.L. (1969), p. 562.
[12]	D.H. Saxon	Private Communication
[13]	Morrison	Phys.Rev. 165, 1699 (1968).

APPENDIX A

AMBIGUITIES IN THE $K^+\pi^+\pi^-$ FINAL STATE

The Van Hove plot of Chapter 1, Fig. 1.8, clearly demonstrates where the kinematic ambiguities of the $K^+\pi^+\pi^-p$ channel lie. The KINEMATICS program cannot distinguish a K^+ from a π^+ in those events in which the $K\pi\pi$ system has a large forward laboratory momentum with the K^+ and π^+ having similar momenta. These events lie in a very restricted region of phase space, largely around the Q region. Their presence does not seriously bias the $K\pi\pi$ mass spectrum as the value of the $K\pi\pi$ mass does not differ greatly from one identification to the other. A comparison of the $K\pi\pi$ mass spectra for the unique and ambiguous fits confirms this. However, the Dalitz plot distributions will be affected. As pointed out in Chapter 3 almost the entire ρ signal observed in Fig. 3.10 comes from the ambiguous events. There is, however, a clear ρ signal in the $K^0\pi^0\pi^+$ system, so the ρ^0 observed in $K^+\pi^+\pi^-p$ must be partially real.

In Fig. A.1 the probability of the kinematic fit 1 is plotted against that of fit 2 for those events in which either fit has $K^+\pi^+\pi^-$ mass in the region 1.2 to 1.4 GeV/c^2. The events have been divided into three regions as shown in the figure, i.e.,

a) the regions running along the axes of the plot

b) the diagonal band

c) the regions in between.

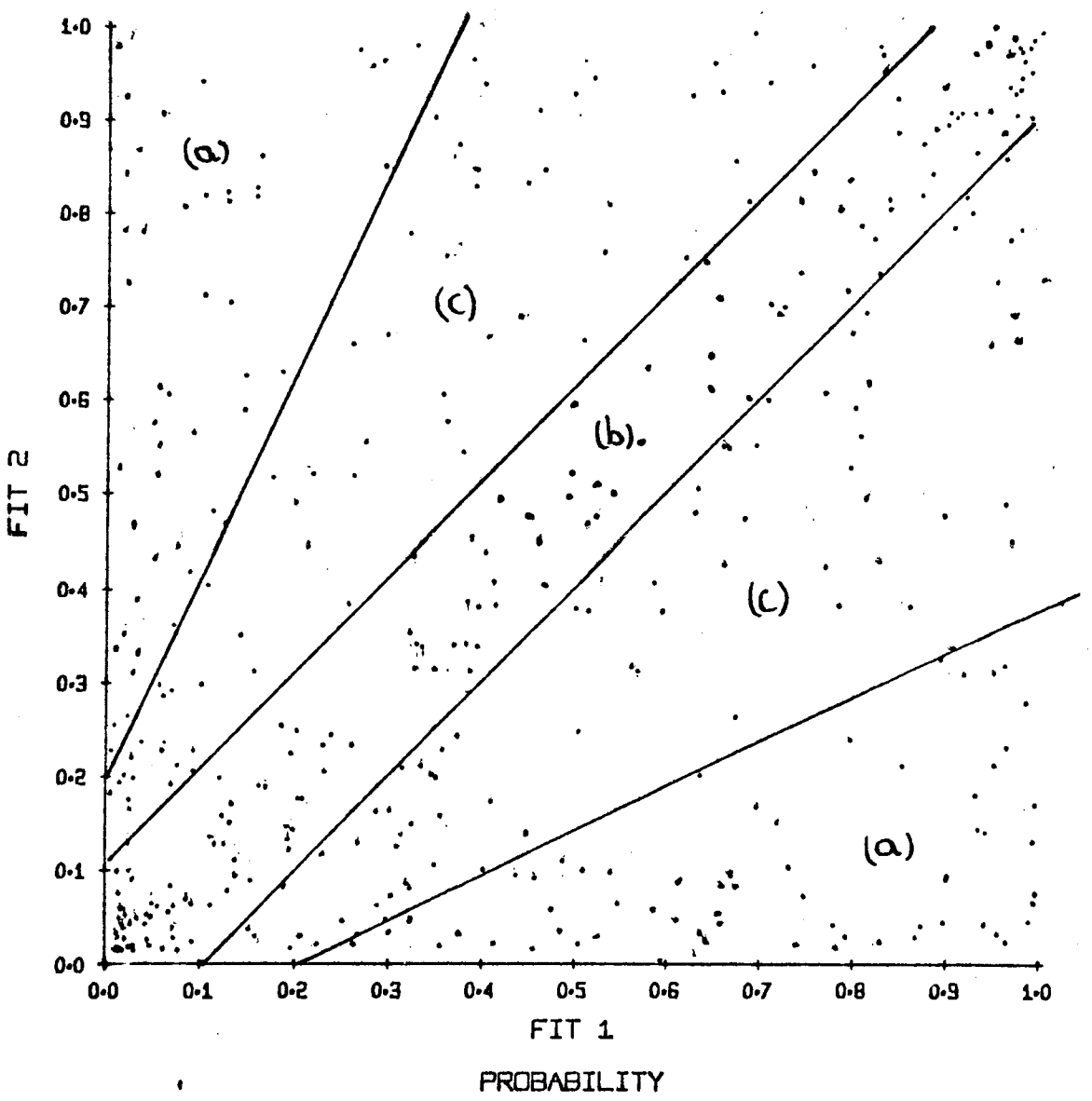
1·0
0·9
0·8
0·7
0·6
0·5
0·4
0·3
0·2
0·1
0·0
FIT 2
(a)
(c)
(b)
(c)
(a)
0·0
0·1
0·2
0·3
0·4
0·5
0·6
0·7
0·8
0·9
1·0
FIT 1
PROBABILITY

Fig. A.1

The selection of the higher probability fit for regions (a) and (c) is thought to be largely correct. This belief is based on the probability scatter plot for region (a) and on the contrast in the $K^+\pi^-$ mass spectra for the high and low probability fits for region (c) (see Fig. A.2). A clear $K^*(890)$ signal is seen for the higher probability selection in region (c) which is absent from the lower probability.

The events in regions (a) and (c) do not contribute a significant ρ signal in the $\pi^+\pi^-$ region when the higher probability fit is taken. However, if the lower probability fit is selected, the K^* disappears and a substantial peak develops in the ρ region (see Fig. A.2). This is in agreement with the conclusions of Ferbel et al. (see reference) who pointed out that misidentified K^*'s generate a spurious ρ signal. These events are not seriously ambiguous, though.

The main problem comes from those events falling in region (b), the band of essentially equal probability for either fit. The Dalitz plot for the higher probability fit of these events is shown in Fig. A.3. The events lie preferentially in the K^*-ρ crossover region. It must be emphasised that there is no a priori knowledge of how these events should be distributed, that can be used to separate the correctly and incorrectly identified events. The situation is partially saved by the strong positive correlation found between the points on the Dalitz plot for the two fits. In Fig. A.4 each event is represented by a line connecting the two points corresponding to each fit. It can be seen that each event slides alone a line of constant $K^+\pi^+$ mass, the

Events from region (c)

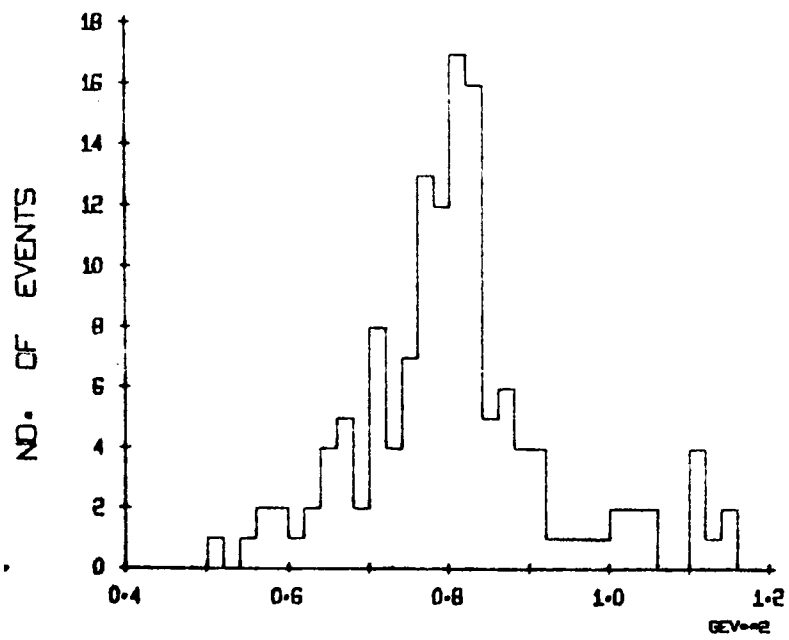

MASS SQ. K+ PI-
HIGH PROBABILITY

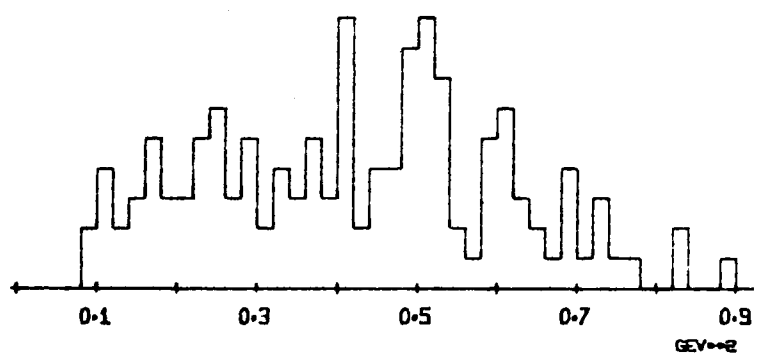

MASS SQ. PI+ PI-
HIGH PROBABILITY

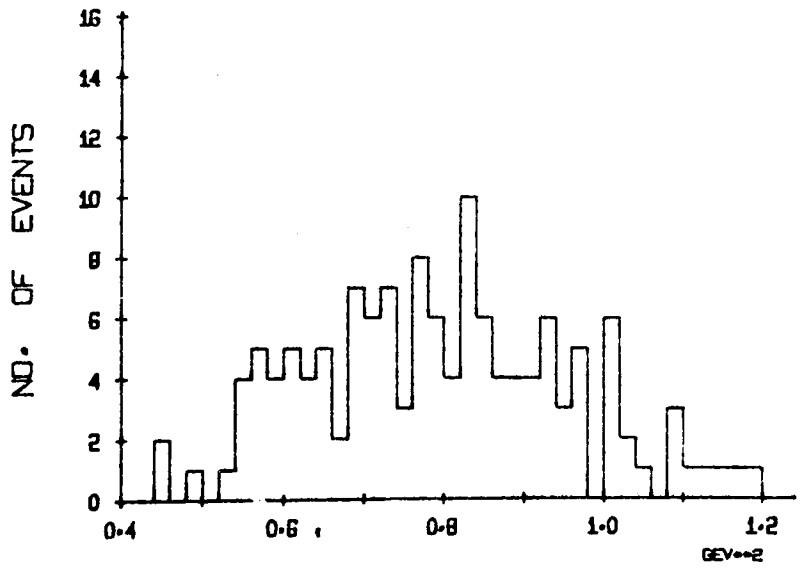

MASS SQ. K+ PI-
LOW PROBABILITY

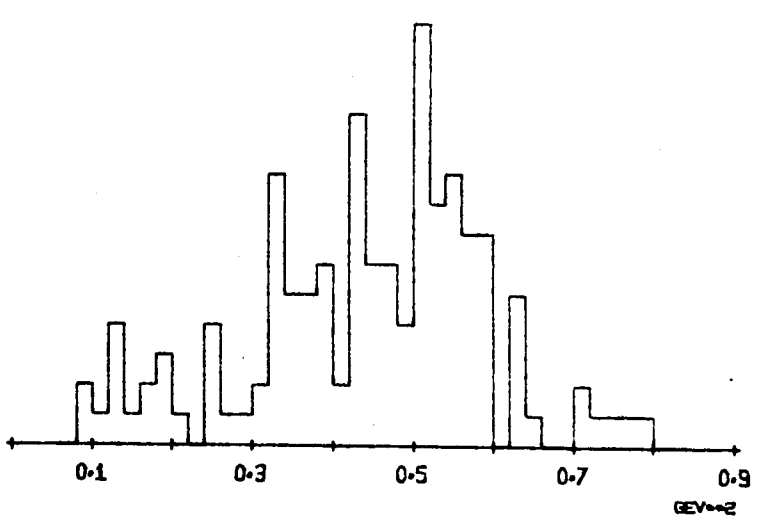

MASS SQ. PI+ PI-
LOW PROBABILITY

Fig. A.2

High probability events
Region (b)

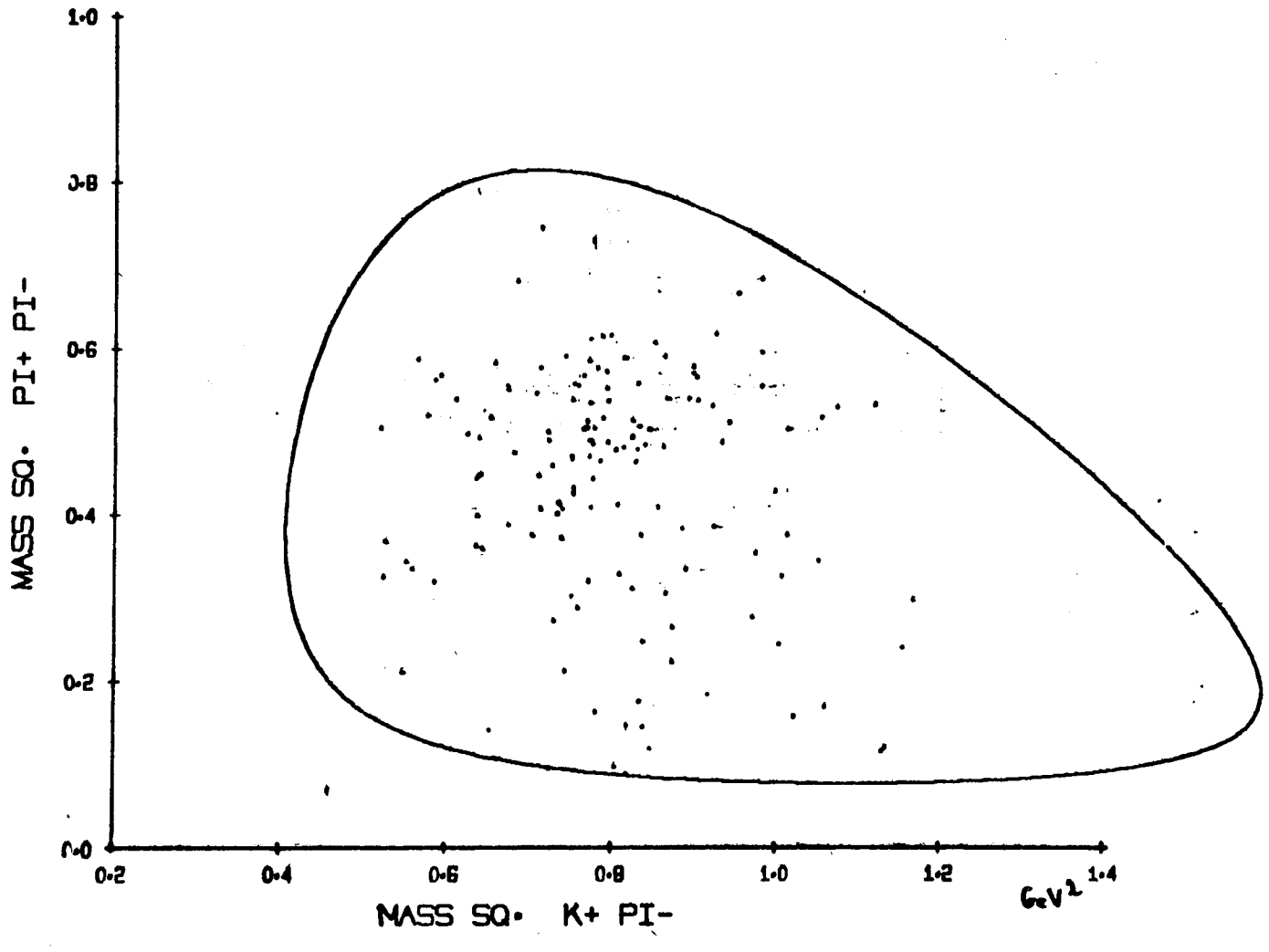

Fig. A.3

length of the line varying with position on the plot. A short line corresponds to a high positive correlation between the two positions, and there is a concentration of such short lines in the region where the K^* and ρ bands cross. Out of the 147 events falling in region (b) and plotted in Fig. A.4, 47 are found in the region defined by $M(K^+\pi^-) = 890 \pm 50$ and $M(\pi^+\pi^-) = 765 \pm 120$ GeV/c^2, for both interpretations.

Thus there appears to be $\sim$ 100 events out of a total of 1246 events in the Q, whose possible misidentification could matter. Of these, half will presumably be correct by random chance, leaving $\sim 4\%$ of the events in the Q for which there is a misidentification which is significant. Although this fraction is small, the effect suggested by Ferbel et al. may be at work giving a disproportionate effect on the ρ amplitude fitted to the data.

To test this possibility, for each of these 100 events, the fit giving a $K\pi$ mass nearest the $K^*(890)$ was taken as the correct one, and the $\pi^+\pi^-$ mass projection was plotted for these events together with the rest used in the Dalitz plot fits. When compared with the projection for the overall higher probability fit selections, the two were found to be identical within statistical errors. The projections of the Dalitz plot given in Chapter 3 must be essentially correct. In conclusion, although there appears to be no clear way of estimating what effect this small number of misidentified events has on the maximum likelihood fitting of Chapter 3, the evidence available shows no indication of a bias in any

Region (b)

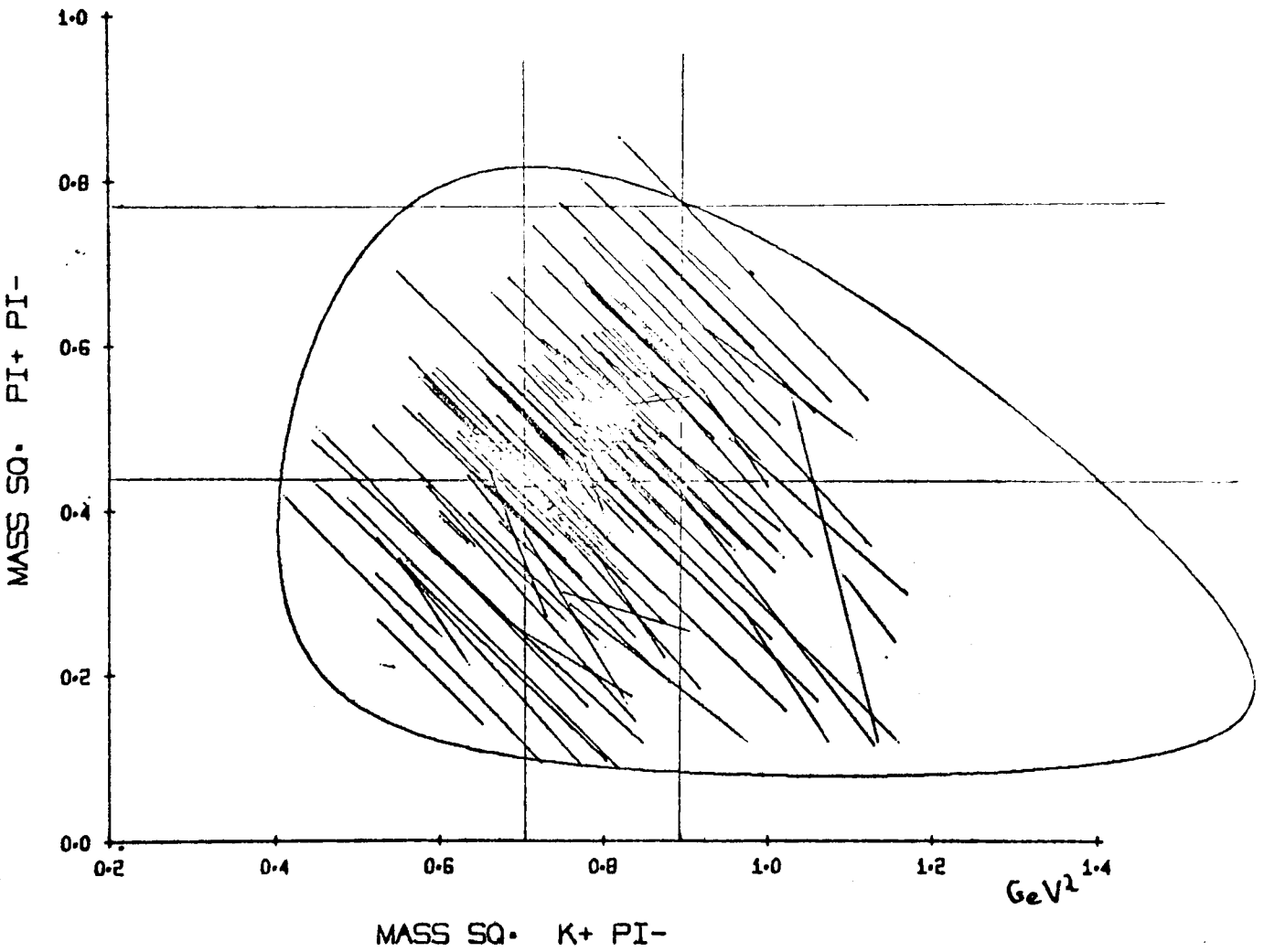

Fig. A.4

particular direction.

Reference

T. Ferbel et al. University of Rochester Report UR-875-304 (1970).

APPENDIX B

CALCULATION OF $K\pi\pi$ ANGULAR DISTRIBUTIONS

A brief outline is given here of the theory involved in the analysis of the moments of the $K\pi\pi$ system (Chapter 3). For the quasi two-to-three-body scattering process of Fig. 3.6 (i.e., $e + K^+ \rightarrow K\,\pi\,\pi$), the transition amplitude from initial to final states may be written as

$$T = \sum_{J\Lambda\lambda} \sqrt{\frac{2J+1}{4\pi}}\; \mathcal{D}^{J}_{\Lambda\lambda}(\psi, \Theta, \phi)\; B^{\lambda}_{J\Lambda}(s, s_i) \qquad (1)$$

where J is the total angular momentum

Λ is the projection of J on the $K\pi\pi$ decay plane normal

λ is the helicity of the incoming virtual particle

s is the invariant mass squared of the $K\pi\pi$ system

s_i are the invariant masses of each pair of outgoing particles.

The angles (ψ, Θ, ϕ) are a set of Euler angles transforming one of the sets of axes defined in Section (6) into the other. The $B^{\lambda}_{J\Lambda}$ are reduced matrix elements which are independent of the magnetic substate in which the system is produced. The expression (1) is essentially the same as that derived by Branson, Landshoff and Taylor (Chapter 3, reference [16]) but uses the fact that all the final state particles have spin zero.

Parity conservation applied to the reduced matrix elements gives the relation

$$B^{\lambda}_{J\Lambda} = \eta_i \, \eta_f \, (-1)^{J+\Lambda} \, B^{-\lambda}_{J\Lambda} \qquad (2)$$

where η_i and η_f are respectively the products of the intrinsic parities of the particles in the initial and final states. For $J^P = 0^+$ exchange, $\lambda = 0$, and (2) becomes $B_{J\Lambda} = (-1)^{J+\Lambda} B_{J\Lambda}$ restricting $J+\Lambda$ to even values only. For pion exchange ($J^P = 0^-$), only odd values of $J+\Lambda$ would be allowed. With λ set equal to zero in (1) the ϕ dependence drops out and the $\mathcal{D}^J_{\Lambda 0}$ may be written in terms of spherical harmonics using the relation [1]

$$\mathcal{D}^J_{\Lambda 0}(\psi, \Theta, \phi) = \sqrt{\frac{4\pi}{(2J+1)}} \; Y^{\Lambda *}_J(\Theta, \psi) \qquad (3)$$

The intensity, given by the modulus squared of (1), may then be expanded into sums of spherical harmonics to give

$$I = \sum_{JJ'\Lambda\Lambda'\ell} \sqrt{\frac{(2J+1)(2J'+1)}{4\pi\,(2\ell+1)}} \, (-1)^{\Lambda'} \, C^{J\;J'\;\ell}_{\Lambda\;-\Lambda'\;(\Lambda-\Lambda')} \, C^{J\;J'\;\ell}_{0\;0\;0}$$

$$\cdot \; B_{J\Lambda} \, B^{*}_{J'\Lambda'} \, Y^{\Lambda-\Lambda'}_{\ell}(\Theta, \psi) \qquad (4)$$

All values of J and Λ are <u>a priori</u> possible. For 1^+ and 2^- production only, the non-zero $B_{J\Lambda}$ are B_{11} and B_{1-1} for 1^+ and B_{22}, B_{20}, B_{2-2} for 2^-. In Table B.1 the corresponding

Table B 1

Expansion of theoretical angular distribution into moments w_L^M for $1^+ + 2^-$ states

Moment	Expression
w_0^0	$\lvert B_{1-1}\rvert^2+\lvert B_{11}\rvert^2+\lvert B_{2-2}\rvert^2+\lvert B_{20}\rvert^2+\lvert B_{22}\rvert^2$
w_1^1	$1/\sqrt{5}(B_{20}B_{1-1}^*-B_{11}B_{20}^*)+\sqrt{6/5}(B_{22}B_{11}^*-B_{1-1}B_{22}^*)$
w_2^0	$-1/\sqrt{5}(\lvert B_{11}\rvert^2+\lvert B_{1-1}\rvert^2)+2\sqrt{5/7}(\lvert B_{20}\rvert^2-\lvert B_{2-2}\rvert^2-\lvert B_{22}\rvert^2)$
w_2^2	$-\sqrt{6/5}B_{11}B_{1-1}^*-2\sqrt{5/7}(B_{22}B_{20}^*+B_{20}B_{22}^*)$
w_3^1	$1/\sqrt{35}\left[\sqrt{3}(B_{1-1}B_{2-2}^*-B_{22}B_{11}^*)+3\sqrt{2}(B_{11}B_{20}^*-B_{20}B_{1-1}^*)\right]$
w_3^3	$3/\sqrt{7}(B_{11}B_{2-2}^*-B_{22}B_{1-1}^*)$
w_4^0	$1/7(\lvert B_{2-2}\rvert^2+\lvert B_{22}\rvert^2+6\lvert B_{20}\rvert^2)$
w_4^2	$\sqrt{15}/7(B_{22}B_{20}^*+B_{20}B_{2-2}^*)$
w_4^4	$\sqrt{10/7}(B_{22}B_{2-2}^*)$

The moments discussed in the text of Chapter 3, section 6, unlike the ones given here, are normalised to $w_0^0 = 1$.

values of w_L^m are given for this hypothesis by evaluating expression (4). These calculations were made by hand and checked by using a program CLEBGN to evaluate the sum of Clebsch-Gordan coefficients.

The formulae in Table B.1 are consistent with the predictions of Berman and Jacob given in Chapter 3, formula (6). For pure 1^+ the ratio of w_2^0/w_0^0 is uniquely equal to $-\frac{1}{\sqrt{5}}$ (i.e., ≈ -0.447) and for pure 2^- there is one parameter in the w_L^0 moments, the ratio of $|B_{22}|^2 + |B_{2-2}|^2$ to $|B_{20}|^2$ in analogue to the parameter K. The interference between 1^+ and 2^- occurs in the moments w_1^1, w_3^1 and w_3^3.

If the exchange particle 'e' has well-defined intrinsic parity (and spin zero) then from (2), only $B_{J\Lambda}$ terms where $J + \Lambda$ is even for even P or odd for odd P can occur. This results in only the moments w_L^m for which $(L + m)$ is even appearing. Odd values of $L + m$, which would be parity violating for a real scattering process, can only occur with interference between exchanges of even and odd parity (e.g. Pomeron and pion exchange). In the data these moments are consistent with zero.

The parameters in the fits of Chapter 3, Section (6) were the real and imaginary parts of each $B_{J\Lambda}$ used. As was pointed out there, the evaluation of the χ^2 given in Table 3.1 included all moments up to w_4^4 and thus contain a quantitative test of the statement above, that the exchange particle had unique intrinsic parity.

Reference

[1] Brink and Satchler - Angular Momentum (Clarendon Press, 1968), Appendix V.

APPENDIX C

CALCULATION OF DALITZ PLOT POPULATIONS

1. Isospin considerations

The decay of a $K\pi\pi$ system for a particular spin-parity state into $K^*\pi$ and $K\rho$ with the Bose symmetry of the two π's taken into account may be written as

$$\langle K\pi\pi| = \frac{1}{\sqrt{2}}\left\{\langle K_1^*\pi_2| + \langle K_2^*\pi_1|\right\} + ae^{i\beta}\langle K\rho| \qquad (1)$$

where either π_1 or π_2 is in the K^*. For $I = 1/2$, on labelling the charge states, equation (1) becomes

$$\begin{aligned}
&\frac{1}{\sqrt{2}}\left\{\left[\sqrt{\tfrac{2}{3}}\langle K_1^{*0}\pi^+_2| - \sqrt{\tfrac{1}{3}}\langle K_1^{*+}\pi^0_2|\right]\right.\\
&\left.+\left[\sqrt{\tfrac{2}{3}}\langle K_2^{*0}\pi^+_1| - \sqrt{\tfrac{1}{3}}\langle K_2^{*+}\pi^0_1|\right]\right\}\\
&+ ae^{i\beta}\left[\sqrt{\tfrac{2}{3}}\langle K^0\rho^+| - \sqrt{\tfrac{1}{3}}\langle K^+\rho^0|\right] \qquad (2)
\end{aligned}$$

With the inclusion of the isospin factors for the decay of the vector mesons, the amplitudes for the two charge states of interest take the form:

(1) $K^+\pi^+\pi^-$

$$\begin{aligned}
&\left\{-\sqrt{\tfrac{2}{3}}\,A(\underline{p}_{\pi_2^+},\underline{q}_{K^+})\;BW(K^+,\pi_1^-) + \sqrt{\tfrac{1}{6}}\,ae^{i\beta}A(\underline{p}_{K^+},\underline{q}_{\pi_1^-})\;BW(\pi_1^-,\pi_2^+)\right\}\\
+&\left\{-\sqrt{\tfrac{2}{3}}\,A(\underline{p}_{\pi_1^+},\underline{q}_{K^+})\;BW(K^+,\pi_2^-) - \sqrt{\tfrac{1}{6}}\,ae^{i\beta}A(\underline{p}_{K^+},\underline{q}_{\pi_1^+})\;BW(\pi_1^+,\pi_2^-)\right\}
\end{aligned}$$

(3)

(2) $K^o\pi^o\pi^+$

$$\left\{\frac{1}{3} A(\underline{p}_{\pi_2^+},\underline{q}_{K^o})\ BW(K^o,\pi_1^o) - \frac{1}{3} A(\underline{p}_{\pi_1^o},\underline{q}_{K^o})\ BW(K^o,\pi_2^+)\right.$$

$$\left. - \alpha e^{i\beta}\sqrt{\frac{1}{3}}\ A(\underline{p}_{K^o},\underline{q}_{\pi_1^o})\ BW(\pi_1^o,\pi_2^+)\right\}$$

$$+\left\{-\frac{1}{3} A(\underline{p}_{\pi_2^-},\underline{q}_{K^o})\ BW(K^o,\pi_1^+) + \frac{1}{3} A(\underline{p}_{\pi_1^+},\underline{q}_{K^o})\ BW(K^o,\pi_2^o)\right.$$

$$\left. + \alpha e^{i\beta}\sqrt{\frac{1}{3}}\ A(\underline{p}_{K^o},\underline{q}_{\pi_1^+})\ BW(\pi_1^+,\pi_2^o)\right\} \qquad (4)$$

where the factors $A(\underline{p},\underline{q})$ and BW are defined in section 7 of Chapter 3.

2 Angular Momentum Properties

To evaluate the factors $A(\underline{p},\underline{q})$, the $K\pi\pi$ system was assumed to be produced in a state with angular momentum J and projection M = 0 with respect to the incoming K^+ as Z axis. (This latter assumption is for convenience only and does not affect the Dalitz plot populations.) The function $A(\underline{p},\underline{q})$ for natural spin parity states is then given by

$$A(\underline{p},\underline{q}) = \sum_{L_Z} C^{J\ \ 1\ \ J}_{L_Z\ -L_Z\ 0}\ Y_J^{L_Z}(\underline{p})\ Y_1^{-L_Z}(\underline{q})\ p^J \qquad (5)$$

and for unnatural spin-parity states by

$$A(\underline{p},\underline{q}) = \sum_{L_Z} C^{J-1\ \ 1\ \ J}_{L_Z\ -L_Z\ \ 0}\ Y^{L_Z}_{J-1}(\underline{p})\ Y_1^{-L_Z}(\underline{q})\ p^{J-1} \qquad (6)$$

where for the latter states J+1 waves have been neglected. The factors p^L are centrifugal barrier terms for the initial state of the decay chain. The corresponding factors for the vector meson decay have been included in the Breit-Wigner formulae. The arguments $\underline{p}$ and $\underline{q}$ of the spherical harmonics are the polar and azimuthal angles of the relevant particle momentum vectors, defined in Table C.1, measured with respect to the external set of axes Oxyz of Chapter 3, section 6. The K meson has been chosen as the indicator of K^* decay and π_1 as indicator of ρ decay. This ensures a consistent definition of the phase β between expressions (3) and (4). The final states $< K^+\pi_1^+\pi_2^-|$ and $<K^+\pi_1^-\pi_2^+|$ are orthogonal and so do not interfere on squaring the amplitudes. Choosing the π^+ as indicator of ρ decay for the experimental analysis reverses the sign of the ρ amplitude in the latter case, since $Y_1^0(\underline{q})$ is odd under $\underline{q} \to -\underline{q}$. The square of equation (3) yields equation (10) and (4) equation (11) of Chapter 3.

This analysis using SU(2) only, leaves an ambiguity of 180 degrees in the phase β since if π_2 had been chosen instead of π_1, the difference would have been $\beta \to -\beta$. This ambiguity can only be removed by going to SU(3) and writing an amplitude symmetric in all three particles.* The values of

* Using SU(3), Bowler has determined that for the phase convention applied here, β = 0 corresponds to the K^* with C = +1, and β = π corresponds to the K^* with C = -1.

Table C.1

Angular terms for decay of the Q via $K^*\pi$ and Kρ, before integration over the orientation of the Dalitz plot in space.

Spin Parity State	$A(\underline{p},\underline{q}) \times (4\pi)$
0^-	$-\sqrt{3}(\underline{p}.\underline{q})$
1^+(s-wave)	$\sqrt{3}q_z$
1^+(d-wave)	$\sqrt{3/2}(q_z-3(\underline{p}.\underline{q})p_z)$
2^-	$\sqrt{3/2}(3p_zq_z-\underline{p}.\underline{q})$
1^-	$3/\sqrt{2}(\underline{p}\wedge\underline{q})_z$
2^+	$3\sqrt{5/2}(\underline{p}\wedge\underline{q})_zp_z$

Barrier factors have been neglected in this table. $\underline{p}$ is a unit vector specifying the direction of the recoiling pseudo-scalar in the $K\pi\pi$ centre of mass and $\underline{q}$ is a unit vector specifying the direction of one of the vector decay products in the vector centre of mass.

$A(\underline{p},\underline{q})$ in terms of the components of the unit vectors $\underline{p}$ and $\underline{q}$ are given for various hypotheses in Table C.1.

The final stage in the calculation is a rotation of axes so that these vectors are defined with respect to the internal axes OXYZ (Chapter 3, section 6). The variables are now the spherical polar angles ($\textcircled{H}$, ψ) of the incident K^+, and the angles lying in the $K\pi\pi$ plane. Integration of equations (11) and (12) of Chapter 3 over $\textcircled{H}$ and ψ yield the theoretical Dalitz plot distributions which may be expressed as :

(1) $K^+\pi^+\pi^-$

$$\frac{4}{9} \left|BW(K^+,\pi^-)\right|^2 G(K^+,\pi^+) + \frac{1}{3} \left|BW(\pi^+,\pi^-)\right|^2 G(\pi^+,K^+)$$

$$+ \frac{4}{3\sqrt{3}} \text{Re} \left\{ BW(K^+,\pi^-)^* \, a e^{i\beta} \, BW(\pi^+,\pi^-) \right\} C(K^+,\pi^+) \qquad (7)$$

(2) $K^0\pi^0\pi^+$

$$\frac{2}{9} \left| BW(K^0,\pi^0)\right|^2 G(K^0,\pi^+) + \frac{2}{9} \left|BW(K^0,\pi^+)\right|^2 G(K^0,\pi^0)$$

$$- \frac{4}{9} \text{Re} \left\{ BW(K^0,\pi^0)^* \, BW(K^0,\pi^+) \right\} C(\pi^0,\pi^+)$$

$$+ \frac{2}{3} a^2 \left|BW(\pi^0,\pi^+)\right|^2 G(\pi^+,K^0)$$

$$+ \frac{4}{3\sqrt{3}} \text{Re} \left\{ BW(K^0,\pi^0)^* \, a e^{i\beta} \, BW(\pi^0,\pi^+) \right\} C(K^0,\pi^+)$$

$$+ \frac{4}{3\sqrt{3}} \text{Re} \left\{ BW(K^0,\pi^+)^* \, a e^{i\beta} \, BW(\pi^0,\pi^+) \right\} C(K^0,\pi^0) \qquad (8)$$

where the factors C and G are given in Table C.2. These

Table C 2

Dalitz plot population terms for decay via $K^*\pi$ and $K\rho$.

Spin Parity State	G(1,2)	C(1,2)
0^-	$3\cos^2\delta_1 p_2^2$	$3\cos\delta_1\cos\delta_2 p_1 p_2$
1^+(s-wave)	1	$\cos(\delta_1+\delta_2-\Delta_{12})$
2^-	$(3/10)(3+\cos^2\delta_1)p_2^2$	$(3/10)(3\cos(\delta_1+\delta_2-2\Delta_{12})+\cos\delta_1\cos\delta_2)p_1 p_2$
1^-	$(3/2)\sin^2\delta_1 p_2^2$	$-(3/2)\sin\delta_1\sin\delta_2 p_1 p_2$
2^+	$(3/2)\sin^2\delta_1 p_2^4$	$-(3/2)\cos\Delta_{12}\sin\delta_1\sin\delta_2 p_1^2 p_2^2$

The angle Δ_{12} is between particles 1 and 2 measured in the three particle centre of mass, δ_1 is this angle measured in the centre of mass of particles 1 and 3, and δ_2 is this angle measured in the centre of mass of particles 2 and 3. The centrifugal barrier terms are the appropriate powers of the momentum p of the recoiling pseudoscalar in the three particle centre of mass.

integrations were checked by comparing the Dalitz plot projections calculated from the formulae (8) and (9) with those obtained by Monte Carlo generation of phase space weighted with the intensities of formulae (10) and (11) of Chapter 3 using the relevant terms from Table C.1.

3 Inclusion of Kϵ Amplitudes

In these analyses the ϵ was represented by an s-wave Breit-Wigner of the form

$$BW_\epsilon = \frac{\sqrt{\Gamma_r \frac{M_r}{q_r}}}{(M-M_r) + i\frac{\Gamma}{2}} \quad ; \quad \Gamma = \Gamma_r \frac{M_r}{q_r} \frac{q}{M} \qquad (9)$$

with the notation of Chapter 3, section 7. The expression (1) was correspondingly modified to read

$$\frac{1}{\sqrt{2}} \left\{ \langle K_1^* \pi_2 | + \langle K_2^* \pi_1 | \right\} + \alpha e^{i\beta} \langle K\rho | + \gamma e^{i\delta} \langle K\epsilon | \qquad (10)$$

for states of unnatural spin-parity. The additional isospin factors give

$$\gamma e^{i\delta} \left\{ \frac{1}{3} A_\epsilon (\underline{p}_{K^+}, \underline{q}_{\pi_1^+}) BW_\epsilon(\pi_1^+, \pi_2^-) + \frac{1}{3} A_\epsilon(\underline{p}_{K^+}, \underline{q}_{\pi_1^-}) BW_\epsilon(\pi_1^-, \pi_2^+) \right\} \qquad (11)$$

to be added to (3) with

$$A_\epsilon(\underline{p},\underline{q}) = Y_J^0(\underline{p})\, Y_0^0(\underline{q})\, p^J \qquad (12)$$

Integration over $\textcircled{H}$ and ψ leads to (7) with the additional terms

$$\frac{2}{9}\,|BW_\epsilon|^2\,G_\epsilon - \frac{4}{3}\sqrt{\frac{2}{3}}\,\mathrm{Re}\left\{BW(K^+,\pi^-)^*\,\gamma e^{i\delta}\,BW_\epsilon\right\}C_{K\epsilon}(K^+,\pi^+)$$

$$-\frac{2}{3}\sqrt{2}\,\mathrm{Re}\left\{BW(\pi^+,\pi^-)^*\,\alpha\gamma e^{i(\delta-\beta)}\,BW_\epsilon\right\}C_{\rho\epsilon}(\pi^+,\pi^-) \qquad (13)$$

The terms G_ϵ , $C_{K\epsilon}$ and $C_{\rho\epsilon}$ for the spin parities 0^-, 1^+, 2^- are given in Table C.3.

4 Fitting Procedure

The fitting of the Dalitz plot distributions to both final states simultaneously was performed by minimising the logarithm of the likelihood function which was defined to be :

$$\mathcal{L} = -\ln\left\{\frac{\prod_{i=1}^{N} L_i^{\,a}\;\prod_{j=1}^{M} P\,L_j^{\,b}}{\left[\int (L^a + PL^b)\,d\Omega\right]^{M+N}}\right\} \qquad (14)$$

where N and M are the number of events studied in $K^+\pi^+\pi^-$ (channel a) and $K^o\pi^+\pi^o$ (channel b) respectively and L^a and L^b are the corresponding intensities for the two channels. The constant P (of value 0.65) is a factor representing the a priori probability ratio of observing the two channels allowing for both the difference in the film samples in the analysis of the two channels and for the loss of unseen K^o mesons. The integral in the denominator is over phase space (Ω). It was evaluated for each bin by numerical integration

Table C 3

Dalitz plot population terms involving the Kϵ decay mode.

Spin Parity State	G_ϵ	$C_{K\epsilon}$	$C_{\rho\epsilon}$
0^-	1	$\sqrt{3}\cos\delta_1 p_2$	$-\sqrt{3}\cos\delta_2 p_1$
1^+	p_1^2	$\cos(\delta_1-\Delta_{12})p_1$	$\cos\delta_2 p_1$
2^-	p_1^4	$1/4\sqrt{6/5}(\cos\delta_1+3\cos(\delta_1-2\Delta_{12}))$ $p_1^2 p_2$	$\sqrt{6/5}\cos\delta_2 p_1^3$

The notation is as Table C.2

over the Dalitz plot at the central value of the energy for that bin.

This normalisation procedure proved inadequate in the first bin where the tail of the ρ started appearing only at the upper end of the region. For this bin, normalisation was carried out by sub-dividing it into 5 smaller regions, calculating the normalisation for each sub-region and summing over the five terms. In higher bins where the normalisations increased approximately linearly with mass, this procedure proved unnecessary, as was verified by repeating this process in bin 2 for some fits. Essentially identical results were obtained to those where the standard normalisation procedure was used.